REPUBLIQUE ALGERIENNE DEMOCRATIQUE ET POPULAIRE
الجمهورية الجزائرية الديمقراطية الشعبية

MINISTRY OF HIGHER EDUCATION
AND SCIENTIFIC RESEARCH

HIGHER SCHOOL IN APPLIED SCIENCES
–T L E M C E N–

ESSA Tlemcen-تلمسان

المدرسة العليا في العلوم التطبيقية
École Supérieure en Sciences Appliquées

وزارة التعليم العالي والبحث العلمي

المدرسة العليا في العلوم التطبيقية
ـ تلمسان ـ

Final Degree Project

For obtaining the Engineering diploma

Field : Industrial engineering
Major: Industrial management and logistics

Presented by : Mohammed Abdelkader EL AHMAR

Subject

A MILP Model for the optimisation of disassembly and remanufactring operations in Circular Supply Chain

Publicly defended, on 22/06/2025 , in front of the jury composed of:

Mr Mohammed Bennekrouf	Associate Professor	ESSA. Tlemcen	President
Mr Fouad Maliki	Associate Professor	ESSA. Tlemcen	Thesis Director
Mr Taha Arbaoui	Professor	INSA Lyon	Thesis co-Director
Mrs Nour El Houad Sekkal	Assistant Professor	ESSA. Tlemcen	Examiner 1
Mr Haddou Benderbal Hichem	Associate Professor	Aix-Marseille Uni	Examiner 2

Année universitaire : 2025 /2026


بسم الله الرحمن الرحيم

Acknowledgment

First and foremost, I would like to express my profound gratitude to Allah, the Almighty, for granting me the strength, perseverance, and intellectual capacity required to complete this Master's thesis successfully. Without this divine grace, the culmination of this demanding academic endeavor would not have been possible.

I wish to express my deepest and most sincere appreciation to my Thesis Director, Mr. Fouad Maliki . His unwavering support, continuous guidance, and immense pedagogical acumen have been invaluable throughout this research journey. I am truly grateful for his constant availability, his constructive feedback, and the rigorous academic standards he instilled in me. His methodical approach to Operations Research and Optimization has profoundly shaped my academic perspective and provided the essential framework necessary to navigate the complexities of this study.

I am equally grateful to my Co-Supervisor, Professor Taha Arbaoui. His extensive expertise, insightful recommendations, and significant scientific contributions have substantially enriched the theoretical and practical quality of this work. His critical insights and unwavering encouragement have been instrumental in overcoming the analytical challenges encountered during the modeling and computational phases of this thesis. The opportunity to benefit from his wealth of knowledge in the field has been a distinct privilege.

It is a profound honor for me that Mr. Mohammed Bennekrouf has graciously accepted the invitation to preside over the jury for this thesis defense. I extend my sincere thanks to him for his interest in this research, for his leadership during the defense, and for honoring this academic presentation with his esteemed presence.

My profound gratitude also extends to the distinguished examiners of my thesis committee: Mrs. Nour El Houad Sekkal, and Mr. Haddou Benderbal Hichem. I deeply appreciate the time, thoroughness, and effort they dedicated to evaluating this work. Their valuable feedback, constructive criticisms, and pertinent questions will undoubtedly enhance the final quality of this research and provide vital direction for my future academic or professional endeavors in Supply Chain Management.

Dedication

I want to dedicate this work to my loving parents, Mr. Miloud El Ahmar and Mrs. Samia Faraoun, who have been there for me in every moment of my life. I want to thank them for their endless support and for granting me every opportunity so I could reach my dreams. Their unconditional love has shaped me into the man I am today, and I will be grateful for as long as I live.

To my little sister, Hidayet El Ahmar, my source of support and hope in this life: Thank you for all your encouragement and help throughout my life, and thank you for filling my days with cherished memories that I can always look back on.

To my grandparents, Mohammed Faraoun and Fatiha Gerryvile: Thank you for being pillars of strength in my life, and for always being a safety net to catch me each time I fail.

I also dedicate this to the loving memory of my late grandfather Abderlkader El Ahmar. Though he is unfortunately not here to witness this day, I carry his memory in my heart and hope this achievement makes him proud

I also extend my heartfelt thanks to my extended family—my aunts, uncles, and cousins—for their love, respect, encouragement, and constant support. May this humble work reflect my sincere gratitude for their unwavering moral support.

To my classmates: Thank you for making these the best three years of my life, full of joy and unforgettable moments.

A special thank you to my professor, Fouad Maliki, who was a true mentor to me throughout my education, helping me achieve things I once thought impossible.

Lastly, to everyone who contributed in any way to the completion of this work: your guidance, support, and presence were essential throughout this journey. I thank you from the bottom of my heart for your help and encouragement in bringing this project to life.

"Despite everything, it's still you."

— Toby Fox, *Undertale*

Abstract

The transition to circular supply chains (CSCs) is a strategic imperative for balancing environmental sustainability with economic resource recovery. However, managing End-of-Life (EoL) products through disassembly and remanufacturing presents complex operational challenges. To address these systemic complexities, this thesis proposes a deterministic Mixed Integer Linear Programming (MILP) model designed to optimize decision-making within a multi-period CSC environment.

The proposed MILP optimization framework determines the optimal quantities of EoL products to disassemble and components to remanufacture, aiming to maximize overall system profitability. It rigorously integrates essential operational constraints, including inventory flow balances, capacity limitations, and demand fulfillment. Due to the scarcity of real-world industrial data, a customized synthetic dataset was generated to computationally implement and exactly solve the optimization model.

Computational experiments and graphical analyses of key performance indicators illustrate critical dynamics regarding inventory, production scheduling, and financial performance. From a managerial perspective, the results demonstrate that synchronously optimizing disassembly and remanufacturing significantly minimizes inventory holding costs while maximizing resource utilization. Ultimately, this thesis provides a robust decision-support tool for industry practitioners, offering a scalable mathematical framework that enhances both the economic viability and environmental sustainability of product recovery operations.

Résumé

La transition vers les chaînes d'approvisionnement circulaires (CAC) est un impératif stratégique pour allier durabilité environnementale et récupération de valeur. Cependant, la gestion des produits en fin de vie via le désassemblage et la refabrication pose des défis opérationnels complexes. Cette thèse propose un modèle déterministe de programmation linéaire en nombres entiers mixtes (MILP) pour optimiser la prise de décision dans une CAC multi-périodes.

Le cadre d'optimisation MILP détermine les quantités optimales de produits à désassembler et de composants à refabriquer afin de maximiser le profit économique. Il intègre rigoureusement des contraintes de capacité, de gestion des stocks et de satisfaction de la demande. En l'absence de données industrielles réelles, un ensemble de données synthétiques a été généré pour implémenter et résoudre le modèle de manière exacte.

Les expériences de calcul et l'analyse graphique des indicateurs de performance illustrent les dynamiques d'inventaire, de production et de rentabilité. D'un point de vue managérial, l'optimisation synchrone du désassemblage et de la refabrication minimise les coûts de stockage tout en maximisant l'utilisation des ressources. En conclusion, cette thèse fournit un outil d'aide à la décision pertinent, améliorant à la fois la viabilité économique et environnementale des opérations de récupération.

الملخص

يعد الانتقال إلى سلاسل التوريد الدائرية ضرورة استراتيجية للجمع بين الاستدامة البيئية واستعادة القيمة. ومع ذلك، فإن إدارة المنتجات في نهاية دورة حياتها من خلال التفكيك وإعادة التصنيع تطرح تحديات تشغيلية معقدة. تقترح هذه الأطروحة نموذجاً حتمياً للبرمجة الخطية المختلطة ذات الأعداد الصحيحة (بيبع) لتحسين اتخاذ القرار في سلسلة توريد دائرية متعددة الفترات.

يحدد إطار عمل التحسين بيبع الكميات المثلى للمنتجات التي يجب تفكيكها والمكونات التي يجب إعادة تصنيعها لتعظيم الأرباح الاقتصادية، مع دمج قيود السعة وتدفق المخزون وتلبية الطلب. ونظراً لندرة البيانات الصناعية الواقعية، تم إنشاء مجموعة بيانات تركيبية (اصطناعية) لتنفيذ النموذج وحله حسابياً بدقة.

تكشف التجارب الحسابية والتحليل البياني لمؤشرات الأداء عن ديناميكيات المخزون والإنتاج والربحية. من منظور إداري، يثبت البحث أن التحسين المتزامن للتفكيك وإعادة التصنيع يقلل بشكل كبير من تكاليف التخزين ويزيد من الاستفادة من الموارد. في الختام، توفر هذه الأطروحة أداة فعالة لدعم اتخاذ القرار، مما يعزز الجدوى الاقتصادية والاستدامة البيئية لعمليات استعادة المنتجات.

Contents

List of Figures **15**

List of Tables **17**

Abreviations list **17**

Introduction **19**

1 Reverse Logistics and Engineering **22**
1.1 Introduction to Reverse Logistics and Engineering 22
1.2 Definition of Reverse Logistics 23
1.3 Importance of Reverse Logistics in Modern Industry 23
1.4 Key Drivers of Reverse Logistics Systems 24
1.4.1 Environmental and Legislative Drivers 24
1.4.2 Economic Drivers 24
1.4.3 Corporate Social Responsibility and Competitive Pressure . . 25
1.5 Reverse Logistics vs. Forward Logistics 25
1.6 Components of Reverse Logistics Systems 25
1.6.1 Collection Systems and Return Channels 25
1.6.2 Product Recovery Options: Reuse, Repair, Remanufacturing, and Recycling 26
1.7 Environmental and Economic Impact of Reverse Logistics 26
1.7.1 Environmental Impact 26
1.7.2 Economic Impact 27

2 Disassembly in Reverse Logistics Systems **28**
2.1 Definition of Disassembly 28
2.2 Role of Disassembly in Reverse Logistics Systems 28
2.3 Types of Disassembly 29

2.3.1 Complete vs. Selective Disassembly . . . 29
2.3.2 Destructive vs. Non-Destructive Disassembly . . . 29
2.4 Disassembly Process and Structure . . . 29
2.4.1 Product Structure Representation . . . 29
2.4.2 Disassembly Sequences . . . 31
2.5 Disassembly Planning Problems . . . 31
2.5.1 Sequence Planning . . . 31
2.5.2 Line Design . . . 31
2.5.3 Resource Allocation . . . 31
2.6 Solution Approaches . . . 32
2.6.1 Exact Methods . . . 32
2.6.2 Heuristics and Metaheuristics . . . 32
2.6.3 Simulation Approaches . . . 33
2.7 Pricing of Recovered Components . . . 34
2.7.1 General Pricing Strategies . . . 34
2.7.2 Dynamic Pricing: Definition and Mechanism . . . 34
2.7.3 Benefits of Dynamic Pricing . . . 35
2.7.4 How Demand Affects Pricing . . . 36

Conclusion **41**

3 Mathematical Formulation **43**
3.1 Introduction . . . 43
3.1.1 Motivation and Context . . . 43
3.1.2 Circular Economy Relevance . . . 43
3.1.3 Generality and Transferability . . . 44
3.1.4 Scope and Applicability . . . 44
3.1.5 Structure of the Document . . . 45
3.2 Generalized Product Decomposition Framework . . . 45
3.2.1 The Product Decomposition Graph . . . 45
3.2.2 Node Classification Taxonomy . . . 46
3.2.3 Generic PDG Diagram . . . 46
3.3 Modelling Assumptions . . . 47
3.4 Mathematical Formulation . . . 48
3.4.1 Sets and Indices . . . 48
3.4.2 Parameters . . . 48
3.4.3 Recovery Yield . . . 50
3.4.4 Dual-Channel Demand Models . . . 50
3.4.5 Dual-Channel Normalized Isoelastic Pricing . . . 51
3.4.6 Decision Variables . . . 53
3.4.7 Objective Function . . . 53
3.4.8 Constraints . . . 54

3.4.9 Complete Model Statement . . . 56
3.5 Structural Generalization Analysis . . . 57
3.5.1 Dimensions of Abstraction . . . 57
3.5.2 Key Invariants Preserved . . . 57
3.5.3 Industrial Instantiation Protocol . . . 58
3.6 Application Examples . . . 58
3.6.1 Example 1: Electric Vehicle Battery Pack (Motivating Instance) 58
3.6.2 Example 2: Smartphone Disassembly . . . 59
3.6.3 Example 3: Industrial Robot Arm . . . 59
3.7 Advanced Extensions . . . 59
3.8 Conclusion . . . 60

4 Model Execution 63
4.1 Problem Description . . . 64
4.1.1 System Overview . . . 64
4.1.2 Quantities and Scenario Approach . . . 64
4.1.3 Key Structural Adaptations . . . 64
4.2 Battery Pack Network . . . 65
4.2.1 Node Set . . . 65
4.2.2 Level Structure . . . 65
4.2.3 Index Subsets . . . 66
4.2.4 Integer Yield on AND Arcs . . . 66
4.2.5 Remanufacturing Assembly Ratios . . . 67
4.2.6 Network Diagram . . . 67
4.3 Mathematical Formulation . . . 67
4.3.1 Sets and Indices . . . 67
4.3.2 Parameters . . . 67
4.3.3 Demand Models . . . 70
4.3.4 Dual-Channel Normalized Isoelastic Pricing . . . 71
4.3.5 Decision Variables . . . 73
4.3.6 Objective Function . . . 73
4.3.7 Constraints . . . 74
4.3.8 Complete Model Statement . . . 76
4.4 Structural Analysis and Economic Interpretation . . . 78
4.4.1 Yield: Two Operational Modes . . . 78
4.4.2 Interaction: Yield × Demand . . . 78
4.4.3 Structure of the Split Inventory Balance . . . 78
4.4.4 Generality of the Constraint Structure . . . 79
4.5 Implementation Notes . . . 79
4.6 Conclusion . . . 80
4.7 The Network Model . . . 81
4.7.1 Node Set CC . . . 81

4.8 Edge Set AA — Directed Multigraph . . . 81
4.9 Mathematical Form (Option C) . . . 82
4.9.1 Set definitions . . . 82
4.9.2 Quantity function qq . . . 82
4.9.3 Direction indicator . . . 83
4.9.4 Absolute quantity at pack level . . . 83
4.9.5 Flow conservation check ΦPhi . . . 83
4.10 Data generation . . . 85
4.10.1 Literature Review . . . 85
4.10.2 Research Problem and Context . . . 85
4.10.3 Related Literature . . . 85
4.11 Extracted Parameters – from Article . . . 88
4.12 Missing Data Analysis . . . 88
4.13 Real Data Collected . . . 89
4.13.1 Secondary-Market Prices for Forward Channel . . . 89
4.13.2 Remanufactured Channel Prices . . . 89
4.13.3 Disassembly Cost Literature Benchmarks . . . 90
4.13.4 Pack-Level Battery Economics . . . 90
4.14 Synthetic Data Generation Methodology . . . 90
4.14.1 Guiding Principles . . . 90
4.14.2 Market Price Ceilings $P_{it}^{\max,f}$ and $P_{kt}^{\max,r}$ . . . 90
4.14.3 Disassembly Costs C_i^{dis} . . . 90
4.14.4 Remanufacturing Costs C_k^{rmfg} . . . 91
4.14.5 Holding Costs h_i . . . 91
4.14.6 Capacity Parameters . . . 91
4.14.7 EOL Supply S_t . . . 92
4.14.8 Isoelastic Parameters $(\alpha_i, \beta_i, \gamma_i)$ . . . 92
4.14.9 Remanufactured Demand Bounds $d_k^{r,\min}$, $d_k^{r,\max}$ . . . 92
4.14.10 Cost-Recovery Base Price κ_i . . . 92
4.15 Final Generated Dataset . . . 94
4.15.1 Node Reference Table . . . 94
4.15.2 Network and Yield Parameters . . . 94
4.15.3 Isoelastic Pricing Parameters . . . 94
4.15.4 Demand Parameters . . . 95
4.15.5 Operational Parameters Summary . . . 95
4.15.6 Constraint Count for Reference Horizons . . . 96
4.16 Assumptions . . . 96
4.17 Limitations . . . 97
4.18 Model execution . . . 98
4.18.1 Scope and Objectives . . . 98
4.19 Bill-of-Materials and Node Definitions . . . 98
4.20 Key Performance Indicators . . . 99

4.21 Period-by-Period Results ($t = 1 \ldots 20$) 100
4.22 Node Revenue Analysis 100
4.23 Results Visualisations 101
4.23.1 BOM Structure and Supply Chain Network 101
4.23.2 Demand and Price Structure 102
4.23.3 Fixed Remanufacturing 103
4.23.4 Financial Performance 106
4.23.5 Full KPI Dashboard 108
4.24 Conclusions 108
4.24.1 Key Findings 108
4.24.2 Interruptions 109
4.24.3 Model Limitations and Future Extensions 109

List of Figures

2.1 Schematic AND/OR graph for a five-component product. AND-arcs indicate parallel disassembly steps; OR-arcs represent alternative sequences leading to the same state (adapted from Homem de Mello and Sanderson 1990). 30

2.2 A standard downward-sloping market demand curve for a recovered component. At equilibrium price P^* the quantity demanded equals Q^*. A price increase above P^* reduces quantity demanded; a price decrease below P^* raises it (after Marshall 1890). 37

2.3 An outward shift in demand from D_1 to D_2 raises both the equilibrium price ($P_1^* \rightarrow P_2^*$) and equilibrium quantity ($Q_1^* \rightarrow Q_2^*$). For a reverse logistics operator holding a fixed stock of recovered parts, this shift justifies a price increase and signals an opportunity to expand disassembly capacity. 38

2.4 Elastic versus inelastic demand curves. The steep curve represents inelastic demand (common for scarce or specialised recovered components with no close substitutes); the flatter curve represents elastic demand (common for standard parts available from multiple suppliers). Firms should raise prices when facing inelastic demand and lower prices when demand is elastic to maximise total revenue (after Marshall 1890). 39

2.5 Optimal dynamic price path $P^*(t)$ over a twelve-period selling horizon for a fixed stock of recovered components, compared with a static reference price $\bar{P}$. The dynamic policy undersells early (capturing volume) and charges a premium as inventory depletes, yielding strictly higher expected revenue than the static price in all scenarios except the trivial case of perfectly flat demand (after Gallego and Van Ryzin 1994). 40

3.1 Generic four-level Product Decomposition Graph (PDG) with $|V| = 10$ nodes, 9 decomposition arcs, and 5 reconditioning arcs. Orange nodes (V_M): remanufacturable intermediates, governed by constraint **(B1)**. Green nodes (V_L): leaf recoverable nodes, governed by constraint **(B2)**. This topology is instantiated for the Nissan Leaf 24 kWh battery pack in Section 3.6.1. 47

4.1 AND-arc disassembly network for the Nissan Leaf 24 kWh battery pack (10 nodes, 9 disassembly arcs, 5 remanufacturing arcs). Orange nodes ($_M = \{N_4, N_7\}$): remanufacturable intermediates governed by constraint **(B1)**. Green nodes ($_L$): leaf nodes governed by constraint **(B2)**. 68

4.2 AND-arc disassembly Bill-of-Materials for the Nissan Leaf 24 kWh battery pack. Nodes N4 and N7 (highlighted in orange and green) are the two remanufacturable nodes C^M. Edge labels show β (nominal yield) and α (recovery yield). 101

4.3 Isoelastic forward price trajectories P^f_{it} across all nine saleable nodes. Prices oscillate sinusoidally; dashed lines show the time-varying price ceiling. 102

4.4 Dual-channel price comparison for the two remanufacturable nodes. The remanufactured price P^r_{kt} commands a substantial premium (shaded area) over the forward channel price P^f_{kt}, justifying remanufacturing investment. 102

4.5 Isoelastic demand curves for N4 (Battery Modules) and N7 (AESC Cells). Scatter points show realised (P, D) pairs over the planning horizon. 103

4.6 Top row — remanufacturing starts $r_{k,t}$ are now properly non-zero (previously all zero in v2). Bottom row — certified-refurb sales $Y^r_{k,t}$ track starts with one-period lag, fed exclusively from $I^{\text{rmfg}}_{k,t}$ (purple dotted). 103

4.7 Material flow into remanufacturing per period. Top: units consumed from I^{fwd} (core module/cell plus replacement parts). Bottom: resulting dual-pool inventory dynamics — forward stock (coloured) and certified-refurb stock (purple) evolve independently. 104

4.8 Dual-pool inventory for N4 and N7. I^{fwd} (solid) and I^{rmfg} (dashed purple) are strictly separated. Horizontal dotted lines mark the independent capacity limits. 104

4.9 Waterfall margin decomposition for N4 remanufacturing. The corrected margin of \$41.12/module explicitly deducts the opportunity cost of diverting a used module from the forward pool. 105

4.10 **B**oth remanufacturing revenue (green) and cost (red) are non-zero. Cost = $C_k^r \cdot r_{k,t}$ is charged when a batch starts; revenue arrives one period later from I^{rmfg} sales. 105
4.11 Revenue vs. total cost (top) and period profit (bottom). Stacked bars show forward (blue) and remanufacturing (green) revenue channels. Nearly All 50 periods are profitable. 106
4.12 Stacked cost decomposition. Disassembly dominates. Holding and disposal costs are negligible by comparison. 106
4.13 Cumulative profit trajectory $Z(t)$ reaching \$283,721 at $t = 50$. Growth is monotone and convex, reflecting the progressive ramp-up of the remanufacturing channel once the I_rmfg pool is seeded. 107
4.14 Total revenue per node over the full horizon. N4 Battery Modules generate by far the largest remanufacturing revenue (green bar segment), followed by N7 Cells. N3 BMS units command the highest forward prices. 107
4.15 Capacity utilisation. Left: disassembly lines — N0 (pack) operates near full capacity; N4 and N7 disassembly run below the 80% threshold. 107
4.16 Consolidated KPI dashboard for MILP. 108

List of Tables

1.1 Principal differences between forward and reverse logistics (adapted from Tibben-Lembke and Rogers 2002 and Fleischmann et al. 2001) . 25

2.1 Comparison of pricing strategies for recovered components (synthesised from Guide et al. 2003, Kotler and Armstrong 2016, and Gallego and Van Ryzin 1994) 40

3.2 Model parameters for the generalized framework. 48
3.1 Sets and index notation for the generalized framework. 51
3.3 Decision variables of the generalized framework. 53
3.4 Constraint inventory for a PDG with $|V_R|$ recoverable nodes, $|V_M|$ remanufacturable intermediates, $|V_L|$ leaf nodes, $|V_D|$ decomposable nodes, $|V|$ total nodes, and $\sum_{k_M} |(k)|$ reconditioning child-pairs. 57
3.5 Abstraction map from battery-specific to generalized framework. . . 62

4.1 Node set : identifiers, labels, level, role, and absolute pack-level quantity Q^{abs}. 65
4.3 Model parameters. 68
4.2 Sets and index notation. 71
4.4 Decision variables. 73
4.5 Constraint inventory (T = number of planning periods). 77
4.6 Node set C with identifiers, labels, and absolute quantities in one complete battery pack. 81
4.7 Complete arc set A. Every row appears as a bidirectional pair. q_{unit} = quantity per parent; q_{abs} = absolute count in pack. 81
4.8 How each element of the directed graph is used in engineering and operations applications. 84
4.9 All values are **[R]** real (from article). 88
4.10 Observed secondary-market prices for forward channel nodes. **[R]** Real data (R). 89

4.11 Observed prices for remanufactured (certified) components. [R] Real (R). 89
4.12 Complete node reference table with all parameters. Data-type legend applies. 93
4.13 AND-arc yield parameters. All values [R] real (from article) except $\bar{\alpha}_{ij}$. 94
4.14 Forward-channel isoelastic parameters. [S] Synthetic (S) unless noted. 94
4.15 Remanufactured-channel isoelastic parameters. [S] Synthetic (S) unless noted. 94
4.16 Forward-channel demand range parameters per node. [I] Inferred (I) or [S] synthetic (S). 95
4.17 Full operational parameter summary. Data-type legend applies. . . . 95
4.18 Model size for representative planning horizons (T). [R] R – formula from article, $42T$. 96
4.19 Node definitions, roles, and key parameters 98
4.20 Financial KPIs — MILP v3 Fixed Model 99
4.21 Operational totals — full $T = 50$ horizon 99
4.22 Operational decisions and economics per period (first 20 of 50) 100
4.23 Node-level revenue breakdown over the full $T = 50$ horizon 100

Abreviations list

1. AESC : Automotive Energy Supply Corporation (manufacturer of the Nissan Leaf pouch cells, node N7)
2. BMS : Battery Management System (node N3)
3. BOM : Bill of Materials
4. CBC : COIN-OR Branch and Cut (open-source MILP solver used via PuLP)
5. CD : Set of disassembly nodes, $C^D = \{N0, N4, N7\}$
6. CM : Set of remanufacturable nodes, $C^M = \{N4, N7\}$
7. CS : Set of sellable (forward-market) nodes, C^S
8. CSV : Comma-Separated Values
9. EOL : End-of-Life (battery packs entering the reverse-logistics system)
10. GA : Genetic Algorithm
11. JSON : JavaScript Object Notation
12. KPI : Key Performance Indicator
13. kWh : Kilowatt-hour
14. LBC : Li-ion Battery Controller (sub-component of node N3)
15. LiPF6 : Lithium Hexafluorophosphate (electrolyte, node N11)
16. LMO : Lithium Manganese Oxide (cathode material, node N8)
17. LP : Linear Programming
18. MCMB : Mesocarbon Microbeads (anode material, node N9)
19. MILP : Mixed-Integer Linear Programming
20. MIP : Mixed-Integer Programming
21. NSGA-II : Non-dominated Sorting Genetic Algorithm II
22. PE/PP : Polyethylene/Polypropylene (separator material, node N10)
23. PGFPlots : PGF/TikZ-based plotting package for LaTeX
24. PuLP : Python linear/mixed-integer programming modelling library
25. ROI : Return on Investment
26. SBX : Simulated Binary Crossover
27. MILP : Mixed:Integer Linear Programme
28. EOL : End:of Life
29. BOM : Bill of Materials
30. CBC : Coin:or Branch and Cut (solver)

31. PuLP : Python LP (Linear Programming library)
32. BMS : Battery Management System
33. LBC : Lithium Battery Controller (Pack BMS variant)
34. EV : Electric Vehicle
35. SoH : State of Health
36. AESC : Automotive Energy Supply Corporation
37. LMO : Lithium Manganese Oxide
38. MCMB : Mesocarbon Microbeads
39. PE/PP : Polyethylene/Polypropylene
40. OR : Operations Research
41. LP : Linear Programme
42. MIP/MILP : Mixed-Integer (Linear) Programme
43. VSS : Value of the Stochastic Solution
44. EVPI : Expected Value of Perfect Information
45. EV : Expected Value (solution)
46. WS : Wait-and-See
47. RH : Rolling Horizon
48. SP : Stochastic Programme
49. SAA : Sample Average Approximation
50. MC : Monte Carlo
51. CV : Coefficient of Variation
52. MPC : Model Predictive Control
53. KPI : Key Performance Indicator
54. EOQ : Economic Order Quantity
55. VRP : Vehicle Routing Problem
56. ATEX : Atmosphères Explosibles (hazardous area classification)
57. B2B : Business to Business
58. BNEF : BloombergNEF
59. OEM : Original Equipment Manufacturer
60. ESSA : École Supérieure des Sciences Appliquées
61. INSA : Institut National des Sciences Appliquées
62. DISP : Décision et Information pour les Systèmes de Production (lab)
63. CITI : Centre of Innovation in Telecommunications and Integration of services (lab)
64. CVaR : Conditional Value-at-Risk
65. IQR : Interquartile Range

Introduction

For over a century, global industrial development has been primarily driven by a linear economic paradigm, often characterized by a "take-make-dispose" model of production and consumption. While this paradigm has yielded unprecedented economic growth and technological advancement, it has simultaneously precipitated severe environmental degradation, accelerated resource depletion, and exacerbated global climate change Geissdoerfer et al. (2017). The extraction of virgin raw materials, coupled with the generation of massive volumes of solid waste and greenhouse gas emissions, has pushed ecological systems toward their planetary boundaries. In response to these pressing sustainability challenges, governments, industries, and academia have increasingly advocated for a paradigm shift toward more sustainable industrial frameworks.

The Circular Economy (CE) has emerged as a compelling and viable alternative to the traditional linear model. Rooted in the principles of designing out waste, keeping materials in use for as long as possible, and regenerating natural systems, the circular economy seeks to decouple economic growth from resource consumption Ellen MacArthur Foundation (2013). Rather than treating end-of-life (EoL) products as waste, the circular economy views them as valuable repositories of materials and components that can be recovered and reintroduced into the economic cycle.

Effective End-of-Life product management is the cornerstone of operationalizing the circular economy. Within this domain, various product recovery options exist, ranging from basic material recycling to high-value recovery processes such as repair, refurbishing, and remanufacturing Ilgin and Gupta (2010). Among these, disassembly and remanufacturing stand out as highly critical operations. Remanufacturing involves rebuilding a product to its original specifications using a combination of reused, repaired, and new parts, thereby recovering a significant portion of the geometric form and intrinsic value of the original product Lund (1984). Disassembly, on the other hand, is the prerequisite systematic dismantling of EoL products to extract functional components and subassemblies. Together, these operations not only prevent products from ending up in landfills but also dramatically reduce the energy and raw material requirements compared to manufacturing entirely new

products. Consequently, optimizing these interrelated operations is a fundamental prerequisite for the financial and ecological viability of modern industrial systems.

Despite the recognized importance of disassembly and remanufacturing, integrating these operations into a unified, financially optimized production plan remains a formidable operational challenge. The core problem lies in making optimal, dynamic decisions regarding whether a specific batch of returned products should be disassembled for parts, directly remanufactured, or held in inventory, all while seeking to maximize the economic performance of the circular supply chain. This decision-making process is complicated by numerous operational challenges and trade-offs. Firstly, there is an inherent mismatch between the supply of returned products and the market demand for recovered components and remanufactured goods. Disassembly operations yield a predetermined set of components based on the product's structure, but the demand for these individual components may be asymmetrical. This often leads to the accumulation of unnecessary inventory for certain parts while others remain heavily constrained. Secondly, there is a constant trade-off between immediate processing and inventory holding. Holding returned products or disassembled components incurs inventory carrying costs, yet processing them prematurely might lead to excessive remanufacturing costs or the degradation of parts before they can be sold. Furthermore, dynamic economic factors heavily influence these decisions. The costs associated with disassembly, inspection, remanufacturing, and storage, coupled with the fluctuating market prices for secondary materials and remanufactured products, require 3 a multi-period planning horizon. The lack of a robust, deterministic planning tool can lead to severe operational inefficiencies, including capacity bottlenecks, excessive inventory holding costs, and missed market opportunities. Therefore, there is a critical need for a comprehensive decision-support model that can simultaneously optimize inventory, disassembly, and remanufacturing decisions over a specified planning horizon.

Chapter 1

Reverse Logistics and Engineering

1.1 Introduction to Reverse Logistics and Engineering

The latter decades of the twentieth century witnessed a profound shift in how organisations and researchers conceptualise the supply chain. While the classical supply chain model directed attention almost exclusively toward the efficient forward movement of goods from raw materials to end consumers, growing environmental pressures, regulatory mandates, and economic opportunities have compelled practitioners and scholars to examine what happens *after* the point of consumption. The discipline that emerged—reverse logistics—has since developed into a rich, multidisciplinary field intersecting operations research, environmental science, engineering design, and strategic management.

Thierry et al. (1995) were among the first to formalise the concept of product recovery management, outlining a hierarchy of options ranging from direct reuse to material recycling and energy recovery. Shortly thereafter, Rogers and Tibben-Lembke (1999) provided the field with one of its earliest and most widely cited definitions, establishing the dual objectives of value capture and environmental responsibility that continue to govern the field. Stock (1992), whose white paper is widely credited with introducing the term in an academic context, emphasised the management of returned, recalled, and obsolete products as well as hazardous materials.

Engineering plays a central role within this framework. Products must be designed with end-of-life disassembly in mind, recovery facilities must be configured and managed, and logistics networks must be optimised under conditions of uncertainty that seldom arise in conventional forward supply chains. The sub-discipline of *reverse engineering* complements reverse logistics by supplying the technical intelligence needed to make recovery processes economically viable (**?**).

The importance of the field is reflected in the rapid growth of its literature. Govindan et al. (2015), surveying 242 articles, document how research has expanded from early descriptive studies to sophisticated quantitative models addressing network design,

inventory management, forecasting of return flows, and the integration of reverse logistics into broader closed-loop supply chain frameworks. Trochu et al. (2025) identify five key themes shaping contemporary scholarship: integration of digital technologies (IoT, blockchain, AI), sustainability and circular economy principles, omni-channel reverse logistics, servitisation models, and collaborative supply chain integration.

1.2 Definition of Reverse Logistics

Definitions of reverse logistics have proliferated as the field has matured, and some authors note that definitional diversity is itself a source of conceptual confusion (de Brito and Dekker, 2003).

The earliest formulations focused on backward goods flows. Murphy and Poist (1989) introduced the notion of reverse goods flows, and Carter and Ellram (1998) expanded the concept by incorporating environmental considerations. The definition that achieved widest adoption is that of Rogers and Tibben-Lembke (1999): *"the process of planning, implementing, and controlling the efficient, cost-effective flow of raw materials, in-process inventory, finished goods, and related information from the point of consumption to the point of origin for the purpose of recapturing value or proper disposal."* This formulation emphasises purpose—value recovery or responsible disposal—rather than merely the direction of flow.

Dowlatshahi (2000) complemented this by defining reverse logistics as a process in which a manufacturer systematically accepts previously shipped products or parts from the point of consumption for possible recycling, remanufacturing, or disposal. The European Working Group on Reverse Logistics (RevLog) extended the destination beyond the point of origin to "a point of recovery or proper disposal," acknowledging that recovered materials frequently enter entirely different supply chains (de Brito and Dekker, 2003).

An important distinction, articulated by Guide and Van Wassenhove (2009), lies between reverse logistics and closed-loop supply chain management (CLSCM). CLSCM encompasses the design, control, and operation of systems to maximise value creation over the entire product life cycle. Reverse logistics constitutes the return-flow component of CLSCM, while the overarching framework addresses the coordination of both flow directions to achieve systemic efficiency.

1.3 Importance of Reverse Logistics in Modern Industry

The strategic importance of reverse logistics has grown substantially, driven by environmental, economic, legislative, and reputational forces. Govindan et al. (2015)

observe that companies whose products are subject to regeneration can achieve cost savings of up to 60 per cent compared with the manufacture of entirely new products. Industries such as automotive, consumer electronics, aerospace, and pharmaceuticals have integrated reverse logistics into their core operational strategies, recognising that returned products represent a valuable secondary resource stream (**?**).

From an environmental standpoint, effective reverse logistics reduces the quantity of products consigned to landfill, lowers demand for virgin raw materials, and cuts greenhouse gas emissions associated with primary manufacturing (Fleischmann et al., 2001). The emergence of the circular economy has further elevated the strategic profile of reverse logistics; it is the operational infrastructure through which the circular ideal is realised (Atasu et al., 2009).

1.4 Key Drivers of Reverse Logistics Systems

1.4.1 Environmental and Legislative Drivers

Legislation mandating manufacturer responsibility for end-of-life product management is the most visible driver of reverse logistics systems. The EU WEEE Directive (2002), the End-of-Life Vehicles Directive (2000), and Extended Producer Responsibility (EPR) policies have compelled manufacturers across a wide range of sectors to establish take-back and recovery systems. Similar legislation in North America, Japan, South Korea, and China has created a global regulatory landscape that treats reverse logistics as a compliance requirement rather than a voluntary initiative (Atasu et al., 2009).

Beyond mandatory compliance, firms increasingly adopt proactive environmental strategies. Srivastava (2007) demonstrates that green supply chain management—which integrates environmental thinking into supply chain design and operations—explicitly encompasses reverse logistics as a key lever for reducing the environmental footprint of production systems.

1.4.2 Economic Drivers

The economic case rests on the residual value embedded in used products and the cost of primary resource inputs. Guide et al. (2003) demonstrate that remanufactured products can be sold at price points comparable to new goods while being produced at significantly lower cost, provided that the quality of the remanufacturing process is adequately controlled.

Customer return rates in e-commerce routinely reach 20 to 30 per cent, and the costs of managing, inspecting, and re-selling returned merchandise can erode profitability significantly if not managed systematically (Rogers et al., 2002). Firms that invest in efficient reverse logistics therefore enjoy a competitive advantage from both lower

total supply chain costs and the ability to offer customer-friendly return policies.

1.4.3 Corporate Social Responsibility and Competitive Pressure

Ravi and Shankar (2005) use interpretive structural modelling to show that organisational variables such as top management commitment and cross-functional integration are among the most critical enablers of effective reverse logistics implementation, suggesting that cultural and governance factors are as important as operational capabilities.

1.5 Reverse Logistics vs. Forward Logistics

While both domains concern the movement of goods, information, and funds along a supply chain, they differ substantially in the structure of flows, the degree of uncertainty, and the value-creation logic. Tibben-Lembke and Rogers (2002) identify numerous operational asymmetries: reverse logistics shipments tend to be smaller, less uniform, and more costly per unit than forward shipments; packaging is frequently absent or damaged; the condition of returned products is unknown until inspection; and the appropriate disposition decision must be determined product by product.

Table 1.1: Principal differences between forward and reverse logistics (adapted from Tibben-Lembke and Rogers 2002 and Fleischmann et al. 2001)

Dimension	Forward Logistics	Reverse Logistics
Flow direction	Origin → consumer	Consumer → recovery point
Product condition	Known, standardised	Unknown, heterogeneous
Product variety	Limited	High
Demand	Predictable	Uncertain
Supply of inputs	Manufacturer-controlled	Consumer-driven, variable
Packaging	Standard	Often absent or damaged
Network structure	One-to-many (distribution)	Many-to-one (collection)
Disposition decision	Not required	Central challenge
Cost visibility	High	Low

From a network design perspective, forward logistics follows a one-to-many distribution structure, whereas reverse logistics requires a many-to-one collection structure, creating challenges for vehicle routing, facility location, and inventory management (Fleischmann et al., 2001).

1.6 Components of Reverse Logistics Systems

1.6.1 Collection Systems and Return Channels

The collection phase is the point at which used products re-enter the supply chain, and its design fundamentally shapes the efficiency and cost of the entire system.

Manufacturer take-back schemes, retailer-based collection points, third-party logistics providers, and municipal collection infrastructure each present different trade-offs between coverage, unit collection cost, and the quality of items recovered (Fleischmann et al., 2000).

Fleischmann et al. (2000) develop facility location models for reverse logistics networks, demonstrating that the optimal configuration depends heavily on the spatial distribution of end-of-life product generation, the unit transportation cost, and the minimum scale required for economically viable processing.

1.6.2 Product Recovery Options: Reuse, Repair, Remanufacturing, and Recycling

Thierry et al. (1995) provide the foundational taxonomy still widely referenced in the literature:

- **Direct reuse**: The product is redistributed without any technical intervention, either in the same or a secondary market.
- **Repair**: Minor restoration operations return the product to working condition, preserving its identity and basic function.
- **Remanufacturing**: A product is disassembled, cleaned, inspected, refurbished, and reassembled to an "as-new" standard with a comparable warranty. Guide et al. (2003) demonstrate that remanufacturing can recover up to 85 per cent of the value of the original product while consuming only a fraction of the energy and material inputs of primary manufacturing.
- **Recycling**: Material content is recovered through disassembly, sorting, and reprocessing. The economic viability depends on commodity prices, sorting technology, and the energy intensity of reprocessing.
- **Energy recovery**: Incineration with energy capture, appropriate only when material recovery is infeasible.
- **Disposal**: Landfilling—the last resort, representing total value loss and the highest environmental cost.

1.7 Environmental and Economic Impact of Reverse Logistics

1.7.1 Environmental Impact

Remanufacturing typically consumes 85 per cent less energy than primary manufacturing and generates substantially lower levels of solid waste and atmospheric emissions (Guide et al., 2003). At the material level, recycling diverts resources from landfill and reduces the demand for energy-intensive primary production; the recycling of one tonne of aluminium avoids the emission of approximately nine tonnes

of CO_2 equivalent compared with primary smelting.

A systems perspective incorporating Life Cycle Assessment (LCA) methodology is therefore necessary to evaluate the net environmental benefit of any reverse logistics system (Moheb-Alizadeh et al., 2023).

1.7.2 Economic Impact

At the firm level, benefits arise from recovered value through remanufacturing and recycling, the avoidance of raw material purchasing costs, and the mitigation of disposal fees. Guide et al. (2003) estimate that the remanufacturing industry in the United States alone generated revenues exceeding $53 billion annually. Tibben-Lembke and Rogers (2002) show that transportation in reverse logistics is expensive relative to forward logistics, partly because return shipments are smaller and less consolidated, motivating careful balance between the cost of recovery operations and the economic value those operations generate (Fleischmann et al., 2001).

Chapter 2

Disassembly in Reverse Logistics Systems

2.1 Definition of Disassembly

Disassembly is the systematic process of separating a product into its constituent parts, sub-assemblies, components, or other groupings through a sequence of operations that may include unfastening joints, extracting fasteners, cutting, breaking, or otherwise severing connections between parts (Gungor and Gupta, 1999). Unlike assembly—a convergent, deterministic, and highly repeatable process—disassembly is a divergent process whose complexity is compounded by uncertainty about the product's condition, the integrity of fasteners and joints, the degree of corrosion or contamination, and the economic value of the components to be retrieved.

Lambert (1997) emphasises the purposive character of disassembly: the objective is not merely separation per se but the retrieval of parts or materials that will yield economic and/or environmental value in subsequent recovery operations. From a computational perspective, Gungor and Gupta (1999) characterise disassembly sequence planning (DSP) as NP-complete, meaning that the solution space grows combinatorially with the number of components.

2.2 Role of Disassembly in Reverse Logistics Systems

Disassembly occupies a pivotal position within reverse logistics systems. It transforms an end-of-life product from an undifferentiated physical object into a collection of separable value streams: reusable components, parts suitable for remanufacturing, materials amenable to recycling, and waste streams requiring disposal (**?**). Without disassembly, most forms of product recovery beyond direct reuse are precluded.

Guide (2000) identified disassembly as one of seven complicating characteristics of production planning and control in remanufacturing environments, alongside un-

certain timing and quantity of returns, the need to balance returns with demands, the uncertainty in materials recovered, the requirement for a reverse logistics network, material matching restrictions, and stochastic processing times.

2.3 Types of Disassembly

2.3.1 Complete vs. Selective Disassembly

Complete disassembly refers to the full decomposition of a product into all its individual constituent parts. All joints are severed and all components are separated until no further subdivision is possible without destroying material integrity. Complete disassembly maximises the range of recovery options but incurs the highest processing time and labour cost (Gungor and Gupta, 1999).

Selective (partial) disassembly stops short of full decomposition, extracting only those components targeted for recovery—typically highest-value items or those containing regulated hazardous materials—and leaving the remainder intact for bulk recycling or disposal. Lambert (1999) develops an analytical framework for selective disassembly that accounts for accessibility constraints imposed by the product structure. Bentaha et al. (2015) develop stochastic models for selective disassembly line balancing, acknowledging that task processing times are uncertain owing to product heterogeneity and variation in joint condition.

2.3.2 Destructive vs. Non-Destructive Disassembly

Non-destructive disassembly preserves the integrity of all components removed and is required whenever the goal is recovery of components for direct reuse or remanufacturing (Gungor and Gupta, 1999). **Destructive disassembly** permits deliberate fracture, cutting, or shearing of joints or components to gain access to target items. Deniz and Ozcelik (2019) show that introducing a partial destructive mode substantially broadens the feasible solution space of disassembly line balancing problems and can improve economic performance by reducing idle time at workstations.

2.4 Disassembly Process and Structure

2.4.1 Product Structure Representation

Before a disassembly sequence can be planned, the structural relationships between components must be represented in a formal mathematical model. Three broad families have been developed: matrix-based models, graph-based models, and hybrid approaches (Laili et al., 2021).

Graph-based Representations

The most influential graph-based representation is the **AND/OR graph** introduced by Homem de Mello and Sanderson (1990) and adapted for disassembly. In an AND/OR graph, nodes represent product states (configurations of remaining components), AND-arcs represent operations that must be performed together (parallel steps), and OR-arcs represent alternative ways of achieving the same state. The AND/OR graph compactly encodes all feasible disassembly sequences and forms the basis for optimal sequence selection via dynamic programming, MILP, or heuristic search (Koc et al., 2009).

The **adjacency graph** focuses on binary contact or fastening relationships between pairs of components, represented as edges between component-nodes. The **disassembly constraint graph** (or precedence graph) represents ordering constraints directly as a directed acyclic graph, and is the most common input representation used in disassembly line balancing research (Laili et al., 2021).

Figure 2.1 illustrates the general structure of an AND/OR graph for a simple five-component product.

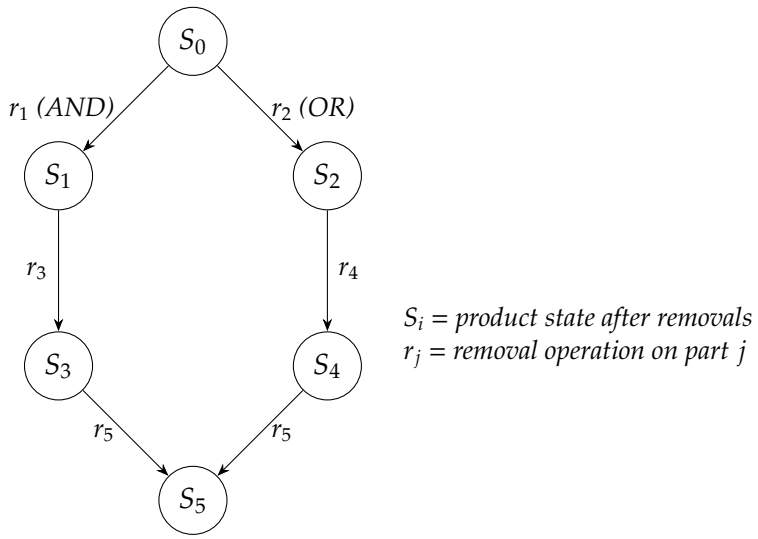

Figure 2.1: Schematic AND/OR graph for a five-component product. AND-arcs indicate parallel disassembly steps; OR-arcs represent alternative sequences leading to the same state (adapted from Homem de Mello and Sanderson 1990).

Matrix-based Representations

Huang and Huang (2002) introduce the **disassembly matrix**, in which entry (i, j) encodes the precedence relationship between component i and component j. A related formulation is the **Relationship Matrix** proposed by Yu and Li (2006), from which feasible assembly and disassembly sequences can be directly derived using a set of inference rules.

2.4.2 Disassembly Sequences

A disassembly sequence is an ordered list of operations specifying the part-removal order, the tool or method used for each removal, and—in parallel or robotic disassembly—the assignment of operations to agents or workstations (Laili et al., 2021). The quality of a sequence is evaluated against multiple criteria simultaneously, including total disassembly time, the number of tool changes, the number of changes in disassembly direction, energy consumption, and the economic profit realised from recovered components (Issaoui et al., 2016).

2.5 Disassembly Planning Problems

2.5.1 Sequence Planning

Disassembly sequence planning (DSP) is the problem of finding an optimal or near-optimal ordering of removal operations subject to the precedence constraints imposed by the product structure. DSP is NP-hard, meaning that exact methods cannot scale to large products within reasonable computational time (Gungor and Gupta, 1999; Tseng et al., 2008).

A practically important variant is *selective* DSP, in which the planner must simultaneously determine which components to target for recovery and in what order to remove them (Lambert, 1999). Selective DSP introduces a binary decision variable for each component (recover or not) and couples it with the sequencing variables, substantially expanding the solution space (Liu et al., 2023).

2.5.2 Line Design

When the volume of end-of-life products is sufficiently large, disassembly is performed on a *disassembly line*. The **Disassembly Line Balancing Problem** (DLBP) assigns tasks to workstations such that precedence constraints are respected, workload is distributed evenly, and the number of workstations or the cycle time is minimised (Gungor and Gupta, 2001).

Key distinctions in the DLBP literature include: (i) complete vs. partial (selective) variants (Unsal et al., 2024); (ii) straight, U-shaped, or two-sided line layouts (Wang et al., 2020); (iii) deterministic vs. stochastic task times (Bentaha et al., 2015); (iv) hybrid destructive/non-destructive modes (Deniz and Ozcelik, 2019; Wang et al., 2024); and (v) human–robot collaborative work cells (Hjorth and Chrysostomou, 2022).

2.5.3 Resource Allocation

Resource allocation encompasses decisions about the assignment of human workers, robotic systems, tools, and equipment to disassembly tasks and workstations. Tool selection is a particularly important dimension: different tools differ in speed, precision, applicability to different joint types, and cost (Ren et al., 2020). In robotic

disassembly systems, resource allocation extends to the assignment of motions, force constraints, and sensor feedback loops to individual operations. The integration of adaptive control strategies into the scheduling framework remains an active area of research (Hjorth and Chrysostomou, 2022; Trochu et al., 2025).

2.6 Solution Approaches

2.6.1 Exact Methods

Mixed-Integer Linear Programming

MILP is the most widely used exact method for disassembly planning problems (Guo et al., 2023). Binary variables encode the assignment of tasks to workstations, continuous variables represent cycle times or costs, and linear constraints capture precedence relations, workload balance requirements, and resource capacities. MILP models can typically be solved to optimality by commercial solvers for instances involving up to several tens of tasks. Koc et al. (2009) present two exact MILP formulations for the DLBP using AND/OR graph precedence structures.

Dynamic Programming

Dynamic programming (DP) decomposes the planning problem into a sequence of smaller sub-problems and combines solutions to obtain a globally optimal plan. DP is well-suited to problems with overlapping sub-problems and optimal sub-structure, properties exhibited by sequence planning problems defined over AND/OR graph representations (Homem de Mello and Sanderson, 1990). The principal limitation is the curse of dimensionality: the state space grows exponentially with the number of components, limiting applicability to small products.

2.6.2 Heuristics and Metaheuristics

Genetic Algorithms

Genetic Algorithms (GAs), inspired by the principles of natural selection, iteratively evolve a set of candidate solutions through selection, crossover, and mutation (Belhadj et al., 2022). In the disassembly context, a solution is encoded as a permutation of component removal operations; crossover and mutation operators are designed to respect precedence constraints.

Tseng et al. (2008) develop a GA for product DSP that demonstrates superior performance relative to earlier exact and heuristic methods on several benchmark products. Ren et al. (2018) develop a GA for asynchronous parallel disassembly planning, identifying significantly faster disassembly processes than synchronous parallel methods. Tian et al. (2020) apply a GA to the DSP of end-of-life electric vehicle batteries, combining the frame-subgroup structural representation with genetic search.

Ant Colony Optimisation

Ant Colony Optimisation (ACO) simulates the pheromone-trail communication behaviour of foraging ants. Issaoui et al. (2016) present an ACO-based approach for automated DSP from CAD models, incorporating criteria such as part volume, tool changes, and disassembly direction changes, comparing it favourably with GA in terms of solution quality and convergence speed.

Other Metaheuristics

A wide range of additional metaheuristics has been applied to disassembly planning. Simulated Annealing (SA) probabilistically accepts worse solutions to escape local optima. Particle Swarm Optimisation (PSO) models the collective motion of a swarm of solutions through the objective function landscape. Artificial Bee Colony (ABC) algorithms model the foraging behaviour of honey bees. The Water Cycle Algorithm (WCA) and the Flower Pollination Algorithm (FPA) have been applied to U-shaped and two-sided DLBP variants (Wang et al., 2020, 2024). Liu et al. (2023) propose a hybrid metaheuristic for selective DSP under uncertainty, representing uncertain task times as trapezoidal fuzzy numbers and using a multi-objective evolutionary algorithm to generate a Pareto-optimal front balancing profit, time, and environmental impact.

Expert Systems and Petri Nets

Prior to the widespread adoption of metaheuristics, rule-based expert systems and Petri net models were used to encode engineering knowledge about disassembly sequences and to simulate disassembly processes (Gungor and Gupta, 1999). Petri nets remain useful as verification tools and for modelling robotic disassembly control logic.

2.6.3 Simulation Approaches

Simulation-based approaches are particularly important for problems involving stochastic elements or complex interactions among workers, robots, and workstations. Discrete-Event Simulation (DES) models the disassembly process as a sequence of events occurring over time and can estimate system performance under realistic conditions. DES is commonly used to validate analytical models and explore the sensitivity of performance to key parameters (Foulloy et al., 2025).

Agent-based simulation (ABS) models individual workers or robots as autonomous agents whose behaviour emerges from local decision rules. ABS has been applied to model human–robot collaborative disassembly work cells (Hjorth and Chrysostomou, 2022). Digital twin technology represents the frontier of simulation-based approaches, enabling continuous monitoring, predictive maintenance, and dynamic re-planning of disassembly operations (Trochu et al., 2025).

2.7 Pricing of Recovered Components

The economic viability of a reverse logistics system depends not only on the efficiency of disassembly and the yield of recovered components, but also on the prices at which those components can be sold. Pricing of recovered parts and remanufactured goods is therefore a critical dimension of reverse logistics management, yet one that has received comparatively less theoretical attention in the engineering literature than in economics and marketing. This section reviews general pricing strategies, explains the rationale for dynamic pricing, and analyses how market demand shapes the pricing outcomes of recovered components.

2.7.1 General Pricing Strategies

Kotler and Armstrong (2016) identify three broad orientations that underpin all specific pricing strategies in commercial settings:

- **Cost-plus (cost-oriented) pricing**: The firm determines the total cost of recovering, disassembling, testing, and reconditioning a component and adds a fixed percentage mark-up to arrive at the selling price. This approach is straightforward and guarantees cost coverage, but it ignores demand-side information and may result in prices that are either too high (suppressing demand) or too low (forgoing obtainable revenue).
- **Value-based (customer-oriented) pricing**: The price is set based on the perceived value delivered to the buyer—typically relative to the price of an equivalent new component—rather than on the cost of recovery. For remanufactured parts, this perceived value depends on quality guarantees, warranty terms, and brand reputation (Guide et al., 2003). Atasu et al. (2009) demonstrate that remanufactured goods can often sustain prices of 50–80 per cent of new-part prices when accompanied by appropriate quality assurance.
- **Competition-based (market-oriented) pricing**: The firm sets prices primarily in response to competitor prices, whether from other remanufacturers, new-part suppliers, or grey-market importers. This orientation is common in markets where recovered components are readily substitutable and price transparency is high.

In the context of recovered components, a hybrid approach that combines cost-plus logic (to ensure financial sustainability of the recovery operation) with value-based and competitive adjustments (to capture available consumer surplus) is generally recommended in the literature (Guide et al., 2003).

2.7.2 Dynamic Pricing: Definition and Mechanism

Dynamic pricing—also referred to as demand-based pricing, variable pricing, or surge pricing—is a revenue management strategy in which the seller continuously adjusts the price of a product in response to real-time changes in market conditions,

most notably demand intensity, inventory levels, and competitive behaviour (Gallego and Van Ryzin, 1994). Unlike static pricing, which fixes a single price for an extended period, dynamic pricing treats the price itself as a decision variable that can be optimised jointly with inventory and capacity decisions over time.

The theoretical foundations of dynamic pricing in operations research were established by Gallego and Van Ryzin (1994), who formulated the problem of a seller with a fixed inventory facing a Poisson arrival stream of price-sensitive customers and derived the structure of the optimal dynamic pricing policy as a function of remaining inventory and time to the sales deadline. The key insight was that the optimal price is a monotone decreasing function of remaining inventory: as stock diminishes, the seller should increase prices to ration access to the remaining units among the highest-valuing customers.

In the context of recovered parts and remanufacturing, dynamic pricing is motivated by two features that are particularly pronounced in reverse logistics settings:

1. **Supply uncertainty**: The quantity and quality of components that will become available from a given batch of end-of-life products are uncertain until disassembly and inspection are complete. Dynamic pricing allows the seller to adjust prices upward when a scarce high-demand part is found to be available in limited quantities, and downward when an over-supply materialises.
2. **Demand heterogeneity**: Buyers of recovered components range from professional repair shops (who are relatively price-sensitive but purchase in volume) to individual consumers performing one-off repairs (who may be less price-sensitive but require instant availability). Dynamic pricing can exploit this heterogeneity by offering lower prices in advance (to attract volume buyers who plan ahead) and higher prices for last-minute or urgent purchases (Gallego and Van Ryzin, 1994).

2.7.3 Benefits of Dynamic Pricing

The academic and practitioner literature identifies several categories of benefit associated with dynamic pricing relative to static pricing.

Revenue Maximisation

Gallego and Van Ryzin (1994) prove that an optimally chosen dynamic pricing policy always achieves at least as high an expected revenue as the best static price, and in most practical scenarios achieves strictly higher revenue. The intuition is straightforward: a static price can be optimal only for the particular demand realisation it was designed for; as actual demand deviates from the forecast—which it invariably does—the static price becomes suboptimal. Dynamic pricing eliminates this rigidity. Empirical studies in airline revenue management, hotel pricing, and retail markdown optimisation confirm revenue improvements of 3 to 8 per cent rel-

ative to naive static pricing rules, with higher gains in settings with greater demand volatility (Gallego and Van Ryzin, 1994).

Inventory Efficiency

By raising prices when demand is high relative to available supply, dynamic pricing prevents premature stockout of high-value components. Conversely, by lowering prices when demand is soft, it accelerates the liquidation of slow-moving inventory, reducing holding costs and the risk of obsolescence. In the remanufacturing context, where recovered parts may have a limited shelf life before technological obsolescence renders them unmarketable, timely liquidation through price reduction can be critical to overall system profitability (Guide et al., 2003).

Demand Smoothing

Dynamic pricing serves as a mechanism for transferring demand from peak periods to off-peak periods. By charging higher prices during periods of peak demand—for example, immediately after a product recall creates a sudden surge in demand for replacement parts—the seller can incentivise less urgent buyers to defer their purchases, thereby flattening the demand curve and reducing the operational strain on the disassembly and reconditioning system. This demand-smoothing function reduces the required capacity of the recovery facility and lowers overall system costs (Gallego and Van Ryzin, 1994).

Signal of Quality

In markets for recovered components, buyers face significant uncertainty about product quality—a classic problem of information asymmetry first formalised by Akerlof (1970). A higher price can serve as a credible signal of quality when the seller has invested in rigorous testing and quality assurance, helping to differentiate genuine high-quality remanufactured parts from low-quality imitations.

2.7.4 How Demand Affects Pricing

The Law of Demand and the Demand Curve

The foundational relationship between price and quantity demanded is captured in the **law of demand**, formulated by Marshall (1890): all else equal, the quantity of a good demanded by the market decreases as its price increases and increases as its price decreases. This inverse relationship is typically represented graphically as a downward-sloping demand curve in price–quantity space, illustrated in Figure 2.2.

The demand curve for recovered components is shaped by factors including: the price of equivalent new parts (the key substitute), the age distribution of the installed base (which determines the size of the potential buyer population), consumer atti-

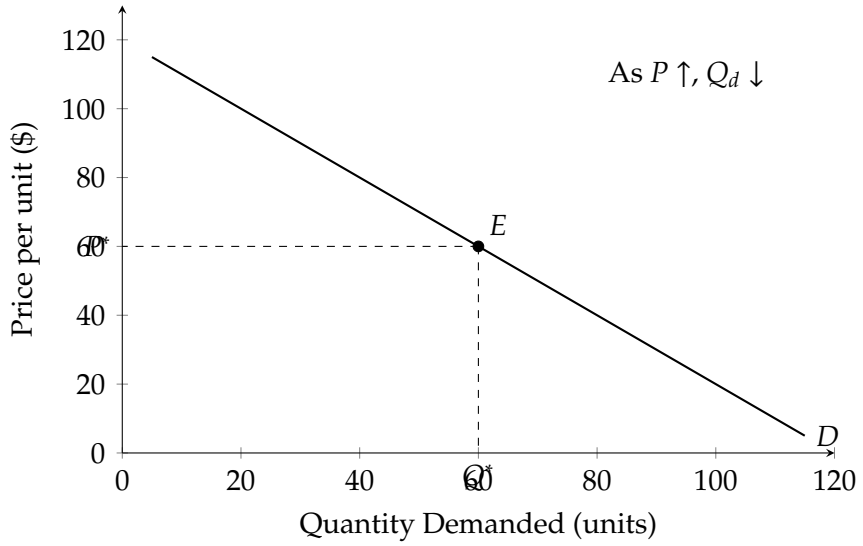

Figure 2.2: A standard downward-sloping market demand curve for a recovered component. At equilibrium price P^* the quantity demanded equals Q^*. A price increase above P^* reduces quantity demanded; a price decrease below P^* raises it (after Marshall 1890).

tudes toward remanufactured goods, and the availability of warranty and quality assurance mechanisms (Atasu et al., 2009; Guide et al., 2003).

Demand Shifts and Their Pricing Implications

Demand is not static; it shifts in response to changes in external conditions. An **outward demand shift** (increase in demand at every price level) is typically driven by growth in the installed base of the parent product, a rise in the price of new substitute parts, or an improvement in consumer awareness of and confidence in remanufactured quality. An outward shift raises both the equilibrium price and the equilibrium quantity, as illustrated in Figure 2.3.

Price Elasticity of Demand

Not all markets respond to price changes with the same sensitivity. The concept of **price elasticity of demand** (PED), introduced formally by Marshall (1890), quantifies this sensitivity:

$$\varepsilon = \frac{\partial Q / Q}{\partial P / P} = \frac{\partial Q}{\partial P} \cdot \frac{P}{Q} \tag{2.1}$$

where Q is quantity demanded, P is price, and $\varepsilon < 0$ by the law of demand. When $|\varepsilon| > 1$, demand is *elastic*: a percentage increase in price produces a larger percentage decrease in quantity demanded, so total revenue falls. When $|\varepsilon| < 1$, demand is *inelastic*: quantity demanded is relatively insensitive to price changes, and total revenue rises when price increases. When $|\varepsilon| = 1$, demand is *unit-elastic* and total revenue is unchanged by a small price change.

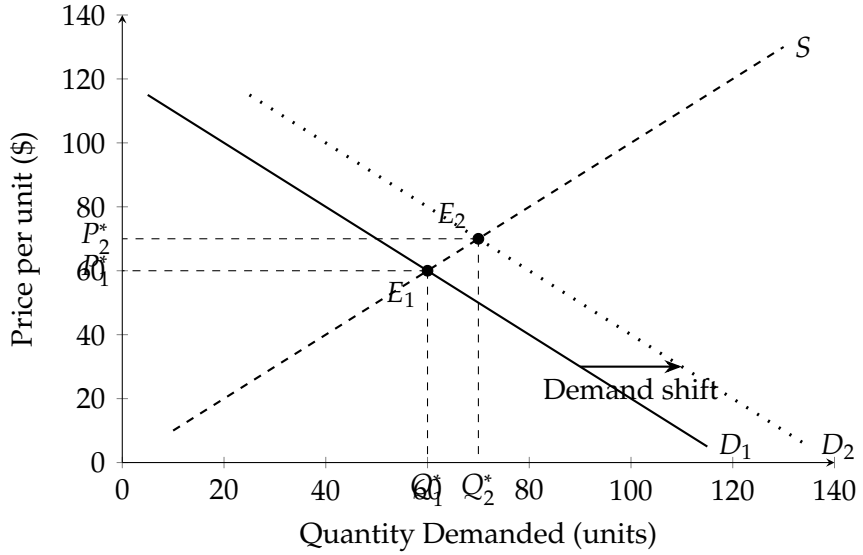

Figure 2.3: An outward shift in demand from D_1 to D_2 raises both the equilibrium price ($P_1^* \rightarrow P_2^*$) and equilibrium quantity ($Q_1^* \rightarrow Q_2^*$). For a reverse logistics operator holding a fixed stock of recovered parts, this shift justifies a price increase and signals an opportunity to expand disassembly capacity.

Figure 2.4 illustrates the contrast between elastic and inelastic demand curves in price–quantity space.

For recovered components, price elasticity depends on the availability of substitutes (new or alternative used parts), the share of the recovered part cost in the total repair bill (the *importance effect*: a small-value part in a major repair tends to exhibit inelastic demand), and the urgency of the repair. Empirical evidence from the automotive aftermarket, one of the largest markets for remanufactured parts, suggests that price elasticities for common engine and drivetrain components lie in the range -1.2 to -2.0, indicating moderately elastic demand (Guide et al., 2003).

Dynamic Pricing Over Time and Inventory Depletion

Figure 2.5 illustrates the typical pattern of optimal dynamic prices over a finite selling horizon for a fixed stock of recovered components. When inventory is abundant relative to remaining demand, prices are set low to stimulate purchases. As inventory depletes or as the end-of-season deadline approaches, prices are raised to ration the remaining units among the highest-valuing customers—a policy known as dynamic mark-up (Gallego and Van Ryzin, 1994).

Implications for Reverse Logistics System Design

The integration of dynamic pricing into a reverse logistics framework has several systemic implications. First, the pricing policy must be co-ordinated with the disassembly and inventory scheduling system: a decision to raise prices for a particular recovered part should signal to the disassembly planner that more effort should be

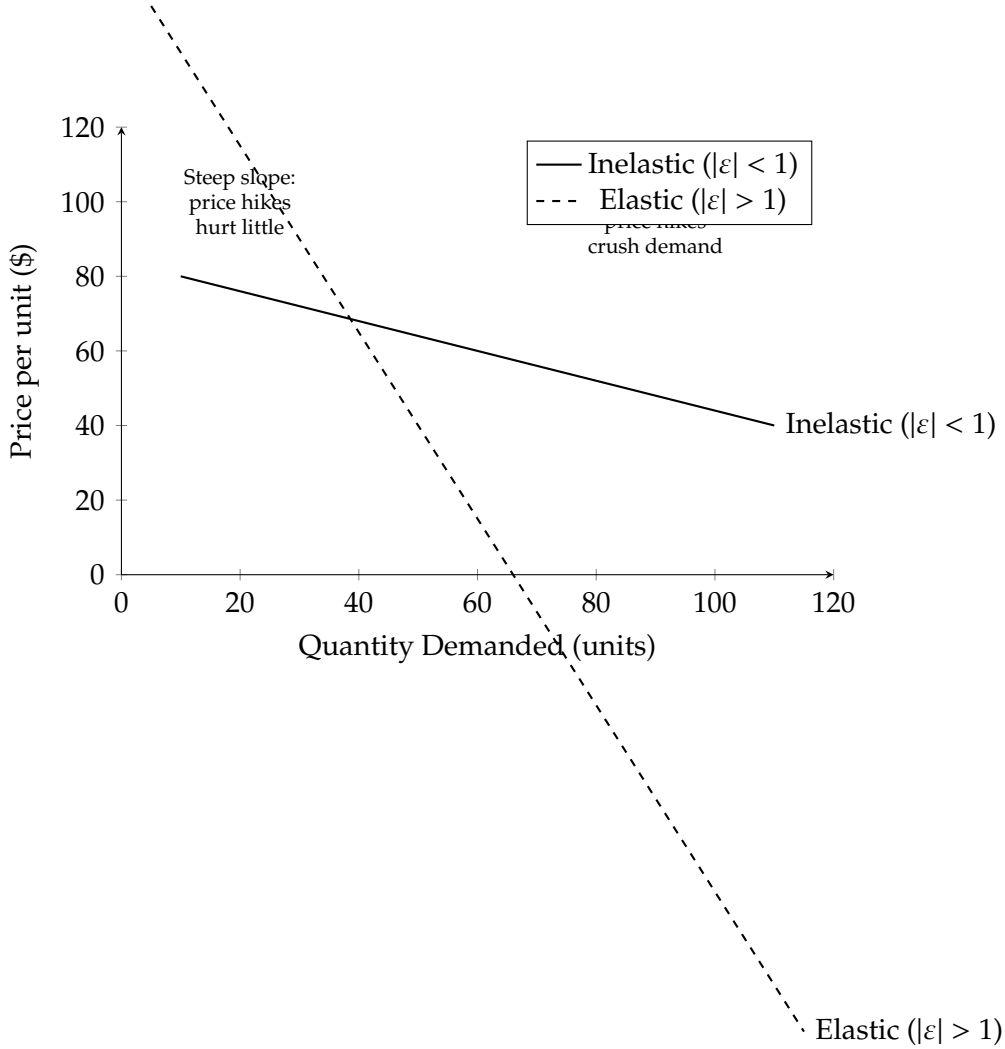

Figure 2.4: Elastic versus inelastic demand curves. The steep curve represents inelastic demand (common for scarce or specialised recovered components with no close substitutes); the flatter curve represents elastic demand (common for standard parts available from multiple suppliers). Firms should raise prices when facing inelastic demand and lower prices when demand is elastic to maximise total revenue (after Marshall 1890).

allocated to recovering that part from incoming end-of-life products, and vice versa (Guide, 2000). Second, the forecasting of demand—which is an input to the dynamic pricing algorithm—requires data integration across the forward supply chain (to estimate the size and age distribution of the installed base) and the reverse logistics system (to estimate the yield of recovered components from incoming products). Third, the use of dynamic pricing may affect consumer behaviour in ways that feedback into the reverse logistics system: if buyers of recovered components learn that prices will fall in later periods, they may strategically defer purchases, increasing the holding costs and obsolescence risk for the seller (Gallego and Van Ryzin, 1994).

Table 2.1 summarises the three main pricing strategies and their suitability in the recovered-component market context.

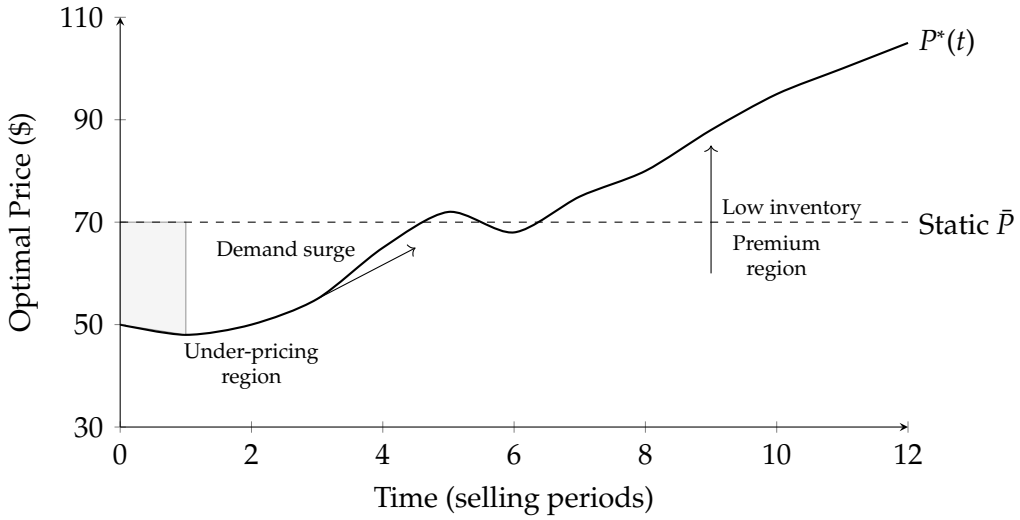

Figure 2.5: Optimal dynamic price path $P^*(t)$ over a twelve-period selling horizon for a fixed stock of recovered components, compared with a static reference price $\bar{P}$. The dynamic policy undersells early (capturing volume) and charges a premium as inventory depletes, yielding strictly higher expected revenue than the static price in all scenarios except the trivial case of perfectly flat demand (after Gallego and Van Ryzin 1994).

Table 2.1: Comparison of pricing strategies for recovered components (synthesised from Guide et al. 2003, Kotler and Armstrong 2016, and Gallego and Van Ryzin 1994)

Strategy	Mechanism	Advantages	Limitations
Cost-plus	Fixed mark-up over recovery cost	Simple; guarantees cost coverage	Ignores demand; may over- or under-price
Value-based	Price anchored to perceived value vs. new part	Captures consumer surplus; rewards quality investment	Requires willingness-to-pay data; complex to implement
Dynamic (demand-based)	Real-time price adjustment to demand, inventory, and competition	Maximises revenue; smooths demand; optimises inventory turn	Requires data infrastructure; may trigger consumer backlash

Conclusions

This thesis has reviewed the interrelated fields of reverse logistics, disassembly planning, and pricing dynamics for recovered components, tracing their development from early definitional work in the 1990s through to sophisticated multi-objective, stochastic, and digitally-enabled models of the present day. Several cross-cutting themes and open challenges deserve emphasis.

Uncertainty. Uncertainty pervades both domains. In reverse logistics, the timing, quantity, and quality of returns are uncertain; in disassembly, task times, joint conditions, and the economic value of recovered components all exhibit significant variability. The development of robust and distributionally robust formulations remains an active frontier (Liu et al., 2023).

Human–robot collaboration. The integration of robots into disassembly operations offers potential for dramatic throughput increases, but poses significant planning and control challenges. Human factors—fatigue, skill variation, ergonomic risk—must be incorporated into planning models alongside purely economic and technical criteria (Hjorth and Chrysostomou, 2022).

Dynamic pricing integration. While dynamic pricing theory is well-developed in the revenue management literature, its integration with the operational planning of disassembly systems—so that pricing signals drive disassembly priorities and vice versa—remains largely unexplored. Joint optimisation of disassembly scheduling and dynamic pricing represents a significant research opportunity (Gallego and Van Ryzin, 1994; Guide, 2000).

Digital technologies. Trochu et al. (2025) identify the integration of digital technologies as the most rapidly growing theme in contemporary reverse logistics research. IoT-enabled product condition monitoring, AI-driven demand forecasting for dynamic pricing, and digital twins for disassembly line management represent particularly promising directions.

Circular economy integration. Reverse logistics and disassembly planning have traditionally been treated as end-of-life activities. The circular economy perspective calls for their integration into the product design phase and into forward supply

chain planning, with pricing policies that reflect the true life-cycle cost of components and incentivise their return and recovery.

In summary, the fields reviewed in this thesis have matured considerably over the past three decades, developing from largely qualitative frameworks to sophisticated quantitative models. The challenges that remain are correspondingly more complex, requiring interdisciplinary approaches that combine operations research, artificial intelligence, robotics, product design, environmental science, and pricing analytics to deliver the resource-efficient, high-value recovery systems that the circular economy demands.

Chapter 3

Mathematical Formulation

3.1 Introduction

3.1.1 Motivation and Context

The accelerating adoption of circular economy principles across manufacturing, electronics, automotive, and consumer goods sectors has generated substantial demand for quantitative decision-support tools that can plan the recovery, decomposition, reconditioning, and resale of end-of-life (EOL) products (Guide et al., 2003; Thierry et al., 1995). Mathematical programming models for EOL product management have, to date, largely been developed in a domain-specific manner: a model designed for battery pack disassembly encodes the battery bill of materials (BOM) directly into its constraint structure, making the model non-transferable to, for example, printed circuit board recycling, power tool refurbishment, or automotive transmission remanufacturing. This specificity imposes a significant cost on the research community: each new application domain requires a near-complete model redesign, even when the underlying operational logic is structurally identical.

The present work addresses this gap by performing a rigorous *structural abstraction* of a domain-specific EOL battery disassembly planning model, lifting it into a generalized *product-agnostic* framework. The key insight is that any multi-level product decomposition process, regardless of the specific materials or components involved, can be represented as a finite directed acyclic graph in which each arc carries a integer recovery yield and a fixed assembly consumption ratio. This observation, combined with abstract node classification into decomposable, remanufacturable, and leaf-only classes, yields a single set of constraints and a single objective function that applies to any such system.

3.1.2 Circular Economy Relevance

From the perspective of circular economy strategy, the three primary value-recovery pathways for EOL products are:

(i) **Direct resale** of recovered subassemblies and components in the forward secondary market;

(ii) **Reconditioning** (repair, remanufacturing, or refurbishment) of intermediate subassemblies for resale in the certified secondary market; and

(iii) **Material recovery** of constituent recoverable materials (metals, polymers, rare earths, chemicals) for commodity re-entry.

The framework developed here explicitly models all three pathways simultaneously, accounting for their interactions through inventory pools, common capacity constraints, and dual-channel demand-driven pricing.

3.1.3 Generality and Transferability

The generalized framework introduced here achieves transferability through four design principles:

P1. Graph abstraction. The product BOM is represented as an abstract directed acyclic graph (DAG) with a pure AND-arc structure, parameterized only by node class assignments and arc weight vectors. No product-specific constraint is hardcoded.

P2. Node classification. Nodes are classified into four abstract roles—root, decomposable intermediate, remanufacturable intermediate, and leaf—using three set memberships. This classification drives the inventory balance structure without reference to physical identity.

P3. Demand abstraction. Demand is parameterized through sensitivity coefficients and isoelastic price-elasticity parameters, both estimable from market data for any product category.

P4. Parametric pricing. The dual-channel isoelastic pricing mechanism normalizes prices to market-defined bounds without encoding product-specific price levels into the model constraints.

3.1.4 Scope and Applicability

Applicable Product Systems The generalized framework can be instantiated for, among others:

- **Energy storage systems:** battery packs (Li-ion, NiMH, lead-acid), fuel cells, supercapacitors
- **Consumer electronics:** smartphones, laptops, tablets, household appliances
- **Automotive:** vehicles (level-0), powertrains, engines, transmissions, electronic control units
- **Machinery and equipment:** industrial robots, CNC machines, turbines, compressors
- **Medical devices:** imaging systems, surgical instruments, diagnostic equip-

ment

- **Aerospace:** avionics, actuators, landing gear subassemblies
- **Modular consumer products:** power tools, bicycles, office furniture, modular electronics

In each case, the user supplies: (i) the PDG topology, (ii) the node class assignments, (iii) the arc parameters, and (iv) the demand and pricing parameters. All constraint equations and the objective function remain unchanged.

3.1.5 Structure of the Document

Section 3.2 introduces the generalized Product Decomposition Graph and its node classification taxonomy. Section 4.16 states the modelling assumptions. Section 3.4 develops the complete mathematical formulation. Section 3.5 provides a systematic analysis of the abstractions introduced and their industrial interpretations. Section 3.6 illustrates instantiation for three distinct product families. Section 3.8 concludes.

3.2 Generalized Product Decomposition Framework

3.2.1 The Product Decomposition Graph

Definition 1 (Product Decomposition Graph)**.** *A **Product Decomposition Graph** (PDG) is a finite, directed, acyclic graph $G = (V, R)$ where:*

- *$V = \{v_0, v_1, \ldots, v_n\}$ is the set of $n+1$ nodes, each representing a distinct product entity (complete product, subassembly, component, or recoverable material);*
- *R is the set of directed decomposition arcs, where (i, j) denotes that decomposing one unit of node i (the parent) yields a quantity of node j (the child);*
- *the graph is a pure AND-arc hierarchy: decomposing one unit of any node i_D simultaneously yields recoverable quantities of* all *children $j \in (i)$;*
- *v_0 is the unique root node, representing the complete EOL product unit arriving at the facility.*

Definition 2 (Hierarchy Level)**.** *The **hierarchy level** of node i, denoted (i), is the length of the unique path from v_0 to i in G. The level partition is:*

$$V_\ell = \{i : (i) = \ell\}, \qquad \ell = \{0, 1, \ldots, L\}, \tag{3.1}$$

where L is the maximum depth of the PDG. The root satisfies $V_0 = \{v_0\}$. For any non-root node $i \setminus \{v_0\}$, let (i) denote the unique parent of i under the AND-arc hierarchy.

3.2.2 Node Classification Taxonomy

All operational logic in the model is driven by four mutually exhaustive, partially overlapping node classes:

Definition 3 (Node Classes)**.** *Given a PDG $G = (V, R)$:*

$V_D \subseteq V$	*Decomposable nodes: have at least one outgoing arc in R*
$V_R = V \setminus \{v_0\}$	*Recoverable nodes: all nodes except the root*
$V_M \subseteq V_{RD}$	*Remanufacturable intermediates: can be reconditioned and resold in the secondary market*
$V_L = V_{RM}$	*Leaf recoverable nodes: sold in the forward market only; not reconditioned; may or may not be further decomposed*

Structural role of V_M versus V_L. The partition $V_R = V_{ML}$ (disjoint) is the single structural decision that determines which of the two inventory balance constraint classes applies to each recoverable node. A node i belongs to V_M if and only if it is commercially viable to recondition it into a certified unit for the secondary market. This is an operational and economic decision, not an intrinsic physical property: the same component may be classified as V_M in one deployment context (when reconditioning is profitable) and as V_L in another (when the reconditioning cost exceeds the secondary market price).

3.2.3 Generic PDG Diagram

Figure 3.1 illustrates the abstract structure of a four-level PDG with two remanufacturable intermediate nodes and seven leaf nodes, matching the Nissan Leaf battery instantiation from which this framework is derived. The diagram uses generic identifiers; any physical product can be substituted by reassigning node labels and arc parameters.

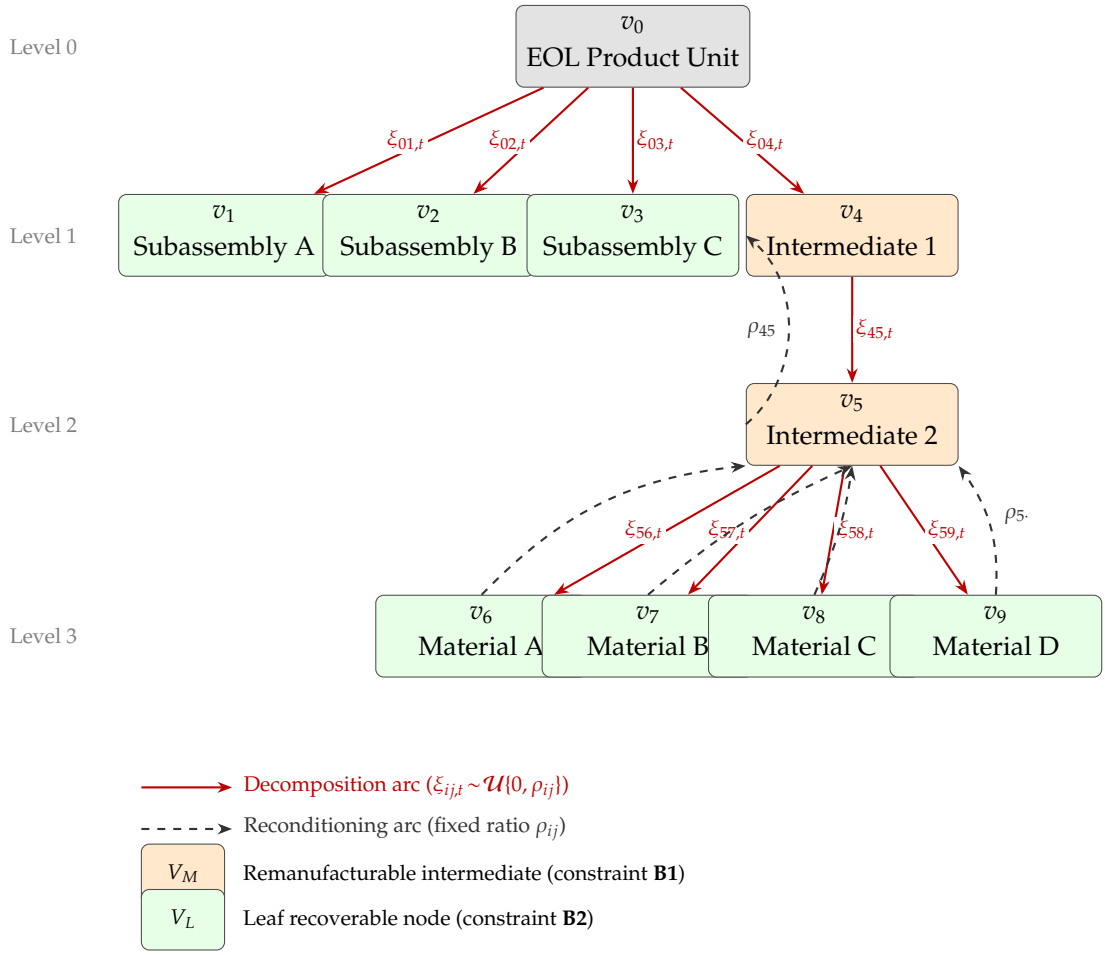

Figure 3.1: Generic four-level Product Decomposition Graph (PDG) with $|V| = 10$ nodes, 9 decomposition arcs, and 5 reconditioning arcs. Orange nodes (V_M): remanufacturable intermediates, governed by constraint **(B1)**. Green nodes (V_L): leaf recoverable nodes, governed by constraint **(B2)**. This topology is instantiated for the Nissan Leaf 24 kWh battery pack in Section 3.6.1.

3.3 Modelling Assumptions

The following assumptions define the operational context of the generalized framework. They are stated in abstract terms; their domain-specific interpretations vary by application.

Assumption 1. *Pure AND Decomposition : The PDG $G = (V, R)$ is a pure AND-arc hierarchy. Initiating the decomposition of one unit of any node i_D simultaneously triggers a recovery of* every *child $j \in (i)$. No OR-arc structure (selective routing) or Big-M linking constraint is required.*

Assumption 2. *Integer Recovery Yield : The number of child-j units recovered per parent-i unit decomposed in period t is a non-negative integer drawn from a discrete uniform distribution on $\{0, 1, \ldots, \rho_{ij}\}$. Yields are independent across arcs, periods, and units processed. Once realized, the yield is fixed for the entire duration of period t.*

Assumption 3. *Uncertainty Resolution : All quantities (yields and demands) are drawn and known to our model at the beginning of each period and thereafter treated as deterministic coefficients within that period's MILP.*

Assumption 4. *Dual-Pool Inventory Architecture : For each recoverable node i_R, There are two inventory pool one for via direct decomposition and the other for reconditioning. Holding costs and inventory capacity limits apply uniformly to the two stocks.*

Assumption 5. *Configurable Lead Times : Decomposition and reconditioning operations are subject to integer lead times $L_i^{\text{dec}} \geq 0$ and $L_k^{\text{rec}} \geq 0$, respectively. Child inventory from decomposing i in period t arrives in period $t + L_i^{\text{dec}}$. A unit reconditioned in period t consumes child components in period t and becomes available in period $t + L_k^{\text{rec}}$.*

Assumption 6. *Dual-Channel Market Independence : The forward market (direct resale of recovered nodes) and the secondary market (resale of reconditioned intermediates) are independent demand pools. Sales to one channel do not substitute for sales to the other.*

Assumption 7. *Isoelastic Demand Structure : Market demand in each channel follows an isoelastic (constant price-elasticity) function: $D = \alpha\gamma P^{-\beta}$, with $\beta > 1$ required for the existence of a finite profit-maximizing price. Parameters α, β, and γ are estimated independently for each node–channel pair from historical price–quantity data.*

Assumption 8. *No Binary Variables : The PDG is a pure AND hierarchy (Assumption 1), which eliminates the need for binary arc-selector variables. All decision variables are non-negative integers.*

3.4 Mathematical Formulation

3.4.1 Sets and Indices

3.4.2 Parameters

Table 3.2: Model parameters for the generalized framework.

Symbol	Domain	Definition
Product supply		
A_t	$\mathbb{Z}_{\geq 0}$	Number of EOL product units arriving at the facility in period t
recovery yield (decomposition arcs)		
ρ_{ij}	$\mathbb{Z}^+$	**Nominal maximum yield** on arc (i, j), equal to the reconditioning consumption ratio: the number of child-j units required to recondition one unit of the nearest remanufacturable ancestor of j in V_M

continued...

Symbol	Domain	Definition
$\xi_{ij,t}$	$\mathcal{U}\{0,\ldots,\rho_{ij}\}$	integer recovery yield on arc (i,j) in period t; realized at the start of period t and fixed as a MILP coefficient (Assumption 2)
$\bar{\xi}_{ij}$	$\mathbb{R}_{>0}$	Expected recovery yield: $\bar{\xi}_{ij} = \rho_{ij}/2$
Lead times		
L_i^{dec}	$\mathbb{Z}_{\geq 0}$	Decomposition lead time for node i_D; child inventory from decomposing i in period t arrives in period $t + L_i^{\text{dec}}$
L_k^{rec}	$\mathbb{Z}_{\geq 0}$	Reconditioning lead time for intermediate k_M; a unit reconditioned in period t becomes available in $t + L_k^{\text{rec}}$; child components consumed in period t
Forward-channel demand		
δ_i^{f}	$\mathbb{R}_{\geq 0}$	Demand-sensitivity coefficient for forward sales of i_R; $\delta_{\min} \leq \delta_i^{\text{f}} \leq \delta_{\max}$
σ_i	$[0,1]$	Normalized sensitivity: $\sigma_i = (\delta_i^{\text{f}} - \delta_{\min})/(\delta_{\max} - \delta_{\min})$
$d_i^{\min}, d_i^{\max}$	$\mathbb{R}_{\geq 0}$	Forward demand range bounds: $d_i^{\min} = a + \sigma_i b$, $d_i^{\max} = c + \sigma_i d$; constants $a,b,c,d \geq 0$
D_{it}^{f}	$\mathcal{U}[\lceil d_i^{\min} \rceil, \lfloor d_i^{\max} \rfloor]$	Forward-channel demand for i_R in period t; drawn once per period
Secondary-channel demand		
$d_k^{\text{s,min}}, d_k^{\text{s,max}}$	$\mathbb{R}_{\geq 0}$	Secondary-market demand range bounds for k_M; set from secondary-market observations
D_{kt}^{s}	$\mathcal{U}[\lceil d_k^{\text{s,min}} \rceil, \lfloor d_k^{\text{s,max}} \rfloor]$	Secondary-market demand for reconditioned k_M in period t; drawn once per period
Pricing — forward channel		
$P_{it}^{\max,\text{f}}$	$\mathbb{R}_{\geq 0}$	Forward market price ceiling for i_R in period t; upper bound on $P_{it}^{\text{f}} \in [0, P_{it}^{\max,\text{f}}]$
α_i^{f}	$\mathbb{R}_{>0}$	Isoelastic base demand (market scale) for forward channel of i; estimated via log-log regression
β_i^{f}	$\mathbb{R}_{>1}$	Price elasticity of forward demand ($\beta_i^{\text{f}} > 1$ required for finite profit-maximizing price to exist)
γ_i^{f}	$\mathbb{R}_{\geq 0}$	Demand-sensitivity scaling used in forward isoelastic pricing
Pricing — secondary/remanufactured channel		
$P_{kt}^{\max,\text{s}}$	$\mathbb{R}_{\geq 0}$	Secondary market price ceiling for reconditioned k_M in period t; upper bound on $P_{kt}^{\text{s}} \in [0, P_{kt}^{\max,\text{s}}]$
α_k^{s}	$\mathbb{R}_{>0}$	Isoelastic base demand for secondary channel of k
β_k^{s}	$\mathbb{R}_{>1}$	Price elasticity of secondary-market demand

continued...

Symbol	Domain	Definition
γ_k^{s}	$\mathbb{R}_{\geq 0}$	Demand-sensitivity scaling used in secondary isoelastic pricing
Operational costs		
c_i^{dec}	$\mathbb{R}_{\geq 0}$	Unit decomposition cost at node i_D (labour, tooling, energy per unit processed)
c_k^{rec}	$\mathbb{R}_{\geq 0}$	Unit reconditioning cost for k_M
h_i	$\mathbb{R}_{\geq 0}$	Holding cost per unit of i per period
Capacity and inventory		
Q_i^{dec}	$\mathbb{Z}^+$	Maximum units of i_D decomposed per period
Q_k^{rec}	$\mathbb{Z}^+$	Maximum units of k_M reconditioned per period
Cap_i	$\mathbb{Z}^+$	Maximum end-of-period inventory of i
$w_{i,t}$	$\mathbb{R}_{\geq 0}$	Disposal units of i

3.4.3 Recovery Yield

Physical decomposition of aged or end-of-life products is imperfect: corrosion, thermal degradation, mechanical stress, contamination, or operational wear can render individual components or materials unrecoverable. The recovery yield on each AND arc is modelled as a uniform integer (Assumption 2):

$$\boxed{\xi_{ij,t} \sim \mathcal{U}\{0, 1, \ldots, \rho_{ij}\}, \qquad \xi_{ij,t} \in \mathbb{Z}_{\geq 0}, \qquad \forall\,(i, j, t)} \tag{3.2}$$

The parameter ρ_{ij} serves a dual role:

(i) **Maximum recovery yield:** the theoretical maximum number of child-j units recoverable per parent-i unit decomposed, achieved only in ideal-condition processing.

(ii) **Reconditioning consumption ratio:** the number of child-j units required to recondition one unit of the nearest remanufacturable ancestor k_M of j.

Setting ρ_{ij} equal to the reconditioning consumption ratio ensures that at peak decomposition output the recovered quantities exactly match reconditioning demand, providing a natural supply-demand balance at the component level. The expected yield is $\bar{\xi}_{ij} = \rho_{ij}/2$.

3.4.4 Dual-Channel Demand Models

Two independent demand streams are drawn at the start of each period and fixed as MILP coefficients (Assumption 3).

Table 3.1: Sets and index notation for the generalized framework.

Symbol	Definition
$T = \{1, \ldots, T\}$	Discrete planning periods
$V = \{v_0, v_1, \ldots, v_n\}$	Node set of the PDG; $\lvert V\rvert = n + 1$
$L = \{0, 1, \ldots, L\}$	Set of hierarchy levels; L = maximum PDG depth
V_ℓ (ℓ)	Nodes at hierarchy level ℓ; see (3.1)
$V_D \subseteq V$	Decomposable nodes (have outgoing AND arcs in R)
$V_R = V \setminus \{v_0\}$	Recoverable nodes (all nodes except the EOL product root)
$V_M \subseteq V_{RD}$	Remanufacturable intermediate nodes (reconditioned and resold in secondary market)
$V_L = V_{RM}$	Leaf recoverable nodes (forward market only; not reconditioned)
$R \subseteq V$	Directed decomposition arc set of the PDG
(i)	Children of node i under decomposition: $(i) = \{j : (i, j)\}$
(i)	Unique parent of node $i \setminus \{v_0\}$ under the AND-arc hierarchy

Forward-Channel Demand D^{f}_{it}

Forward-channel demand for recoverable node i_R in period t is drawn from a discrete uniform distribution whose range scales with the product sensitivity coefficient δ^{f}_i:

$$\boxed{D^{\mathrm{f}}_{it} \sim \mathcal{U}\left[\lceil d^{\min}_i \rceil,\ \lfloor d^{\max}_i \rfloor\right],} \quad d^{\min}_i = a + \sigma_i b, \quad d^{\max}_i = c + \sigma_i d, \tag{3.3}$$

where $\sigma_i = (\delta^{\mathrm{f}}_i - \delta_{\min})/(\delta_{\max} - \delta_{\min}) \in [0, 1]$ is the normalized sensitivity and $a, b, c, d \geq 0$ are calibration constants. A higher δ^{f}_i reflects a product node with a broader, more active forward secondary market.

Secondary-Channel Demand D^{s}_{kt}

Demand for reconditioned intermediate k_M in the secondary market in period t is drawn independently:

$$\boxed{D^{\mathrm{s}}_{kt} \sim \mathcal{U}\left[\lceil d^{\mathrm{s},\min}_k \rceil,\ \lfloor d^{\mathrm{s},\max}_k \rfloor\right],} \qquad k_M,\ t. \tag{3.4}$$

The bounds $d^{\mathrm{s},\min}_k$ and $d^{\mathrm{s},\max}_k$ are set from secondary-market observations (e.g. certified-refurbished component markets, industrial spare-part exchanges).

3.4.5 Dual-Channel Normalized Isoelastic Pricing

Both selling channels employ the same three-step isoelastic pricing procedure. Prices are bounded in $[0, P^{\max}]$ by construction, with neither channel imposing a cost floor (Assumption 7).

Forward-Channel Price P^{f}_{it}

Step 1 — Demand-implied isoelastic price. The isoelastic demand model posits $D^{\mathrm{f}}_{it} = \alpha^{\mathrm{f}}_i \gamma^{\mathrm{f}}_i (P^{\mathrm{iso,f}}_{it})^{-\beta^{\mathrm{f}}_i}$. Inverting:

$$P^{\mathrm{iso,f}}_{it} = \left(\frac{D^{\mathrm{f}}_{it}}{\alpha^{\mathrm{f}}_i \gamma^{\mathrm{f}}_i} \right)^{-1/\beta^{\mathrm{f}}_i}, \qquad i_R,\ t. \tag{3.5}$$

The range of $P^{\mathrm{iso,f}}_{it}$ over the demand support $[d^{\min}_i, d^{\max}_i]$ is:

$$P^{\mathrm{iso,f,max}}_i = \left(\frac{d^{\min}_i}{\alpha^{\mathrm{f}}_i \gamma^{\mathrm{f}}_i} \right)^{-1/\beta^{\mathrm{f}}_i}, \qquad P^{\mathrm{iso,f,min}}_i = \left(\frac{d^{\max}_i}{\alpha^{\mathrm{f}}_i \gamma^{\mathrm{f}}_i} \right)^{-1/\beta^{\mathrm{f}}_i}. \tag{3.6}$$

Step 2 — Normalization.

$$\hat{P}^{\mathrm{iso,f}}_{it} = \frac{P^{\mathrm{iso,f}}_{it} - P^{\mathrm{iso,f,min}}_i}{P^{\mathrm{iso,f,max}}_i - P^{\mathrm{iso,f,min}}_i} \in [0,1]. \tag{3.7}$$

Step 3 — Forward selling price.

$$\boxed{P^{\mathrm{f}}_{it} = P^{\mathrm{max,f}}_{it}\ \hat{P}^{\mathrm{iso,f}}_{it} \in \left[0,\ P^{\mathrm{max,f}}_{it}\right]}, \qquad i_R,\ t. \tag{3.8}$$

Secondary-Channel Price P^{s}_{kt}

Step 1 — Demand-implied isoelastic price.

$$P^{\mathrm{iso,s}}_{kt} = \left(\frac{D^{\mathrm{s}}_{kt}}{\alpha^{\mathrm{s}}_k \gamma^{\mathrm{s}}_k} \right)^{-1/\beta^{\mathrm{s}}_k}, \qquad k_M,\ t. \tag{3.9}$$

With range:

$$P^{\mathrm{iso,s,max}}_k = \left(\frac{d^{\mathrm{s,min}}_k}{\alpha^{\mathrm{s}}_k \gamma^{\mathrm{s}}_k} \right)^{-1/\beta^{\mathrm{s}}_k}, \quad P^{\mathrm{iso,s,min}}_k = \left(\frac{d^{\mathrm{s,max}}_k}{\alpha^{\mathrm{s}}_k \gamma^{\mathrm{s}}_k} \right)^{-1/\beta^{\mathrm{s}}_k}. \tag{3.10}$$

Step 2 — Normalization.

$$\hat{P}^{\mathrm{iso,s}}_{kt} = \frac{P^{\mathrm{iso,s}}_{kt} - P^{\mathrm{iso,s,min}}_k}{P^{\mathrm{iso,s,max}}_k - P^{\mathrm{iso,s,min}}_k} \in [0,1]. \tag{3.11}$$

Step 3 — Secondary-market selling price.

$$\boxed{P^{\mathrm{s}}_{kt} = P^{\mathrm{max,s}}_{kt}\ \hat{P}^{\mathrm{iso,s}}_{kt} \in \left[0,\ P^{\mathrm{max,s}}_{kt}\right]}, \qquad k_M,\ t. \tag{3.12}$$

Common bound structure. For both channels, $\hat{P} \in [0,1]$ multiplied by the non-negative market ceiling $P^{\max} \geq 0$ yields a price in $[0, P^{\max}]$ without any auxiliary

constraint or min(·) operator.

Regime	Forward channel	Secondary channel
Max demand (liquid market)	$\hat{P}^{\text{iso,f}}_{it} = 0 \;\Rightarrow\; P^{\text{f}}_{it} = 0$	$\hat{P}^{\text{iso,s}}_{kt} = 0 \;\Rightarrow\; P^{\text{s}}_{kt} = 0$
Min demand (scarcity)	$\hat{P}^{\text{iso,f}}_{it} = 1 \;\Rightarrow\; P^{\text{f}}_{it} = P^{\max,\text{f}}_{it}$	$\hat{P}^{\text{iso,s}}_{kt} = 1 \;\Rightarrow\; P^{\text{s}}_{kt} = P^{\max,\text{s}}_{kt}$

Prices are purely demand-driven. Low realized demand signals scarcity and pushes the price toward the market ceiling; high demand signals a liquid market and pulls the price toward zero.

Parameter Estimation

1. **Market ceilings $P^{\max,\text{f}}_{it}$ and $P^{\max,\text{s}}_{kt}$**: sourced from secondary-market price benchmarks specific to the product category. Seasonal variation may be captured via $P^{\max}_{it} = \bar{P}^{\max}_{i}\Big(1 + \delta_P \sin(2\pi t/T)\Big)$.
2. **Isoelastic parameters $(\alpha^{\text{f}}_i, \beta^{\text{f}}_i)$ and $(\alpha^{\text{s}}_k, \beta^{\text{s}}_k)$**: estimated channel-by-channel via log-log OLS regression:
$$\ln\Big(D^{\text{f}}_{it}/\gamma^{\text{f}}_i\Big) = \ln \alpha^{\text{f}}_i - \beta^{\text{f}}_i \ln P^{\text{f}}_{it} + \varepsilon^{\text{f}}_{it}.$$
Require $\beta > 1$; use industry benchmarks if estimation yields $\hat{\beta} \leq 1$.
3. **Sensitivity coefficients δ^{f}_i, γ^{f}_i, γ^{s}_k**: estimated via seasonal decomposition of the respective demand time series: $\hat{\gamma} = \bar{D}/\bar{\bar{D}}$.

3.4.6 Decision Variables

Table 3.3: Decision variables of the generalized framework.

Symbol	Domain	Definition
q^i_t	$\mathbb{Z}_{\geq 0}$	Units of i_D decomposed in period t
Y^{f}_{it}	$\mathbb{Z}_{\geq 0}$	Units of i_R sold in the forward (primary) market in period t
Y^{f}_{it}	$\mathbb{Z}_{\geq 0}$	Units of k_M sold in the secondary (reconditioned) market in period t
r^k_t	$\mathbb{Z}_{\geq 0}$	Units of k_M for which reconditioning is *initiated* in period t; child components consumed immediately; reconditioned unit available in period $t + L^{\text{rec}}_k$
I^{fwd}_{it}	$\mathbb{Z}_{\geq 0}$	End-of-period inventory of i in period t; for disassembly
I^{rmfg}_{kt}	$\mathbb{Z}_{\geq 0}$	End-of-period inventory of i in period t; for Remanufactured

3.4.7 Objective Function

The planning horizon objective maximizes total net profit across all periods:

$$\max Z = \underbrace{\sum_{i\in C^S}\sum_{t=1}^{T} P^f_{it}\, r^f_{it}}_{\text{forward sales revenue}} + \underbrace{\sum_{k\in C^M}\sum_{t=1}^{T} P^r_{kt}\, r^r_{kt}}_{\text{rmfg sales revenue}} - \underbrace{\sum_{i\in C^D}\sum_{t=1}^{T} C^d_i\, x_{it}}_{\text{disassembly cost}} - \underbrace{\sum_{k\in C^M}\sum_{t=1}^{T} C^r_k\, u_{kt}}_{\text{rmfg cost}} - \underbrace{\sum_i\sum_t h_i\, I^{\text{fwd}}_{it}}_{\text{holding (fwd)}} - \underbrace{\sum_k\sum_t h_k\, I^{\text{rmfg}}_{kt}}_{\text{holding (rmfg)}} - \underbrace{\sum_i\sum_t C^\delta\, w_{it}}_{\text{disposal}} \quad (3.13)$$

(I) Forward revenue from selling recovered nodes at demand-driven price $P^{\text{f}}_{it} \in [0, P^{\max,\text{f}}_{it}]$; high scarcity (low D^{f}_{it}) pushes price toward the market ceiling.

(II) Secondary revenue from selling reconditioned intermediates at price $P^{\text{s}}_{kt} \in [0, P^{\max,\text{s}}_{kt}]$, also demand-driven.

(III) Decomposition operating costs (labour, tooling, energy) at each decomposable node.

(IV) Reconditioning costs (restoration, testing, certification) for each remanufacturable intermediate.

(V) Inventory holding costs penalizing idle stock and incentivizing throughput.

(IV) Disposal costs penalizing the overload on the disassembly .

3.4.8 Constraints

Lead-time conventions. For decomposition: $\tilde{x}^i_\tau \equiv 0$ for $\tau \le 0$ (zero delayed quantity before the horizon). For reconditioning: $\tilde{u}^k_\tau \equiv 0$ for $\tau \le 0$. With all lead times set to 1, child inventory from i decomposed in period $t-1$ arrives in period t.

(A) Root Node Inventory Balance

$$\iota_{v_0,t-1} + A_t - x^{v_0}_t - w_{it} = \iota_{v_0,t}, \qquad \forall\, t, \quad \iota_{v_0,0} = 0.A \quad (3.14)$$

Constraint **(A)** is the EOL product arrival-to-processing balance. A_t units arrive; $x^{v_0}_t$ units are decomposed; the remainder accumulates in inventory (awaiting capacity or market conditions).

(B1) Inventory Balance — Remanufacturable Intermediate Nodes (i_M)

Nodes in V_M receive units from both parent decomposition and reconditioning, and lose units to further decomposition, forward sales, and secondary-market sales. For every i_M and t:

General forward pool (fed by disassembly):

$$I^{\text{fwd}}_{n,t} = I^{\text{fwd}}_{n,t-1} + \alpha_{p(n),n}\, q_{p(n),t-1} - r_{n,t} - q_{n,t} - \Upsilon^f_{n,t} - w_{n,t} - \sum_{m\in C(n)} \beta_{m,n}\, r_{m,t} \quad (3.15)$$

General remanufactured pool (fed only by completed r runs):

$$I^{\text{rmfg}}_{n,t} = I^{\text{rmfg}}_{n,t-1} + r_{n,t-L^r_n} - Y^r_{n,t} \tag{3.16}$$

(B2) Inventory Balance — Leaf Recoverable Nodes (i_L)

Nodes in V_L have no outgoing decomposition arc and are not reconditioned. Their inventory balance is structurally simpler: only inflows from parent decomposition and outflows to forward sales (plus possible consumption in parent reconditioning). For every i_L and t:

$$\boxed{\iota_{i,t-1} + \xi_{(i),i,\,t-L^{\text{dec}}_{(i)}}\, \tilde{x}^{(i)}_{t-L^{\text{dec}}_{(i)}} - \mathbf{1}_{[(i)_M]}\, \rho_{(i),i}\, u^{(i)}_t - Y^{\text{f}}_{it} = \iota_{it}.}\; B2 \tag{3.17}$$

Structural significance of the B1/B2 split. The partition $V_R = V_{ML}$ induces two structurally distinct inventory equations. Constraint **(B1)** captures the bidirectional role of V_M nodes: they simultaneously act as *products* (sold forward or as reconditioned items) and as *assembly inputs* (consumed by their parent's reconditioning process). Constraint **(B2)** captures the unidirectional role of V_L nodes: they receive recovered units from their parent and funnel them exclusively to the forward market. This explicit split makes the flow logic auditable, avoids indicator function clutter in a single combined equation, and is directly portable to any PDG by reassigning nodes between V_M and V_L.

(C) Decomposition Capacity

$$q^i_t \;\le\; Q^{\text{dec}}_i, \qquad \forall\, i_D,\ t. C \tag{3.18}$$

$$w_{it} = max(0, q^i_t - Q^{\text{dec}}_i) \qquad \forall\, i_D,\ t. \tag{3.19}$$

Reflects physical throughput limits (equipment, labour, floor space) at each decomposition station.

(D) Reconditioning Capacity

$$r^k_t \;\le\; Q^{\text{rec}}_k, \qquad \forall\, k_M,\ t. D \tag{3.20}$$

Independent capacity bounds govern each reconditioning level.

(E) Inventory Capacity

$$\iota_{it} \;\le\; \text{Cap}_i, \qquad \forall\, i,\ t. E \tag{3.21}$$

(F) Forward Demand Cap

$$Y^{\text{f}}_{it} \;\le\; D^{\text{f}}_{it}, \qquad \forall\, i_R,\ t. F \tag{3.22}$$

Forward sales cannot exceed the realized period demand.

(H) Generalized Reconditioning Feasibility

Reconditioning of intermediate k can only draw on child-component inventory actually available at the start of the reconditioning run. For every k_M, every child $j \in (k)$, and every t:

$$\boxed{\rho_{k,j}\, r_t^k \;\le\; \iota_{j,t-1} + \xi_{k,j,\,t-L_k^{\mathrm{dec}}}\, \tilde{x}^k_{t-L_k^{\mathrm{dec}}},} \qquad \forall\, k_M,\ j \in (k),\ t.H \tag{3.23}$$

The right-hand side is the total child-j inventory available: carry-over stock $\iota_{j,t-1}$ plus fresh units arriving from decomposing k in the current period.

Binding case (zero yield on critical arc). When $\xi_{k,j,t} = 0$ for some $j \in (k)$, no new child-j inventory arrives. Constraint **(H)** then imposes $r_t^k \le \min_{j\in(k)} \iota_{j,t-1}/\rho_{k,j}$: reconditioning is feasible only when carry-over stock of *every* required component is positive. A single missing component type blocks all reconditioning of k, regardless of the surplus of other components. This "weakest link" property models realistic assembly processes faithfully without additional constraints.

(I) Non-Negativity and Integrality

$$q_t^i,\ Y_{it}^{\mathrm{f}},\ Y_{it}^{\mathrm{f}},\ r_t^k,\ \iota_{it} \;\in\; \mathbb{Z}_{\ge 0}, \qquad \forall\, i,\ k_M,\ t.I \tag{3.24}$$

3.4.9 Complete Model Statement

Complete Generalized MILP — EOL Product Decomposition Planning **Period-start sampling** (before solving period t):

- Draw $\xi_{ij,t} \sim \mathcal{U}\{0, \ldots, \rho_{ij}\}$ for each (i, j).
- Draw $D_{it}^{\mathrm{f}} \sim \mathcal{U}[\lceil d_i^{\min} \rceil, \lfloor d_i^{\max} \rfloor]$ for each i_R.
- Draw $D_{kt}^{\mathrm{s}} \sim \mathcal{U}[\lceil d_k^{\mathrm{s,min}} \rceil, \lfloor d_k^{\mathrm{s,max}} \rfloor]$ for each k_M.

Preprocessing (scalar arithmetic; no new variables):

$$P_{it}^{\mathrm{iso,f}} = \left(D_{it}^{\mathrm{f}} / \alpha_i^{\mathrm{f}} \gamma_i^{\mathrm{f}}\right)^{-1/\beta_i^{\mathrm{f}}}, \qquad \hat{P}_{it}^{\mathrm{iso,f}} = \frac{P_{it}^{\mathrm{iso,f}} - P_i^{\mathrm{iso,f,min}}}{P_i^{\mathrm{iso,f,max}} - P_i^{\mathrm{iso,f,min}}}, \qquad P_{it}^{\mathrm{f}} = P_{it}^{\mathrm{max,f}}\, \hat{P}_{it}^{\mathrm{iso,f}}$$

$$P_{kt}^{\mathrm{iso,s}} = \left(D_{kt}^{\mathrm{s}} / \alpha_k^{\mathrm{s}} \gamma_k^{\mathrm{s}}\right)^{-1/\beta_k^{\mathrm{s}}}, \qquad \hat{P}_{kt}^{\mathrm{iso,s}} = \frac{P_{kt}^{\mathrm{iso,s}} - P_k^{\mathrm{iso,s,min}}}{P_k^{\mathrm{iso,s,max}} - P_k^{\mathrm{iso,s,min}}}, \qquad P_{kt}^{\mathrm{s}} = P_{kt}^{\mathrm{max,s}}\, \hat{P}_{kt}^{\mathrm{iso,s}}$$

Objective: Maximise Z as in (4.42).

Subject to:

(A) Root inventory balance

(B1) Inventory balance — remanufacturable intermediates ($\forall\, i_M,\ t$)

(B2) Inventory balance — leaf recoverable nodes ($\forall\, i_L,\ t$)

(C) Decomposition capacity ($\forall\, i_D,\ t$)

(D) Reconditioning capacity ($\forall\, k_M,\ t$)

(E) Inventory capacity ($\forall\, i,\ t$)

(F) Forward demand cap ($\forall\, i_R,\ t$)

(G) Secondary demand cap ($\forall\, k_M,\ t$)

(H) Reconditioning feasibility ($\forall\, k_M,\ j \in (k),\ t$)

(I) Non-negativity and integrality

Table 3.4: Constraint inventory for a PDG with $|V_R|$ recoverable nodes, $|V_M|$ remanufacturable intermediates, $|V_L|$ leaf nodes, $|V_D|$ decomposable nodes, $|V|$ total nodes, and $\sum_{k_M} |(k)|$ reconditioning child-pairs.

Label	Description	Applies to	Count
(A)	Root inventory balance	$\{v_0\}$	T
(B1)	Inventory balance — intermediates	V_M	$\lvert V_M\rvert \cdot T$
(B2)	Inventory balance — leaf nodes	V_L	$\lvert V_L\rvert \cdot T$
(C)	Decomposition capacity	V_D	$\lvert V_D\rvert \cdot T$
(D)	Reconditioning capacity	V_M	$\lvert V_M\rvert \cdot T$
(E)	Inventory capacity	V	$\lvert V\rvert \cdot T$
(F)	Forward demand cap	V_R	$\lvert V_R\rvert \cdot T$
(G)	Secondary demand cap	V_M	$\lvert V_M\rvert \cdot T$
(H)	Reconditioning feasibility	$\{(k, j) : k_M, j \in (k)\}$	$\left(\sum_{k_M} \lvert(k)\rvert\right) \cdot T$
	Total		$\left(1 + \lvert V_R\rvert + 3\lvert V_M\rvert + \lvert V_L\rvert + \lvert V_D\rvert + \lvert V\rvert + \sum_k \lvert(k)\rvert\right)T$

3.5 Structural Generalization Analysis

3.5.1 Dimensions of Abstraction

Table 3.5 systematically maps each battery-specific construct in the original model to its generalized counterpart in the framework developed here. The table distinguishes between *notational* substitutions (renaming without structural change), *representational* abstractions (lifting a specific structure to a parameterized class), and *architectural* generalizations (restructuring the constraint or objective).

3.5.2 Key Invariants Preserved

The following mathematical properties of the original model are preserved exactly by the generalization:

I1. Pure integer model. All decision variables remain non-negative integers. No binary variables are introduced at any level of generality, provided the PDG is a pure AND hierarchy (Assumption 1).

I2. Scenario-based linearity. All stochastic quantities ($\xi_{ij,t}$, D^{f}_{it}, D^{s}_{kt}) are realized before the MILP is built, ensuring the optimization problem is linear in all variables.

I3. Price bound guarantee. Both $P^{\mathrm{f}}_{it} \in [0, P^{\max,\mathrm{f}}_{it}]$ and $P^{\mathrm{s}}_{kt} \in [0, P^{\max,\mathrm{s}}_{kt}]$ hold by algebraic construction, without auxiliary constraints.

I4. Reconditioning feasibility structure. Constraint **(H)** correctly captures the minimum-availability condition across all required child components, independent of the specific product and its BOM depth.

I5. Scalability. The model size scales as $O(|V| \cdot T)$ constraints and $O(|V| \cdot T)$ variables; no non-linear scaling with hierarchy depth or breadth.

3.5.3 Industrial Instantiation Protocol

To instantiate the framework for a new product system, the practitioner performs the following five steps:

Step 1. Construct the PDG. Enumerate all product entities (product unit, sub-assemblies, components, constituent materials) as nodes v_i. Draw a directed arc (v_i, v_j) for each parent-to-child decomposition relationship.

Step 2. Assign node classes. Partition V into $\{v_0\}$, V_D, V_M, V_L based on: (a) whether the node has outgoing arcs, and (b) whether the corresponding entity is commercially viable to recondition.

Step 3. Set arc parameters. For each (i, j), specify ρ_{ij} from the product BOM or engineering specifications.

Step 4. Calibrate demand and pricing parameters. Estimate $(\alpha^{\mathrm{f}}_i, \beta^{\mathrm{f}}_i, \gamma^{\mathrm{f}}_i)$ and $(\alpha^{\mathrm{s}}_k, \beta^{\mathrm{s}}_k, \gamma^{\mathrm{s}}_k)$ from historical price–quantity data for each node. Source market ceilings $P^{\max,\mathrm{f}}_{it}$ and $P^{\max,\mathrm{s}}_{kt}$ from market benchmarks.

Step 5. Specify operational parameters. Set lead times $(L^{\mathrm{dec}}_i, L^{\mathrm{rec}}_k)$, costs $(c^{\mathrm{dec}}_i, c^{\mathrm{rec}}_k, h_i)$, and capacity bounds $(Q^{\mathrm{dec}}_i, Q^{\mathrm{rec}}_k, \mathrm{Cap}_i)$ from facility operational data.

Steps 1–3 require product engineering knowledge; Steps 4–5 require market and operational data. No modification of any constraint or objective equation is required.

3.6 Application Examples

This section illustrates how the five-step instantiation protocol (Section 3.5) is applied to three distinct product families.

3.6.1 Example 1: Electric Vehicle Battery Pack (Motivating Instance)

Instantiation: Nissan Leaf 24 kWh Battery Pack **PDG topology:** 4-level, 10 nodes, 9 decomposition arcs, 5 reconditioning arcs.

Node assignments: v_0 = Battery Pack (root); V_M = {Modules, Cells}; V_L = {Enclosure, Cooling, BMS, Cathode, Anode, Separator, Electrolyte}.

Arc parameters: $\rho_{v_0,\text{Module}} = 48$, $\rho_{\text{Module,Cell}} = 4$, $\rho_{\text{Cell},j} = 1$ for all intra-cell materials.

Constraint count: $42T$ (using $|V_M| = 2, |V_L| = 7, |V_D| = 3, |V| = 10, \sum |(k)| = 1+4 = 5$).

3.6.2 Example 2: Smartphone Disassembly

Instantiation: Mid-Range Android Smartphone **PDG topology:** 3 levels, 8 nodes, 7 decomposition arcs, 3 reconditioning arcs.

Node assignments: v_0 = Smartphone (root, level 0);
Level 1 (V_{MD}): Screen Assembly, Mainboard — both reconditioned for certified-refurbished market;
Level 1 (V_L): Battery Cell, Housing;
Level 2 (V_L): Camera Module, SoC (from Mainboard), RF Module (from Mainboard).

Arc parameters: $\rho_{v_0,\text{Screen}} = 1$, $\rho_{v_0,\text{Mainboard}} = 1$, $\rho_{\text{Mainboard,SoC}} = 1$, $\rho_{\text{Mainboard,RF}} = 1$, etc.

Constraint count: $(1 + 5 + 2 + 1 + 2 + 8 + 5 + 2 + 3)T = 29T$.

Market context: Certified-refurbished smartphones command secondary prices of 40–70% of new retail; isoelastic pricing captures the well-documented price elasticity of the refurbished handset market ($\hat{\beta}^s \approx 1.8$–$2.4$).

3.6.3 Example 3: Industrial Robot Arm

Instantiation: 6-DOF Industrial Robot Arm **PDG topology:** 3 levels, 12 nodes, 11 decomposition arcs, 4 reconditioning arcs.

Node assignments: v_0 = Robot Arm (root, level 0);
Level 1 (V_M): Joint Actuator Modules (6 units) — high reconditioning value due to precision servo motors; $\rho_{v_0,\text{ActuatorModule}} = 6$.
Level 1 (V_L): Arm Link Segments (structural), End-Effector Bracket, Controller PCB.
Level 2 (V_L from Actuator): Servo Motor, Gear Assembly, Encoder, Harness.

Arc parameters: $\rho_{\text{ActuatorModule,ServoMotor}} = 1$, $\rho_{\text{ActuatorModule,GearAssembly}} = 1$, etc.

Operational context: Decomposition lead times of 2–3 periods (days) for joint disassembly; reconditioning lead time of 5 periods for servo motor refurbishment and testing. Setting $L_i^{\text{dec}} = 2$ and $L_k^{\text{rec}} = 5$ in the parameter table activates the lead-time logic in constraints **(B1)**, **(B2)**, and **(H)** without structural modification.

3.7 Advanced Extensions

The generalized framework is designed to accommodate the following extensions without altering its core constraint structure.

Multi-product families. When multiple EOL product variants share component nodes (parts commonality), the PDG is extended to a multi-root forest: one root $v_0^{(m)}$ per product variant m, with shared child nodes v_{jR} appearing as children of multiple

parents. Constraint **(B1)** and **(B2)** remain unchanged; only the supply term A_t is indexed by product type.

supply. If EOL product arrivals A_t are uncertain, they can be drawn from an appropriate distribution (Poisson, uniform, or empirically fitted) at the start of each period, consistent with the scenario-based approach (Assumption 3).

Or-arc extensions. If the product BOM contains OR arcs (alternative decomposition routes), binary arc-selector variables and Big-M constraints must be introduced. The inventory balance constraints **(B1)** and **(B2)** remain valid; only the yield expression $\xi_{ij,t}\tilde{x}^i_{t-L}$ is replaced by a sum over active arcs.

Non-uniform yield distributions. When empirical yield data are available, the uniform yield distribution $\mathcal{U}\{0,\ldots,\rho_{ij}\}$ can be replaced by any discrete distribution (truncated binomial, empirical, beta-binomial) without altering the model constraints, since yields enter only as fixed coefficients after sampling.

Carbon and resource accounting. Environmental objectives (carbon emissions, material recovery rates, landfill diversion) can be added to the objective function as additional terms, weighted by emission factors or recovery value coefficients, using the same variable set.

3.8 Conclusion

This paper has presented a rigorous structural abstraction of a domain-specific battery disassembly planning model into a fully product-agnostic multi-period MILP framework. The generalization was achieved through four coordinated abstractions: (i) the product BOM was lifted into an arbitrary Product Decomposition Graph parameterized by node class assignments and arc weight vectors; (ii) the yield was decoupled from battery-specific quantities and expressed in terms of a generic recovery yield distribution parameterized by assembly consumption ratios; (iii) the dual-channel isoelastic pricing mechanism was expressed in terms of abstract demand parameters estimable for any product category; and (iv) the inventory balance constraints were restructured into two split-class equations whose applicability depends solely on node class membership, not on physical identity.

The resulting framework satisfies the following properties:

- **Mathematical correctness:** all constraints and the objective function are dimensionally and logically valid for any PDG satisfying the pure AND-arc assumption.
- **Computational tractability:** no binary variables; the model scales as $O(|V| \cdot T)$ in both constraints and variables.

- **Transferability:** instantiation requires only the five-step parameter assignment protocol; no constraint equation is modified.
- **Extensibility:** multi-product families, supply, OR-arc BOMs, and non-uniform yields can be incorporated without disrupting the core structure.

The framework is applicable to any manufactured product whose EOL processing involves hierarchical decomposition, selective reconditioning of intermediate subassemblies, and dual-channel market access. This encompasses the full breadth of reverse logistics and circular economy applications—from consumer electronics and automotive powertrains to industrial machinery and medical devices.

Table 3.5: Abstraction map from battery-specific to generalized framework.

Battery-specific construct	Generalized construct	Abstraction type
Battery pack (root node)	EOL product unit v_0	Representational
Battery modules, cells	Remanufacturable intermediates V_M	Representational
Cathode, anode, separator, electrolyte	Leaf recoverable nodes V_L (materials)	Representational
Enclosure, BMS, cooling	Leaf recoverable nodes V_L (subassemblies)	Representational
N_i notation (fixed indices)	v_i (abstract vertex set)	Notational
Battery BOM (hard-coded levels)	PDG $G = (V, R)$ of arbitrary depth L	Architectural
$\alpha_{ij,t}$ yield (battery-calibrated)	$\xi_{ij,t}$ yield (parameterized via ρ_{ij})	Representational
β_{ij} assembly ratio (BOM-fixed)	ρ_{ij} consumption ratio (user-specified)	Notational
Disassembly lead time L_i^{dis}	Decomposition lead time L_i^{dec}	Notational
Remanufacturing lead time L_k^{rmfg}	Reconditioning lead time L_k^{rec}	Notational
γ_i^{f} (battery sensitivity)	δ_i^{f} (product sensitivity)	Notational
Level-specific constraints (B/C/D/E)	Node-class constraints (B1/B2) via V_M, V_L	Architectural
q_t^i, Y_{it}^{f}, Y_{kt}^{r}, r_t^k, I_{it}	q_t^i, Y_{it}^{f}, Y_{it}^{f}, r_t^k, ι_{it}	Notational
C_i^{dis}, C_k^{rmfg}	c_i^{dec}, c_k^{rec}	Notational
Dual-channel isoelastic pricing (f, r)	Dual-channel isoelastic pricing (f, s)	Representational
Battery-specific $P^{\max}$ values	Abstract market ceilings $P^{\max,\text{f}}$, $P^{\max,\text{s}}$	Representational
Fixed 4-level BOM depth	Configurable L-level PDG	Architectural
$42T$ constraints (10-node instance)	General $\big(\ldots\big)T$ formula (Table 4.5)	Architectural

Chapter 4

Model Execution

This Model presents a multi-period MILP for disassembly planning of end-of-life (EOL) Nissan Leaf 24 kWh battery packs (ZE0/AZE0, 2011–2015; LMO/Graphite chemistry, AESC LEV50 cells). The model operates on a four-level, pure AND-arc hierarchy (10 nodes, 9 disassembly arcs) and incorporates five structural features: *(i)* **integer yield** on each AND arc, drawn from $\mathcal{U}\{0, \ldots, \beta_{ij}\}$ where β_{ij} is the remanufacturing assembly ratio; *(ii)* **sensitivity-driven integer demand** drawn from $\mathcal{U}\left[\lceil d_i^{\min} \rceil, \lfloor d_i^{\max} \rfloor\right]$ whose range scales with the demand-sensitivity coefficient γ_i; *(iii)* **dual-channel normalized isoelastic pricing**: both the forward selling price $P_{it}^{\mathrm{f}} = P_{it}^{\max,\mathrm{f}}\, \hat{P}_{it}^{\mathrm{iso,f}}$ and the remanufactured selling price $P_{kt}^{\mathrm{r}} = P_{kt}^{\max,\mathrm{r}}\, \hat{P}_{kt}^{\mathrm{iso},r}$ are derived purely from their respective inverse isoelastic demand functions (Couzon, Ouazene & Yalaoui, 2019), each guaranteed by construction to lie in $[0, P^{\max}]$; *(iv)* a **shared inventory pool** with per-level capacity limits and lead times L_i^{dis}, L_k^{rmfg} (all currently set to 1); and *(v)* **split level-based inventory balance constraints** that separate intermediate remanufacturable nodes ($_M$) from leaf nodes ($_L$), improving model clarity and portability to arbitrary AND-arc hierarchies. quantities are sampled at the start of each period and enter the MILP as fixed coefficients (scenario-based approach), preserving full integrality. The model has **42T** functional constraints and no binary variables.

4.1 Problem Description

4.1.1 System Overview

We consider a multi-period disassembly planning problem over a finite horizon of T discrete periods = $\{1, \ldots, T\}$. In each period $t \in$, a known quantity S_t of EOL Nissan Leaf 24 kWh battery packs arrives at the disassembly facility. Packs are processed through a four-level AND-arc network that *jointly* produces all sellable sub-components. Intermediate products (N_4 battery modules, N_7 pouch cells) may be further disassembled into lower-level components or reassembled (remanufactured) and sold in a dedicated secondary market. The planner determines, in each period, how many units of each node to disassemble, remanufacture, and sell in each channel, subject to yield, capacity, inventory, and demand constraints.

4.1.2 Quantities and Scenario Approach

Two quantities are drawn randomly at the *start* of each period and are thereafter fixed as deterministic MILP coefficients:

1. **Disassembly yield** $\alpha_{ij,t}$: the number of child-j units recovered per unit of parent i disassembled, drawn from $\mathcal{U}\{0, 1, \ldots, \beta_{ij}\}$ (Section 4.2.4).
2. **Market demand** D_{it}: drawn from a discrete uniform distribution whose range is governed by γ_i (Section 4.3.3).

This *scenario-based* (rolling-horizon) approach preserves full integrality: the MILP solved in period t contains only fixed numerical coefficients, with no embedded uncertainty.

4.1.3 Key Structural Adaptations

1. **No OR arcs.** The battery BOM is a pure AND hierarchy. Disassembling one unit of a parent node simultaneously yields (a realisation of) *all* children's components. No binary arc-selector variables or Big-M constraints are needed.
2. **Dual-channel normalized isoelastic pricing.** Both the forward price and the remanufactured price are derived independently from their respective isoelastic demand functions and normalized to lie in $[0, P^{\max}]$ by construction. Neither channel uses a cost floor; both are purely demand-driven (Section 4.3.4).
3. **Cost-recovery base price.** κ_i equals the accumulated per-unit disassembly cost from root N_0 to node i, computed at expected yields $\bar{\alpha}_{ij} = \beta_{ij}/2$. It serves as the hard lower bound on the selling price.
4. **Shared inventory with level-based lead times.** A single pool I_{it} aggregates all units of product i. Disassembly lead time L_i^{dis} and remanufacturing lead time L_k^{rmfg} are defined per node and currently set to 1 for all $i \in_D$, $k \in_M$.
5. **Split inventory balance constraints.** The inventory balance for sellable nodes

is expressed as *two* separate equations: constraint **(B1)** for intermediate nodes that are both disassembled and remanufactured ($i \in_M$), and constraint **(B2)** for leaf nodes that cannot be further disassembled ($i \in_L$). This separation makes the flow logic explicit for each node class and is directly portable to any AND-arc hierarchy.

6. **Generalized remanufacturing feasibility.** A single level-indexed constraint **(H)** replaces all node-pair-specific feasibility inequalities and applies without modification to any AND-arc product BOM.

4.2 Battery Pack Network

4.2.1 Node Set

The directed graph $G = (,)$ mirrors the BOM of one complete Nissan Leaf 24 kWh battery pack. Busbars (N_5) and thermistors (N_6) are excluded from the model: their recovery adds negligible residual value relative to their disassembly cost and they are not involved in any remanufacturing pathway.

Table 4.1: Node set : identifiers, labels, level, role, and absolute pack-level quantity Q^{abs}.

ID	Label	Level ℓ	Role	Q^{abs}
N_0	Battery Pack	0	Root — EOL input	1
N_1	Outer Enclosure	1	Structural housing	1
N_2	Air-Cooling Manifold	1	Thermal management	1
N_3	Pack BMS (LBC)	1	Electronics / control	1
N_4	Battery Modules	1	Serviceable sub-units	48
N_7	AESC Pouch Cells (2S2P)	2	Electrochemical unit	192
N_8	LMO Cathode	3	Electrode — positive	192
N_9	MCMB Anode	3	Electrode — negative	192
N_{10}	Separator (PE/PP)	3	Ionic membrane	192
N_{11}	Electrolyte ($LiPF_6$)	3	Ion-transport medium	192

4.2.2 Level Structure

The hierarchy is partitioned into four levels. Let $\ell(i) \in \{0,1,2,3\}$ denote the level of node i, and define:

$$_{\ell} = \{i \in : \ \ell(i) = \ell\}, \qquad \ell \in \{0,1,2,3\}. \tag{4.1}$$

$_0 = \{N_0\}$	Root (EOL battery pack)
$_1 = \{N_1, N_2, N_3, N_4\}$	Level-1 components (direct children of N_0)
$_2 = \{N_7\}$	Level-2 component (pouch cells, child of N_4)
$_3 = \{N_8, N_9, N_{10}, N_{11}\}$	Level-3 leaf components (intra-cell materials)

For any node $i \in \backslash\{N_0\}$, let $p(i)$ denote its unique parent under the AND-arc disassembly hierarchy.

4.2.3 Index Subsets

$_D = \{N_0, N_4, N_7\}$	Disassembly nodes (have outgoing AND arcs)
$_S = \backslash\{N_0\} = \{N_1, N_2, N_3, N_4, N_7, N_8, N_9, N_{10}, N_{11}\}$	$\lvert_S\rvert = 9$
$_M = \{N_4, N_7\}$	Intermediates eligible for remanufacturing
$_L =_S \backslash_M = \{N_1, N_2, N_3, N_8, N_9, N_{10}, N_{11}\}$	Leaf nodes (no outgoing dis arc, not rem)
$= \{1, \ldots, T\}$	Planning periods

Node classes and constraint assignment. The split between $_M$ and $_L$ is the structural basis for the two inventory balance constraints introduced in Section 4.3.7:

- $_M = \{N_4, N_7\}$: intermediate nodes that are both *disassembled further* and *remanufactured*. Their inventory balance includes inflows from remanufacturing ($\tilde{r}^i$), outflows to further disassembly (q_t^i), and outflows to the secondary market (Y_{it}^{r}).
- $_L = \{N_1, N_2, N_3, N_8, N_9, N_{10}, N_{11}\}$: leaf nodes that are *sold forward only*. Their inventory balance has no remanufacturing or disassembly outflow terms, keeping the equation structurally simpler.

4.2.4 Integer Yield on AND Arcs

Motivation

Physical disassembly of aged battery packs is imperfect: corrosion, thermal damage, or mechanical stress can render individual components unrecoverable. The yield on each AND arc is modelled as a integer drawn at the start of each period and fixed for that period's MILP.

Yield Distribution

For each AND arc $(i, j) \in$ and period $t \in$:

$$\boxed{\alpha_{ij,t} \sim \mathcal{U}\{0, 1, \ldots, \beta_{ij}\}, \qquad \alpha_{ij,t} \in \mathbb{Z}_{\geq 0},} \tag{4.2}$$

where $\beta_{ij} \in \mathbb{Z}^+$ is the **remanufacturing assembly ratio**: the number of child-j units required to rebuild one unit of intermediate k (the nearest ancestor of j in $_M$). Setting the maximum yield equal to β_{ij} ensures that at peak disassembly output the recovered quantities exactly match remanufacturing needs, providing a natural demand–supply balance.

Nominal Yield Upper Bounds β_{ij}

$$\begin{aligned} \beta_{N_0,N_1} = \beta_{N_0,N_2} = \beta_{N_0,N_3} &= 1, \\ \beta_{N_0,N_4} &= 48, \\ \beta_{N_4,N_7} &= 4, \\ \beta_{N_7,N_8} = \beta_{N_7,N_9} = \beta_{N_7,N_{10}} = \beta_{N_7,N_{11}} &= 1. \end{aligned} \tag{4.3}$$

Consequently:

- $\alpha_{N_0,N_j,t} \sim \mathcal{U}\{0,1\}$ for $j \in \{N_1, N_2, N_3\}$: each level-1 leaf is recovered or lost.
- $\alpha_{N_0,N_4,t} \sim \mathcal{U}\{0,\ldots,48\}$: 0–48 modules recovered per EOL pack.
- $\alpha_{N_4,N_7,t} \sim \mathcal{U}\{0,\ldots,4\}$: 0–4 cells recovered per module.
- $\alpha_{N_7,N_j,t} \sim \mathcal{U}\{0,1\}$ for $j \in \{N_8, N_9, N_{10}, N_{11}\}$: each intra-cell component is recovered (1) or lost (0).

4.2.5 Remanufacturing Assembly Ratios

The same β_{ij} values also serve as remanufacturing consumption rates. One unit of intermediate $k \in_M$ is rebuilt by consuming $\beta_{k,j}$ units of each child $j \in \mathrm{Ch}(k)$ from the inventory:

$$\text{Rebuild one module } N_4: \quad \beta_{N_4,N_7} = 4 \text{ pouch cells.} \tag{4.4}$$

$$\text{Rebuild one cell } N_7: \quad \beta_{N_7,N_8} = 1,\ \beta_{N_7,N_9} = 1,\ \beta_{N_7,N_{10}} = 1,\ \beta_{N_7,N_{11}} = 1. \tag{4.5}$$

4.2.6 Network Diagram

4.3 Mathematical Formulation

4.3.1 Sets and Indices

4.3.2 Parameters

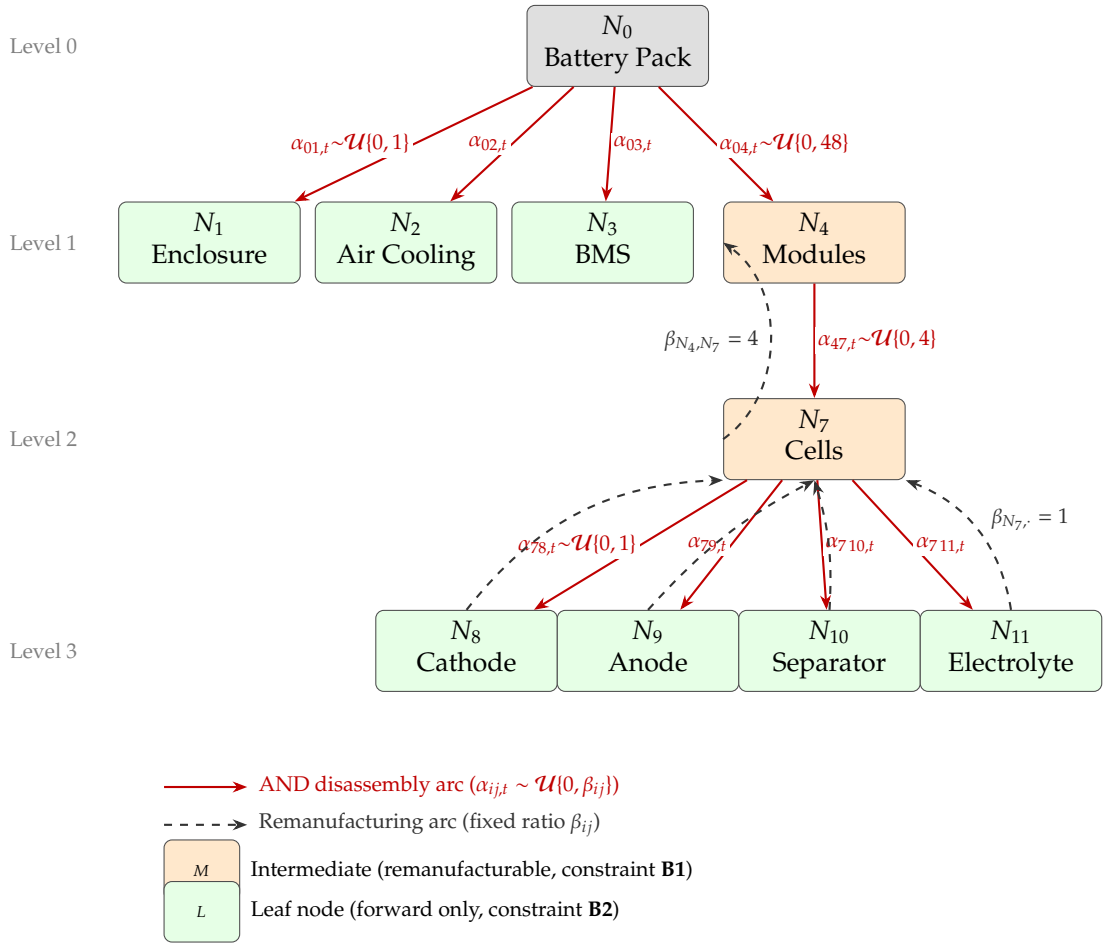

Figure 4.1: AND-arc disassembly network for the Nissan Leaf 24 kWh battery pack (10 nodes, 9 disassembly arcs, 5 remanufacturing arcs). Orange nodes ($_M = \{N_4, N_7\}$): remanufacturable intermediates governed by constraint **(B1)**. Green nodes ($_L$): leaf nodes governed by constraint **(B2)**.

Table 4.3: Model parameters.

Symbol	Domain	Definition
Supply		
S_t	$\mathbb{Z}_{\geq 0}$	EOL battery packs arriving in period t
yield (AND arcs)		
β_{ij}	$\mathbb{Z}^+$	Maximum yield and remanufacturing assembly ratio for arc $(i, j) \in$; values in (4.3)
$\alpha_{ij,t}$	$\mathcal{U}\{0, \ldots, \beta_{ij}\}$	integer yield on arc (i, j) in period t; fixed as MILP coefficient after sampling
$\bar{\alpha}_{ij}$	$\mathbb{R}_{>0}$	Expected yield $\bar{\alpha}_{ij} = \beta_{ij}/2$; used to compute base price κ_i
Lead times		

continued. . .

Symbol	Domain	Definition
L_i^{dis}	$\mathbb{Z}_{\geq 0}$	Disassembly lead time for node $i \in_D$; **currently set to 1** for all $i \in_D$. Child inventory from disassembling i in period t arrives in period $t + L_i^{\text{dis}}$
L_k^{rmfg}	$\mathbb{Z}_{\geq 0}$	Remanufacturing lead time for intermediate $k \in_M$; **currently set to 1** for all $k \in_M$. A unit remanufactured in period t becomes available in $t + L_k^{\text{rmfg}}$; child components are consumed in period t
Sensitivity-driven integer demand		
Forward channel demand ()		
γ_i^{f}	$\mathbb{R}_{\geq 0}$	Demand-sensitivity coefficient for forward sales of $i \in_S$; $\gamma_{\min} \leq \gamma_i^{\text{f}} \leq \gamma_{\max}$
scale_i	$[0, 1]$	Normalised sensitivity: $\text{scale}_i = (\gamma_i^{\text{f}} - \gamma_{\min})/(\gamma_{\max} - \gamma_{\min})$
$d_i^{\min}, d_i^{\max}$	$\mathbb{R}_{\geq 0}$	Forward demand range bounds: $d_i^{\min} = a + \text{scale}_i \cdot b,\ d_i^{\max} = c + \text{scale}_i \cdot d$, $a = 2, b = 4, c = 10, d = 6$
D_{it}^{f}	$\mathcal{U}\left[\lceil d_i^{\min} \rceil, \lfloor d_i^{\max} \rfloor\right]$	Forward-channel demand for $i \in_S$ in period t; drawn once per period
Remanufactured channel demand		
$d_k^{\text{r,min}}, d_k^{\text{r,max}}$	$\mathbb{R}_{\geq 0}$	Remanufactured demand range bounds for $k \in_M$; set from secondary-market observations
D_{kt}^{r}	$\mathcal{U}\left[\lceil d_k^{\text{r,min}} \rceil, \lfloor d_k^{\text{r,max}} \rfloor\right]$	Remanufactured-channel demand for $k \in_M$ in period t; drawn once per period
Pricing — forward channel		
$P_{it}^{\max,\text{f}}$	$\mathbb{R}_{\geq 0}$	Market price ceiling for forward sales of $i \in_S$ in period t; upper bound on P_{it}^{f} ($P_{it}^{\text{f}} \in [0, P_{it}^{\max,\text{f}}]$); sourced from secondary market benchmarks
α_i^{f}	$\mathbb{R}_{>0}$	Isoelastic base demand for the forward channel; estimated via log-log regression on forward price–quantity data
β_i^{f}	$\mathbb{R}_{>1}$	Price elasticity of forward demand; $\beta_i^{\text{f}} > 1$ required for a finite profit-maximising price to exist
γ_i^{f}	$\mathbb{R}_{\geq 0}$	Demand-sensitivity coefficient used in forward pricing
Pricing — remanufactured channel		

continued...

Symbol	Domain	Definition
$P_{kt}^{\max,\mathrm{r}}$	$\mathbb{R}_{\geq 0}$	Market price ceiling for remanufactured sales of $k \in_M$ in period t; upper bound on P_{kt}^{r} ($P_{kt}^{\mathrm{r}} \in [0, P_{kt}^{\max,\mathrm{r}}]$); sourced from certified-refurbished market benchmarks
α_k^{r}	$\mathbb{R}_{>0}$	Isoelastic base demand for the remanufactured channel; estimated via log-log regression on remanufactured price–quantity data
β_k^{r}	$\mathbb{R}_{>1}$	Price elasticity of remanufactured demand
γ_k^{r}	$\mathbb{R}_{\geq 0}$	Demand-sensitivity coefficient used in remanufactured pricing
Costs		
C_i^{dis}	$\mathbb{R}_{\geq 0}$	Unit disassembly cost at node $i \in_D$
C_k^{rmfg}	$\mathbb{R}_{\geq 0}$	Unit remanufacturing cost for $k \in_M$
h_i	$\mathbb{R}_{\geq 0}$	Holding cost per unit of $i \in$ per period
Capacity and inventory		
Q_i^{dis}	$\mathbb{Z}^+$	Maximum units of $i \in_D$ disassembled per period
Q_k^{rmfg}	$\mathbb{Z}^+$	Maximum units of $k \in_M$ remanufactured per period
Cap_i	$\mathbb{Z}^+$	Maximum end-of-period inventory of $i \in$

4.3.3 Demand Models

Two independent demand streams are drawn at the start of each period and fixed as MILP coefficients: one for each selling channel.

Forward Channel Demand D_{it}^{f}

Demand for product $i \in_S$ in the forward market in period t is drawn from a discrete uniform distribution whose range scales with the sensitivity coefficient γ_i^{f}:

$$\boxed{D_{it}^{\mathrm{f}} \sim \mathcal{U}\Big[\lceil d_i^{\min} \rceil,\ \lfloor d_i^{\max} \rfloor\Big],} \quad d_i^{\min} = a + \mathrm{scale}_i \cdot b, \quad d_i^{\max} = c + \mathrm{scale}_i \cdot d, \tag{4.6}$$

where $\mathrm{scale}_i = (\gamma_i^{\mathrm{f}} - \gamma_{\min})/(\gamma_{\max} - \gamma_{\min}) \in [0, 1]$ A higher γ_i^{f} implies a broader and higher forward demand range.

Remanufactured Channel Demand D_{kt}^{r}

Demand for remanufactured intermediate $k \in_M$ in the secondary market in period t is drawn independently from its own discrete uniform distribution:

$$\boxed{D_{kt}^{\mathrm{r}} \sim \mathcal{U}\Big[\lceil d_k^{\mathrm{r},\min} \rceil,\ \lfloor d_k^{\mathrm{r},\max} \rfloor\Big],} \qquad k \in_M,\ t \in . \tag{4.7}$$

Table 4.2: Sets and index notation.

Symbol	Definition
$= \{1, \ldots, T\}$	Planning periods
$= \{N_0, N_1, N_2, N_3, N_4, N_7, \ldots, N_{11}\}$	All product nodes, $\| = 10$
$_\ell$ ($\ell = 0, 1, 2, 3$)	Nodes at level ℓ; see (4.1)
$_D = \{N_0, N_4, N_7\}$	Nodes with outgoing AND disassembly arcs
$_S = \setminus\{N_0\}$	Sellable products, $\|_S\| = 9$
$_M = \{N_4, N_7\}$	Intermediates eligible for remanufacturing
$_L =_S \setminus_M$	Leaf nodes (no outgoing disassembly arc)
	Set of all AND disassembly arcs (i, j)
Ch(i)	Children of node i under disassembly
$p(i)$	Unique parent of node $i \in \setminus\{N_0\}$

The bounds $d_k^{\mathrm{r,min}}$ and $d_k^{\mathrm{r,max}}$ are set from secondary-market observations (e.g. certified module and cell refurbishment platforms). Both demands are drawn independently for each product and period and enter the MILP as fixed integers.

4.3.4 Dual-Channel Normalized Isoelastic Pricing

Both selling channels use the same three-step pricing procedure: invert the isoelastic demand function, normalize the result to $[0, 1]$, and scale by the channel's market ceiling. In both cases the price is bounded between 0 and the market ceiling by construction, with no cost floor.

Forward Channel Price P_{it}^{f}

Step 1 — Isoelastic demand-implied price. The isoelastic model posits $D_{it}^{\mathrm{f}} = \alpha_i^{\mathrm{f}} \gamma_i^{\mathrm{f}} (P_{it}^{\mathrm{iso,f}})^{-\beta_i^{\mathrm{f}}}$. Inverting:

$$P_{it}^{\mathrm{iso,f}} = \left(\frac{D_{it}^{\mathrm{f}}}{\alpha_i^{\mathrm{f}} \gamma_i^{\mathrm{f}}} \right)^{-1/\beta_i^{\mathrm{f}}}, \qquad i \in_S,\ t \in . \tag{4.8}$$

Range over the demand support $[d_i^{\min}, d_i^{\max}]$:

$$P_i^{\mathrm{iso,f,max}} = \left(\tfrac{d_i^{\min}}{\alpha_i^{\mathrm{f}} \gamma_i^{\mathrm{f}}} \right)^{-1/\beta_i^{\mathrm{f}}}, \qquad P_i^{\mathrm{iso,f,min}} = \left(\tfrac{d_i^{\max}}{\alpha_i^{\mathrm{f}} \gamma_i^{\mathrm{f}}} \right)^{-1/\beta_i^{\mathrm{f}}}.$$

Step 2 — Normalization to $[0, 1]$.

$$\hat{P}_{it}^{\mathrm{iso,f}} = \frac{P_{it}^{\mathrm{iso,f}} - P_i^{\mathrm{iso,f,min}}}{P_i^{\mathrm{iso,f,max}} - P_i^{\mathrm{iso,f,min}}} \in [0, 1]. \tag{4.9}$$

Step 3 — Forward selling price.

$$\boxed{P^{\mathrm{f}}_{it} = P^{\max,\mathrm{f}}_{it}\ \hat{P}^{\mathrm{iso,f}}_{it}\ \in\ \left[0,\ P^{\max,\mathrm{f}}_{it}\right],} \qquad i \in_S,\ t \in . \tag{4.10}$$

Remanufactured Channel Price P^{r}_{kt}

Step 1 — Isoelastic demand-implied price. The isoelastic model for the secondary market posits $D^{\mathrm{r}}_{kt} = \alpha^{\mathrm{r}}_k \gamma^{\mathrm{r}}_k (P^{\mathrm{iso,r}}_{kt})^{-\beta^{\mathrm{r}}_k}$. Inverting:

$$P^{\mathrm{iso,r}}_{kt} = \left(\frac{D^{\mathrm{r}}_{kt}}{\alpha^{\mathrm{r}}_k\, \gamma^{\mathrm{r}}_k}\right)^{-1/\beta^{\mathrm{r}}_k}, \qquad k \in_M,\ t \in . \tag{4.11}$$

Range over the remanufactured demand support $[d^{\mathrm{r,min}}_k, d^{\mathrm{r,max}}_k]$:

$$P^{\mathrm{iso,r,max}}_k = \left(\tfrac{d^{\mathrm{r,min}}_k}{\alpha^{\mathrm{r}}_k \gamma^{\mathrm{r}}_k}\right)^{-1/\beta^{\mathrm{r}}_k}, \qquad P^{\mathrm{iso,r,min}}_k = \left(\tfrac{d^{\mathrm{r,max}}_k}{\alpha^{\mathrm{r}}_k \gamma^{\mathrm{r}}_k}\right)^{-1/\beta^{\mathrm{r}}_k}.$$

Step 2 — Normalization to $[0,1]$.

$$\hat{P}^{\mathrm{iso,r}}_{kt} = \frac{P^{\mathrm{iso,r}}_{kt} - P^{\mathrm{iso,r,min}}_k}{P^{\mathrm{iso,r,max}}_k - P^{\mathrm{iso,r,min}}_k}\ \in\ [0,1]. \tag{4.12}$$

Step 3 — Remanufactured selling price.

$$\boxed{P^{\mathrm{r}}_{kt} = P^{\max,\mathrm{r}}_{kt}\ \hat{P}^{\mathrm{iso,r}}_{kt}\ \in\ \left[0,\ P^{\max,\mathrm{r}}_{kt}\right],} \qquad k \in_M,\ t \in . \tag{4.13}$$

Bound Guarantee (Both Channels)

Common bound structure. For both channels, the normalized signal $\hat{P} \in [0,1]$ multiplied by the non-negative market ceiling $P^{\max} \geq 0$ yields a price in $[0, P^{\max}]$ without any additional constraint or min-operator.

Regime	Forward	Remanufactured
Maximum demand (liquid market)	$\hat{P}^{\mathrm{iso,f}}_{it} = 0 \Rightarrow P^{\mathrm{f}}_{it} = 0$	$\hat{P}^{\mathrm{iso,r}}_{kt} = 0 \Rightarrow P^{\mathrm{r}}_{kt} = 0$
Minimum demand (scarcity)	$\hat{P}^{\mathrm{iso,f}}_{it} = 1 \Rightarrow P^{\mathrm{f}}_{it} = P^{\max,\mathrm{f}}_{it}$	$\hat{P}^{\mathrm{iso,r}}_{kt} = 1 \Rightarrow P^{\mathrm{r}}_{kt} = P^{\max,\mathrm{r}}_{kt}$

Neither channel carries a cost floor. Prices are purely demand-driven: low realized demand signals scarcity and pushes the price toward the market ceiling; high demand signals a liquid market and pulls the price toward zero.

Parameter Generation

1. **Market ceilings $P_{it}^{\max,\mathrm{f}}$ and $P_{kt}^{\max,\mathrm{r}}$** — sourced from secondary-market benchmarks for the forward channel (module/cell resale platforms, electrode spot prices) and from certified-refurbished market benchmarks for the remanufactured channel. Seasonal perturbations $P_{it}^{\max} = P_i^{\max}(1+\delta\sin(2\pi t/T))$ capture periodic fluctuations.
2. **Isoelastic parameters $(\alpha_i^{\mathrm{f}}, \beta_i^{\mathrm{f}})$ and $(\alpha_k^{\mathrm{r}}, \beta_k^{\mathrm{r}})$** — estimated independently for each channel via log-log OLS regression:

$$\ln\left(D_{it}^{\mathrm{f}}/\gamma_i^{\mathrm{f}}\right) = \ln\alpha_i^{\mathrm{f}} - \beta_i^{\mathrm{f}}\ln P_{it}^{\mathrm{f}} + \varepsilon_{it}^{\mathrm{f}}, \qquad \ln\left(D_{kt}^{\mathrm{r}}/\gamma_k^{\mathrm{r}}\right) = \ln\alpha_k^{\mathrm{r}} - \beta_k^{\mathrm{r}}\ln P_{kt}^{\mathrm{r}} + \varepsilon_{kt}^{\mathrm{r}}.$$

   Require $\beta > 1$ for both; use industry benchmarks if estimation yields $\hat{\beta} \le 1$.
3. **Sensitivity coefficients γ_i^{f} and γ_k^{r}** — estimated via seasonal decomposition of the respective demand time series: $\hat{\gamma} = \bar{D}/\bar{\bar{D}}$.

4.3.5 Decision Variables

Table 4.4: Decision variables.

Symbol	Domain	Definition
q_t^i	$\mathbb{Z}_{\ge 0}$	Units of $i \in_D$ disassembled in period t
Y_{it}^{f}	$\mathbb{Z}_{\ge 0}$	Units of $i \in_S$ sold in the forward (primary) market in period t
Y_{kt}^{r}	$\mathbb{Z}_{\ge 0}$	Units of $k \in_M$ sold in the remanufactured (secondary) market in period t
r_t^k	$\mathbb{Z}_{\ge 0}$	Units of $k \in_M$ for which remanufacturing is *started* in period t; child components consumed immediately; rebuilt unit available in period $t + L_k^{\mathrm{rmfg}}$
I_{it}^{fwd}	$\mathbb{Z}_{\ge 0}$	End-of-period inventory of i in period t; for disassembly
I_{kt}^{rmfg}	$\mathbb{Z}_{\ge 0}$	End-of-period inventory of i in period t; for Remanufactured

4.3.6 Objective Function

$$\max\ Z = \underbrace{\sum_{i\in C^S}\sum_{t=1}^{T} P_{it}^{f} r_{it}^{f}}_{\text{forward sales revenue}} + \underbrace{\sum_{k\in C^M}\sum_{t=1}^{T} P_{kt}^{r} r_{kt}^{r}}_{\text{rmfg sales revenue}} - \underbrace{\sum_{i\in C^D}\sum_{t=1}^{T} C_i^{d} x_{it}}_{\text{disassembly cost}} - \underbrace{\sum_{k\in C^M}\sum_{t=1}^{T} C_k^{r} u_{kt}}_{\text{rmfg cost}} - \underbrace{\sum_{i}\sum_{t} h_i I_{it}^{\mathrm{fwd}}}_{\text{holding (fwd)}} - \underbrace{\sum_{k}\sum_{t} h_k I_{kt}^{\mathrm{rmfg}}}_{\text{holding (rmfg)}} - \underbrace{\sum_{i}\sum_{t} C^{\delta} w_{it}}_{\text{disposal}} \quad (4.14)$$

4.3.7 Constraints

Lead-time conventions. Define delayed disassembly: $\tilde{q}^{i}_{t-L_i^{\mathrm{dis}}} \equiv 0$ for $t \le L_i^{\mathrm{dis}}$. Define delayed remanufacturing completion: $\tilde{r}^{k}_{t-L_k^{\mathrm{rmfg}}} \equiv 0$ for $t \le L_k^{\mathrm{rmfg}}$. With all lead times currently equal to 1, child inventory from i disassembled in period $t-1$ arrives in period t, and a rebuild started in period $t-1$ is available in period t.

(A) Root Node Inventory Balance

$$I_{N_0,t-1} + S_t - q_t^{N_0} = I_{N_0,t}, \qquad \forall\, t \in, \quad I_{N_0,0} = 0.A \tag{4.15}$$

(B1) Inventory Balance — Intermediate Remanufacturable Nodes ($i \in_M$)

These nodes (N_4 and N_7) receive units from parent disassembly *and* from remanufacturing, and lose units to further disassembly, secondary-market sales, and forward sales. For every $i \in_M$ and $t \in$:

N4 forward pool (fed by disassembly; Y^f and r draw from here):

$$I^{\mathrm{fwd}}_{\mathrm{N4},t} = I^{\mathrm{fwd}}_{\mathrm{N4},t-1} + \alpha_{\mathrm{N0,N4}}\, q_{\mathrm{N0},t-1} - r_{\mathrm{N4},t} - q_{\mathrm{N4},t} - Y^{f}_{\mathrm{N4},t} - w_{\mathrm{N4},t} \tag{4.16}$$

N4 remanufactured pool (fed *only* by completed r runs; Y^r draws here):

$$I^{\mathrm{rmfg}}_{\mathrm{N4},t} = I^{\mathrm{rmfg}}_{\mathrm{N4},t-1} + r_{\mathrm{N4},t-1} - Y^{r}_{\mathrm{N4},t} - w^{\mathrm{rmfg}}_{\mathrm{N4},t} \tag{4.17}$$

N7 forward pool (also absorbs replacement cells consumed by N4-remanufacturing):

$$I^{\mathrm{fwd}}_{\mathrm{N7},t} = I^{\mathrm{fwd}}_{\mathrm{N7},t-1} + \alpha_{\mathrm{N4,N7}}\, q_{\mathrm{N4},t-1} - r_{\mathrm{N7},t} - \beta_{\mathrm{N4,N7}}\, r_{\mathrm{N4},t} - q_{\mathrm{N7},t} - Y^{f}_{\mathrm{N7},t} - w_{\mathrm{N7},t} \tag{4.18}$$

N7 remanufactured pool:

$$I^{\mathrm{rmfg}}_{\mathrm{N7},t} = I^{\mathrm{rmfg}}_{\mathrm{N7},t-1} + r_{\mathrm{N7},t-1} - Y^{r}_{\mathrm{N7},t} - w^{\mathrm{rmfg}}_{\mathrm{N7},t} \tag{4.19}$$

Flow terms.

- $\alpha_{p(i),i,\,t-L^{\mathrm{dis}}_{p(i)}}\, \tilde{q}^{\,p(i)}_{t-L^{\mathrm{dis}}_{p(i)}}$: fresh units arriving from disassembling the parent node.
- $\tilde{r}^{\,i}_{\,t-L_i^{\mathrm{rmfg}}}$: rebuilt units completing remanufacturing (started L_i^{rmfg} periods ago).
- q_t^i: units sent for further disassembly at this node ($i \in_D$, so always active for N_4 and N_7).
- $\mathbf{1}_{[p(i)\in_M]}\, \beta_{p(i),i}\, r_t^{p(i)}$: units consumed as components when *remanufacturing the parent* intermediate. Active only for N_7 (whose parent $N_4 \in_M$); zero for N_4 (whose parent $N_0 \notin_M$).

- Y_{it}^{f}: forward sales.
- Y_{it}^{r}: secondary-market sales of the remanufactured unit.

(B2) Inventory Balance — Leaf Nodes ($i \in_L$)

These nodes ($N_1, N_2, N_3, N_8, N_9, N_{10}, N_{11}$) have no outgoing disassembly arc and are not remanufactured. Their inventory balance is structurally simpler: inflows come only from parent disassembly, and outflows go only to forward sales (and possibly to parent remanufacturing consumption). For every $i \in_L$ and $t \in$:

$$\boxed{I_{i,t-1} + \alpha_{p(i),i,\, t-L^{\mathrm{dis}}_{p(i)}}\, \tilde{q}^{\,p(i)}_{t-L^{\mathrm{dis}}_{p(i)}} - \mathbf{1}_{[p(i)\in_M]}\, \beta_{p(i),i}\, r_t^{p(i)} - Y_{it}^{\mathrm{f}} = I_{it},} \qquad \forall\, i \in_L,\ t \in .B2 \tag{4.20}$$

Flow terms.

- $\alpha_{p(i),i,\, t-L^{\mathrm{dis}}_{p(i)}}\, \tilde{q}^{\,p(i)}_{t-L^{\mathrm{dis}}_{p(i)}}$: fresh units from parent disassembly.
- $\mathbf{1}_{[p(i)\in_M]}\, \beta_{p(i),i}\, r_t^{p(i)}$: units consumed when remanufacturing the parent. Active only for $N_8, \ldots, N_{11}$ (parent $N_7 \in_M$); zero for N_1, N_2, N_3 (parent $N_0 \notin_M$).
- Y_{it}^{f}: forward sales.

Explicit instantiations. For level-1 leaf nodes N_1, N_2, N_3 (parent $N_0 \notin_M$):

$$I_{i,t-1} + \alpha_{N_0,i,\, t-L^{\mathrm{dis}}_{N_0}}\, \tilde{q}^{\,N_0}_{t-L^{\mathrm{dis}}_{N_0}} - Y_{it}^{\mathrm{f}} = I_{it}.$$

For level-3 leaf nodes N_8, N_9, N_{10}, N_{11} (parent $N_7 \in_M$):

$$I_{i,t-1} + \alpha_{N_7,i,\, t-L^{\mathrm{dis}}_{N_7}}\, \tilde{q}^{\,N_7}_{t-L^{\mathrm{dis}}_{N_7}} - \beta_{N_7,i}\, r_t^{N_7} - Y_{it}^{\mathrm{f}} = I_{it}.$$

Why the split matters. Constraint **(B1)** is the richer equation: it captures the bidirectional role of $_M$ nodes — they are simultaneously *products* (sold forward or as remanufactured) and *assembly inputs* (consumed by their own parent's remanufacturing). Constraint **(B2)** is the simpler unidirectional equation for nodes that only flow out: disassembly-in, forward-sales-out. Separating them makes the model easier to audit, extend, and explain. Both equations are portable: to apply the model to a different BOM, assign each sellable node to $_M$ or $_L$, specify its parent $p(i)$ and β_{ij} values, and the two equations apply without modification.

(C) Disassembly Capacity

$$q_t^i \le Q_i^{\mathrm{dis}}, \qquad \forall\, i \in_D,\ t \in .C \tag{4.21}$$

$$w_{it} = max(0, q_t^i - Q_i^{\mathrm{dec}}) \qquad \forall\, i_V,\ t. \tag{4.22}$$

(D) Remanufacturing Capacity

$$r_t^k \le Q_k^{\text{rmfg}}, \qquad \forall\, k \in_M,\ t \in .D \tag{4.23}$$

(E) Inventory Capacity

$$I_{it} \le \text{Cap}_i, \qquad \forall\, i \in,\ t \in .E \tag{4.24}$$

(F) Forward Demand Cap

Forward sales cannot exceed the realized period demand:

$$Y_{it}^{\text{f}} \le D_{it}, \qquad \forall\, i \in_S,\ t \in .F \tag{4.25}$$

(G) Remanufactured Demand Cap

$$Y_{kt}^{\text{r}} \le D_{kt}^{\text{rmfg}}, \qquad \forall\, k \in_M,\ t \in .G \tag{4.26}$$

(H) Generalized Remanufacturing Feasibility

Remanufacturing can only draw on child inventory actually available at the start of the rebuild. For every intermediate $k \in_M$, every child $j \in \text{Ch}(k)$, and every period $t \in$:

$$\boxed{\beta_{k,j}\, r_t^k \;\le\; I_{j,t-1} + \alpha_{k,j,\,t-L_k^{\text{dis}}}\, \tilde{q}_{t-L_k^{\text{dis}}}^k,} \qquad \forall\, k \in_M,\ j \in \text{Ch}(k),\ t \in .H \tag{4.27}$$

The right-hand side is carry-over stock $I_{j,t-1}$ plus fresh units arriving from disassembling k.

Binding case. When $\alpha_{k,j,t} = 0$ on a critical arc, no new child inventory arrives. Constraint **(H)** then imposes $r_t^k \le \min_{j \in \text{Ch}(k)} I_{j,t-1}/\beta_{k,j}$: remanufacturing is feasible only when carry-over stock of *every* required component is sufficient. A single missing component type blocks all rebuilding of k.

(I) Non-Negativity and Integrality

$$q_t^i,\ Y_{it}^{\text{f}},\ Y_{kt}^{\text{r}},\ r_t^k,\ I_{it} \;\in\; \mathbb{Z}_{\ge 0}, \qquad \forall\, i \in,\ k \in_M,\ t \in .I \tag{4.28}$$

4.3.8 Complete Model Statement

Complete MILP — Generalized Disassembly Planning **Period-start sampling** (before solving period t):

- Draw $\alpha_{ij,t} \sim \mathcal{U}\{0, \ldots, \beta_{ij}\}$ for each $(i, j) \in$.
- Draw $D_{it} \sim \mathcal{U}[\lceil d_i^{\min} \rceil, \lfloor d_i^{\max} \rfloor]$ for each $i \in_S$.

Preprocessing (scalar arithmetic, no new variables):

$$P_{it}^{\text{iso}} = \left(\frac{D_{it}}{\alpha_i \, \gamma_i} \right)^{-1/\beta_i}$$

$$\hat{P}_{it}^{\text{iso}} = \frac{P_{it}^{\text{iso}} - P_i^{\text{iso,min}}}{P_i^{\text{iso,max}} - P_i^{\text{iso,min}}} \in [0, 1]$$

$$P_{it} = P_{it}^{\max} \, \hat{P}_{it}^{\text{iso}} \in [0, P_{it}^{\max}]$$

Objective: Maximise Z as in (4.42).

Subject to:

(A) Root inventory balance
(B1) Inventory balance — intermediate nodes ($\forall\, i \in_M,\ t \in$)
(B2) Inventory balance — leaf nodes ($\forall\, i \in_L,\ t \in$)
(C) Disassembly capacity ($\forall\, i \in_D,\ t \in$)
(D) Remanufacturing capacity ($\forall\, k \in_M,\ t \in$)
(E) Inventory capacity ($\forall\, i \in,\ t \in$)
(F) Forward demand cap ($\forall\, i \in_S,\ t \in$)
(G) Remanufactured demand cap ($\forall\, k \in_M,\ t \in$)
(H) Remanufacturing feasibility ($\forall\, k \in_M,\ j \in \text{Ch}(k),\ t \in$)
(I) Non-negativity and integrality

Table 4.5: Constraint inventory (T = number of planning periods).

Label	Description	Applies to	Count
(A)	Root inventory balance	N_0	T
(B1)	Inv. balance — intermediates	$i \in_M$ (2 nodes: N_4, N_7)	$2T$
(B2)	Inv. balance — leaf nodes	$i \in_L$ (7 nodes)	$7T$
(C)	Disassembly capacity	$i \in_D$ (3 nodes)	$3T$
(D)	Remanufacturing capacity	$k \in_M$ (2 nodes)	$2T$
(E)	Inventory capacity	$i \in$ (10 nodes)	$10T$
(F)	Forward demand cap	$i \in_S$ (9 nodes)	$9T$
(G)	Remfg demand cap	$k \in_M$ (2 nodes)	$2T$
(H)	Remfg feasibility	$k \in_M,\ j \in \text{Ch}(k)$ (5 pairs)	$5T$
	Total		**42T**

4.4 Structural Analysis and Economic Interpretation

4.4.1 Yield: Two Operational Modes

High-yield periods ($\alpha_{ij,t} \approx \beta_{ij}$). Disassembly replenishes child inventory at its maximum rate. Forward sales can be served without drawing down carry-over stock. Remanufacturing benefits from abundant component supply; constraint **(H)** is slack. The optimiser focuses on the revenue trade-off between the forward and secondary channel.

Low-yield periods ($\alpha_{ij,t} \approx 0$). Little or no new child inventory arrives from disassembly. The facility relies entirely on carry-over $I_{i,t-1}$. Constraint **(H)** binds, limiting remanufacturing volume. The optimiser shifts toward holding inventory until a high-yield period replenishes stock.

4.4.2 Interaction: Yield × Demand

The two quantities interact through the composite price P_{it} and constraints **(F)** and **(H)**:

- **Low D_{it} (scarcity), high yield:** $\hat{P}^{\text{iso}}_{it}$ is near 1 (scarcity premium), pushing P_{it} toward $P^{\max}_{it}$. Abundant fresh inventory from disassembly and a high per-unit price maximise both volume and margin.
- **High D_{it} (abundant market), low yield:** $\hat{P}^{\text{iso}}_{it}$ is near 0, lowering P_{it} toward zero. Scarce inventory from disassembly must be allocated between forward sales (near-zero margin when demand is high) and remanufacturing (fixed margin $P^{\text{rmfg}}_{k} - \kappa_k - C^{\text{rmfg}}_{k}$), with constraint **(H)** potentially binding.
- **High D_{it}, high yield:** P_{it} is near zero but volume is unconstrained. The optimiser saturates forward demand $Y^{\text{f}}_{it} = D_{it}$ and directs surplus inventory to remanufacturing, where the fixed margin is more attractive.
- **Low D_{it}, low yield:** high margin per unit (P_{it} near $P^{\max}_{it}$) but scarce supply. The optimiser prioritises the highest-margin channel and carries over inventory (at holding cost h_i) to future periods.

4.4.3 Structure of the Split Inventory Balance

The explicit separation of constraints **(B1)** and **(B2)** reflects the structurally distinct roles of the two node classes:

Node class	From disassembly	From remfg	To disassembly	To remfg sales
$_M$ (B1)	x			
$_L$ (B2)	x	×	×	×

Constraint **(B1)** accounts for all four flow directions; constraint **(B2)** accounts only

for inflow from parent disassembly and outflow via forward sales (and consumption by a remanufactured parent, if applicable).

4.4.4 Generality of the Constraint Structure

Constraints **(B1)**, **(B2)**, and **(H)** are formulated for an arbitrary AND-arc hierarchy. To apply the model to a different product, one need only: (i) define the level partition $_{\ell}$, (ii) specify the parent function $p(i)$, (iii) partition sellable nodes into $_{M}$ and $_{L}$, (iv) set the yield upper bounds β_{ij}, and (v) calibrate the pricing parameters per Section 4.3.4. All constraint equations remain identical.

4.5 Implementation Notes

1. **Period-start sampling.** At the start of period t, independently draw:

$$\begin{aligned} &\alpha_{ij,t} \sim \mathcal{U}\{0, \ldots, \beta_{ij}\} && \text{for each } (i,j) \in, \\ &D_{it} \sim \mathcal{U}[\lceil a + \text{scale}_i \cdot b \rceil,\ \lfloor c + \text{scale}_i \cdot d \rfloor] && \text{for each } i \in_S . \end{aligned}$$

2. **Preprocessing before the MILP solve.** All quantities below are scalar constants; no auxiliary variables are required:

$$\begin{aligned} P_{it}^{\text{iso}} &= \left(\frac{D_{it}}{\alpha_i \, \gamma_i} \right)^{-1/\beta_i}, \\ \hat{P}_{it}^{\text{iso}} &= \frac{P_{it}^{\text{iso}} - P_i^{\text{iso,min}}}{P_i^{\text{iso,max}} - P_i^{\text{iso,min}}} \ \in\ [0,1], \\ P_{it} &= P_{it}^{\max} \, \hat{P}_{it}^{\text{iso}} \ \in\ [0,\, P_{it}^{\max}]. \end{aligned}$$

   Guard against division by zero: if $P_i^{\text{iso,max}} = P_i^{\text{iso,min}}$ (degenerate demand range), set $\hat{P}_{it}^{\text{iso}} = 0.5$. Require $\gamma_i > 0$; if $\gamma_{\min} = 0$, use a small floor $\varepsilon > 0$.

3. **Lead-time initialisation.** Set $\tilde{q}^i_{t-L_i^{\text{dis}}} = 0$ for $t \le L_i^{\text{dis}}$ (all $i \in_D$) and $\tilde{r}^k_{t-L_k^{\text{rmfg}}} = 0$ for $t \le L_k^{\text{rmfg}}$ (all $k \in_M$). With current lead times equal to 1, both delays apply only in period $t = 1$.

4. **Lead time modification.** To change lead times, update L_i^{dis} or L_k^{rmfg}; constraints **(B1)**, **(B2)**, and **(H)** automatically incorporate the new values without structural changes.

5. **Base price computation.** Use $\bar{\alpha}_{ij} = \beta_{ij}/2$ in . If empirical recovery rates are available, replace $\beta_{ij}/2$ with the measured mean yield.

6. **Model size and solver.** For $T = 52$ (weekly, one year): $42 \times 52 = 2{,}184$ functional constraints, approximately 1,404 non-negative integer variables. Directly solvable with PuLP/CBC, Gurobi, or CPLEX without decomposition.

4.6 Conclusion

This model has presented a fully-integer multi-period MILP for disassembly planning of EOL Nissan Leaf 24 kWh battery packs, based on a four-level AND-arc BOM with 10 nodes and 9 disassembly arcs. Five structural features are integrated:

1. **integer yield:** $\alpha_{ij,t} \sim \mathcal{U}\{0, \ldots, \beta_{ij}\}$ per AND arc per period; maximum yield equals the remanufacturing assembly ratio.
2. **Sensitivity-driven integer demand:** $D_{it} \sim \mathcal{U}[\lceil a + \text{scale}_i \cdot b \rceil, \lfloor c + \text{scale}_i \cdot d \rfloor]$ with $\text{scale}_i = (\gamma_i - \gamma_{\min})/(\gamma_{\max} - \gamma_{\min})$, $a = 2, b = 4, c = 10, d = 6$.
3. **Normalized isoelastic pricing** (Couzon et al., 2019):

$$P_{it} = P_{it}^{\max}\, \hat{P}_{it}^{\text{iso}}, \quad \hat{P}_{it}^{\text{iso}} = \frac{(D_{it}/\alpha_i\gamma_i)^{-1/\beta_i} - P_i^{\text{iso,min}}}{P_i^{\text{iso,max}} - P_i^{\text{iso,min}}},$$

   guaranteed by construction to lie in $[0, P_{it}^{\max}]$. The price is purely demand-driven with no cost floor; κ_i is retained solely for the remanufactured channel price $P_k^{\text{rmfg}} = \kappa_k + C_k^{\text{rmfg}}$.
4. **Shared inventory with per-level capacity limits:** single I_{it} pool; $q_t^i \le Q_i^{\text{dis}}$, $r_t^k \le Q_k^{\text{rmfg}}$; lead times L_i^{dis} and L_k^{rmfg} (all currently set to 1).
5. **Split level-based inventory constraints:** constraint **(B1)** for intermediate remanufacturable nodes ($_M = \{N_4, N_7\}$) and constraint **(B2)** for leaf nodes ($_L = \{N_1, N_2, N_3, N_8, N_9, N_{10}, N_{11}\}$), together with the generalized remanufacturing feasibility **(H)**, replace all node-specific constraints and are directly portable to any AND-arc product BOM.

The model has **42T** functional constraints and no binary variables, making it directly solvable for standard planning horizons with off-the-shelf integer programming solvers. The forward selling price P_{it} is precomputed as a scalar before each MILP solve and introduces no additional variables or constraints.

4.7 The Network Model

4.7.1 Node Set CC

Every component appearing in the BOM hierarchy is assigned a unique node identifier. Absolute counts are derived from the pack-level quantities shown in the diagram.

Table 4.6: Node set C with identifiers, labels, and absolute quantities in one complete battery pack.

ID	Node Label	Total in Pack	Level / Role
N_0	Battery Pack	1	Level 0 — Root assembly
N_1	Outer Enclosure	1	Level 1 — Structural housing
N_2	Air-Cooling Manifold	1	Level 1 — Thermal management
N_3	Pack BMS (LBC)	1	Level 1 — Electronics / control
N_4	Battery Modules	48	Level 1 — Serviceable sub-units
N_5	AESC Pouch Cells (2S2P)	192	Level 2 — Electrochemical unit
N_6	LMO Cathode	192	Level 3 — Electrode (positive)
N_7	MCMB Anode	192	Level 3 — Electrode (negative)
N_8	Separator PE/PP	192	Level 3 — Ionic membrane
N_9	Electrolyte $LiPF_6$	192	Level 3 — Ion-transport medium

$|C| = 10$ nodes Total cell count: $48 \times 4 = 192$

4.8 Edge Set AA — Directed Multigraph

Each parent–child relationship in the BOM generates **two directed arcs**: one disassembly arc ($\delta = -1$, parent $\rightarrow$ child) and one assembly arc ($\delta = +1$, child $\rightarrow$ parent). The quantity $q(i, j)$ is placed on the arc and denotes the number of child units per parent unit.

Table 4.7: Complete arc set A. Every row appears as a bidirectional pair. q_{unit} = quantity per parent; q_{abs} = absolute count in pack.

Arc #	Source	Target	q_{unit}	q_{abs}	Type (δ)
e_{01}	N_0 Battery Pack	N_1 Outer Enclosure	1	1	**Disassembly** (-1)
e_{02}	N_1 Outer Enclosure	N_0 Battery Pack	1	1	**Assembly** ($+1$)
e_{03}	N_0 Battery Pack	N_2 Air-Cooling Manifold	1	1	**Disassembly** (-1)
e_{04}	N_2 Air-Cooling Manifold	N_0 Battery Pack	1	1	**Assembly** ($+1$)
e_{05}	N_0 Battery Pack	N_3 Pack BMS (LBC)	1	1	**Disassembly** (-1)
e_{06}	N_3 Pack BMS (LBC)	N_0 Battery Pack	1	1	**Assembly** ($+1$)

Arc #	Source	Target	q_{unit}	q_{abs}	Type (δ)
e_{07}	N_0 Battery Pack	N_4 Battery Modules	48	48	**Disassembly** (-1)
e_{08}	N_4 Battery Modules	N_0 Battery Pack	48	48	**Assembly** ($+1$)
e_{09}	N_4 Battery Modules	N_5 AESC Pouch Cells	4	192	**Disassembly** (-1)
e_{10}	N_5 AESC Pouch Cells	N_4 Battery Modules	4	192	**Assembly** ($+1$)
e_{11}	N_5 AESC Pouch Cells	N_6 LMO Cathode	1	192	**Disassembly** (-1)
e_{12}	N_6 LMO Cathode	N_5 AESC Pouch Cells	1	192	**Assembly** ($+1$)
e_{13}	N_5 AESC Pouch Cells	N_7 MCMB Anode	1	192	**Disassembly** (-1)
e_{14}	N_7 MCMB Anode	N_5 AESC Pouch Cells	1	192	**Assembly** ($+1$)
e_{15}	N_5 AESC Pouch Cells	N_8 Separator PE/PP	1	192	**Disassembly** (-1)
e_{16}	N_8 Separator PE/PP	N_5 AESC Pouch Cells	1	192	**Assembly** ($+1$)
e_{17}	N_5 AESC Pouch Cells	N_9 Electrolyte $LiPF_6$	1	192	**Disassembly** (-1)
e_{18}	N_9 Electrolyte $LiPF_6$	N_5 AESC Pouch Cells	1	192	**Assembly** ($+1$)

$|A| = 18$ directed arcs (**9 disassembly** + **9 assembly**)

4.9 Mathematical Form (Option C)

4.9.1 Set definitions

$$C = \{N_0,\ N_1,\ N_2,\ N_3,\ N_4,\ N_5,\ N_6,\ N_7,\ N_8,\ N_9\} \quad |C| = 10 \tag{4.29}$$

$$A \subseteq C \times C \times \mathbb{Z}^+ \times \{-1, +1\} \tag{4.30}$$

Each arc is a 4-tuple $(i,\ j,\ q(i,j),\ \delta)$ where:

- i = source node, j = target node
- $q(i,j) \in \mathbb{Z}^+$ = number of child units per parent unit
- $\delta = -1$ (disassembly, parent $\rightarrow$ child); $\delta = +1$ (assembly, child $\rightarrow$ parent)

4.9.2 Quantity function qq

$$q(N_0,\ N_1) = q(N_0,\ N_2) = q(N_0,\ N_3) = 1 \tag{4.31}$$

$$q(N_0,\ N_4) = 48 \tag{4.32}$$

$$q(N_4,\ N_5) = 4 \tag{4.33}$$

$$q(N_5,\ N_6) = q(N_5,\ N_7) = q(N_5,\ N_8) = q(N_5,\ N_9) = 1 \tag{4.34}$$

Symmetry: $q(i,j) = q(j,i)$ — quantity is conserved across both flow directions.

4.9.3 Direction indicator

$$\delta(i,j) = \begin{cases} -1 & \text{if } i \text{ is the parent of } j \quad \textit{(Disassembly flow)} \\ +1 & \text{if } j \text{ is the parent of } i \quad \textit{(Assembly flow)} \end{cases} \tag{4.35}$$

4.9.4 Absolute quantity at pack level

For any node N_k at depth d below the root, the absolute count in one complete pack is:

$$Q_{\text{abs}}(N_k) = \prod_{(i,j) \in \text{path}(N_0 \to N_k)} q(i,j) \tag{4.36}$$

Applied to all nodes:

$$Q_{\text{abs}}(N_4) = q(N_0, N_4) = 48 \tag{4.37}$$

$$Q_{\text{abs}}(N_5) = q(N_0, N_4) \times q(N_4, N_5) = 48 \times 4 = 192 \tag{4.38}$$

$$Q_{\text{abs}}(N_6) = Q_{\text{abs}}(N_7) = Q_{\text{abs}}(N_8) = Q_{\text{abs}}(N_9) = 192 \times 1 = 192 \tag{4.39}$$

4.9.5 Flow conservation check ΦPhi

$$\Phi_{\text{cells}} = q(N_0, N_4) \times q(N_4, N_5) = 48 \times 4 = \mathbf{192} \tag{4.40}$$

$$\Phi_{\text{electrodes}} = Q_{\text{abs}}(N_5) \times q(N_5, N_6) = 192 \times 1 = \mathbf{192} \tag{4.41}$$

Summary

$$\begin{aligned} |C| &= 10 \text{ nodes} \\ |A| &= 18 \text{ directed arcs} \quad (9 \text{ disassembly} + 9 \text{ assembly}) \\ Q_{\text{abs}}(N_4) &= 48 \text{ modules} \\ Q_{\text{abs}}(N_5) &= 192 \text{ cells} \\ Q_{\text{abs}}(N_{6\text{–}9}) &= 192 \text{ each (cathode, anode, separator, electrolyte)} \\ \Phi_{\text{cells}} &= 48 \times 4 = 192 \\ \Phi_{\text{electrodes}} &= 192 \times 1 = 192 \end{aligned}$$

Table 4.8: How each element of the directed graph is used in engineering and operations applications.

Application	Graph elements used	Formulation
Disassembly planning	All $\delta = -1$ arcs	Traverse from N_0 downward; sequence arcs by tooling constraint. Yield at each level = $q(i, j)$ units per pass.
Assembly sequencing	All $\delta = +1$ arcs	Reverse traversal from leaf nodes to N_0; enforce $q(j, i)$ units consumed per parent build.
Reverse logistics	q_{abs}, arc costs c_{ij}	Minimise $\sum_{(i,j)\in A} c_{ij}\, x_{ij}$ subject to flow conservation Φ.
Spare parts stocking	q_{abs} column	Stock level for $N_k = Q_{\text{abs}}(N_k) \times \alpha$ where α is safety factor.
ILP optimisation	Full arc set A, q, δ	$x_{ij} \in \mathbb{Z}^+$; enforce $\sum_{j:(i,j)\in A} x_{ij} = Q_{\text{abs}}(N_i)$ for all $N_i \in C$.
End-of-life recycling	$\delta = -1$ arcs, N_6–N_9	Follow disassembly path to leaf nodes; assign material-recovery value per 192 units of LMO cathode, graphite anode, separator, electrolyte.

4.10 Data generation

4.10.1 Literature Review

4.10.2 Research Problem and Context

this thesis addresses the multi-period disassembly planning problem for end-of-life (EOL) Nissan Leaf 24 kWh battery packs (model years 2011–2015, ZE0/AZE0 platform, AESC LEV50 LMO/Graphite cells). It formulates a Mixed-Integer Linear Program (MILP) over a four-level AND-arc Bill-of-Materials (BOM) hierarchy with 10 nodes and 9 disassembly arcs, incorporating yield, sensitivity-driven demand, dual-channel normalized isoelastic pricing, shared inventory, and split level-based inventory constraints.

4.10.3 Related Literature

Disassembly Planning – Foundational Works

Gupta and Taleb (1994) Gupta and Taleb (1994) introduced the first formal disassembly planning framework using Material Requirements Planning (MRP) logic. Lambert (2002) Lambert (2002) extended this to AND/OR graph representations, establishing the structural foundation used in the present paper. The work of Thierry et al. (1995) Thierry et al. (1995) formalized the taxonomy of product recovery options—reuse, remanufacturing, recycling—that motivates the dual-channel architecture .

Disassembly Models

Xanthopoulos and Iakovou (2009) Xanthopoulos and Iakovou (2009) first modeled yield in disassembly as a Bernoulli process; the uniform integer formulation $\alpha_{ij,t} \sim \mathcal{U}\{0, \ldots, \beta_{ij}\}$ is a natural extension. Zikopoulos and Tagaras (2008) Zikopoulos and Tagaras (2008) showed that yield significantly impacts inventory policy in reverse logistics. Kim et al. (2009) Kim et al. (2009) proposed the multi-period MRP-style MILP structure that underpins the present model. Rahme et al. (2023) Rahme et al. (2023) incorporated returns into a rolling-horizon disassembly MILP for electronic waste, obtaining a similar scenario-based approach.

Isoelastic Pricing in Circular Economy Models

The isoelastic (constant-elasticity) demand model $D = \alpha\gamma P^{-\beta}$ has been widely applied in revenue management. Couzon, Ouazene, and Yalaoui (2019) Couzon et al. (2019) introduced its use in disassembly planning, deriving the inverse demand function and showing that price elasticity $\beta > 1$ is required for finite profit-maximizing prices to exist. The normalization step $\hat{P}^{\text{iso}} \in [0, 1]$ is an original contribution that ensures $P_{it} \in [0, P_{it}^{\max}]$ without auxiliary variables.

EV Battery End-of-Life Management

The global stock of EOL Nissan Leaf 24 kWh packs is significant. Cumulative Leaf sales exceeded 650,000 units by July 2023 Nissan Motor Co. (2023), with first-generation (2011–2015) vehicles now approaching or beyond 10-year EOL thresholds. Ahmadi et al. (2020) Ahmadi et al. (2020) surveyed end-of-life strategies and reported that remanufacturing at the module level achieves 60–80% cost savings relative to new pack production. The Nissan–Sumitomo joint venture in Japan remanufactures 24 kWh packs for approximately $3,000, recovering modules with $\geq$ 80% state-of-health Green Car Future (2022).

Harper et al. (2019) Harper et al. (2019) modeled the global lithium-ion battery waste stream and projected annual EOL volumes reaching 11 million units by 2030. Richa et al. (2017) Richa et al. (2017) specifically analyzed the US Nissan Leaf fleet, estimating 15,000–30,000 pack retirements per year through 2025.

Battery Disassembly Cost Studies

Lander et al. (2023) Lander et al. (2023) conducted a techno-economic analysis of five commercially available EV battery pack designs, finding that full manual disassembly of a 24 kWh Nissan Leaf pack requires approximately 3.5–5 hours of labor at $25–40/h, yielding a total disassembly cost of $87–200 per pack. Rosenberg et al. (2022) Rosenberg et al. (2022) measured field disassembly times and costs, reporting pack-level disassembly costs of approximately $120 under typical workshop conditions. Liang et al. (2025) Liang et al. (2025) demonstrated that automated robotic disassembly cells can reduce per-module disassembly cost by 40–60% relative to manual operations.

Market Prices for Nissan Leaf Components

Secondary-market prices for Gen-1 (LMO/Graphite, 2011–2015) Nissan Leaf battery modules have been documented extensively. Greentec Auto lists bulk Gen-1 modules at $55–60/kWh (second-life use), equating to approximately $27.50–30.00 per 500 Wh module Greentec Auto (2024). Battery Hookup lists 7.6 V / 500 Wh modules at approximately $40 per unit Battery Hookup (2024). OGSolarStore lists sets of 7 modules at $60/kWh OGSolarStore (2024). Remanufactured certified modules command a premium of 80–150% over used modules, placing certified Gen-1 modules at approximately $55–80 FindMyElectric (2025); Greentec Auto (2024).

For the Battery Management System (BMS/LBC), secondary-market prices range from $150–400 depending on condition Recurrent Auto (2024). Outer enclosures (structural housing) sell for $30–80 on platforms such as eBay and RockAuto. Cooling manifolds (air-cooled Gen-1) have lower residual value at $15–40.

At the sub-cell level, the LMO cathode, MCMB graphite anode, polyethylene/polypropylene

separator, and $LiPF_6$ electrolyte are primarily traded as black-mass inputs to hydrometallurgical recycling. Market prices for these electrode-level materials are reviewed in Section **??**.

Electrode and Electrolyte Material Prices

Manganese (the primary metal in LMO cathode) is significantly cheaper than cobalt or nickel: approximately \$1.5–2.5/kg in 2024 S&P Global (2024). The LMO cathode powder price at industrial scale is approximately \$4–8/kg NEI Corporation (2024). In the AESC LEV50 cell, the cathode contributes approximately 80–120 g of LMO per cell (estimated from 24 kWh / 192 cells / 125 Wh/kg specific energy). At \$6/kg, the material value of the LMO cathode per cell is approximately \$0.48–0.72.

MCMB (mesocarbon microbead) graphite anode powder is priced at \$8–15/kg at industrial scale Benchmark Mineral Intelligence (2024). The separator (PE/PP trilayer, 25 μm, approximately 4 g/cell) has a value of \$0.05–0.15 per cell Liang et al. (2025). $LiPF_6$ electrolyte (approximately 1.2 g/cell for a pouch cell of this size) is priced at approximately \$15–25/kg, yielding \$0.02–0.03/cell IECM Group (2024).

BloombergNEF Battery Price Benchmark

BloombergNEF's 2024 Battery Price Survey documents pack-level costs falling from \$732/kWh in 2010 to \$111/kWh in 2024, a trajectory confirming that EOL 24 kWh packs from 2011–2015 were manufactured at a historically high cost BloombergNEF (2024). This is relevant for computing the cost-recovery base price κ_i (accumulated disassembly cost from root to node i at expected yields).

4.11 Extracted Parameters – from Article

Table 4.9: All values are **[R]** real (from article).

Symbol	Value(s)	Description	Source
Network structure			
$\lvert C\rvert$	10	Total nodes	Article, Sec. 2.1
$\lvert C_S\rvert$	9	Sellable nodes	Article, Sec. 2.3
$\lvert C_D\rvert$	3	Disassembly nodes	Article, Sec. 2.3
$\lvert C_M\rvert$	2	Remanufacturable intermediates	Article, Sec. 2.3
$\lvert C_L\rvert$	7	Leaf nodes	Article, Sec. 2.3
Q^{abs}_{N0}	1	Packs per EOL input unit	Article, Table 1
$Q^{\text{abs}}_{N1,N2,N3}$	1 each	Enclosure, cooling, BMS per pack	Article, Table 1
Q^{abs}_{N4}	48	Battery modules per pack	Article, Table 1
Q^{abs}_{N7}	192	Pouch cells per pack	Article, Table 1
$Q^{\text{abs}}_{N8–N11}$	192 each	Electrode / separator / electrolyte	Article, Table 1
Yield upper bounds (AND arcs)			
$\beta_{N0,N1}$	1	Max yield: enclosure	Article, Eq. (3)
$\beta_{N0,N2}$	1	Max yield: air-cooling manifold	Article, Eq. (3)
$\beta_{N0,N3}$	1	Max yield: BMS	Article, Eq. (3)
$\beta_{N0,N4}$	48	Max yield: modules	Article, Eq. (3)
$\beta_{N4,N7}$	4	Max yield: cells per module	Article, Eq. (3)
$\beta_{N7,N8}$	1	Max yield: LMO cathode	Article, Eq. (3)
$\beta_{N7,N9}$	1	Max yield: MCMB anode	Article, Eq. (3)
$\beta_{N7,N10}$	1	Max yield: PE/PP separator	Article, Eq. (3)
$\beta_{N7,N11}$	1	Max yield: $LiPF_6$ electrolyte	Article, Eq. (3)
Demand model parameters			
a	2	Demand range lower-bound intercept	Article, Eq. (6)
b	4	Demand range lower-bound slope	Article, Eq. (6)
c	10	Demand range upper-bound intercept	Article, Eq. (6)
d	6	Demand range upper-bound slope	Article, Eq. (6)
Lead times (current setting)			
L_i^{dis}	1, $\forall i \in C_D$	Disassembly lead time	Article, Sec. 3.2
L_k^{rmfg}	1, $\forall k \in C_M$	Remanufacturing lead time	Article, Sec. 3.2
Model size			
Constraints	$42T$	Functional constraints	Article, Table 5
Binary vars	0	No binary variables	Article, Sec. 5

4.12 Missing Data Analysis

The following parameter categories are *not* supplied and must be sourced externally or generated synthetically:

1. **Market price ceilings** $P_{it}^{\max,f}$ and $P_{kt}^{\max,r}$ – for all 9 forward-channel nodes and 2 remanufactured-channel nodes, across T periods.
2. **Isoelastic parameters** (α_i^f, β_i^f) and (α_k^r, β_k^r) – demand-model elasticity and base-demand scalars.
3. **Sensitivity coefficients** γ_i^f, γ_k^r and range $[\gamma_{\min}, \gamma_{\max}]$.
4. **Disassembly costs** C_i^{dis} per node $i \in C_D$.
5. **Remanufacturing costs** C_k^{rmfg} per node $k \in C_M$.
6. **Holding costs** h_i per node $i \in C$, per period.
7. **Capacity parameters** Q_i^{dis}, Q_k^{rmfg}, Cap_i.
8. **EOL supply** S_t (packs arriving per period t).
9. **Remanufactured demand bounds** $d_k^{r,\min}$, $d_k^{r,\max}$ for $k \in C_M$.
10. **Seasonal perturbation amplitude** δ for $P_{it}^{\max}$.
11. **Initial inventory** $I_{i,0}$.

4.13 Real Data Collected

4.13.1 Secondary-Market Prices for Forward Channel

Table 4.10 reports market prices collected from verified secondary-market sources (Greentec Auto, Battery Hookup, OGSolarStore, eBay aggregation, Recurrent Auto). These provide the empirical basis for $P_i^{\max,f}$ (the time-invariant component before seasonal perturbation).

Table 4.10: Observed secondary-market prices for forward channel nodes. **[R]** Real data (R).

Node	Component	Low ($)	High ($)	Adopted $\bar{P}^{\max,f}$ ($)	Source
N1	Outer Enclosure	30	80	55	eBay / RockAuto Recurrent Auto (2024)
N2	Air-Cooling Manifold	15	40	27	eBay secondary market
N3	Pack BMS (LBC)	150	400	250	Greentec Auto (2024); Recurrent Auto (2024)
N4	Battery Module	27	55	40	Battery Hookup (2024); Greentec Auto (2024)
N7	AESC Pouch Cell	5	15	9	Encatsu (2024)
N8	LMO Cathode (per cell)	0.40	0.80	0.60	NEI Corporation (2024); S&P Global (2024)
N9	MCMB Anode (per cell)	0.20	0.60	0.40	Benchmark Mineral Intelligence (2024)
N10	PE/PP Separator (per cell)	0.05	0.20	0.12	Liang et al. (2025)
N11	$LiPF_6$ Electrolyte (per cell)	0.02	0.08	0.05	IECM Group (2024)

4.13.2 Remanufactured Channel Prices

Table 4.11: Observed prices for remanufactured (certified) components. **[R]** Real (R).

Node	Component	Low ($)	High ($)	Adopted $\bar{P}^{\max,r}$ ($)	Source
N4	Module (certified refurb)	55	120	85	FindMyElectric (2025); Greentec Auto (2024)
N7	Cell (certified refurb)	10	25	17	Encatsu (2024)

4.13.3 Disassembly Cost Literature Benchmarks

Lander et al. (2023) Lander et al. (2023) report full manual disassembly of a 24 kWh pack costs \$87–200 (3.5–5 h at \$25–40/h). Rosenberg et al. (2022) Rosenberg et al. (2022) measured \$120 under typical workshop conditions. Liang et al. (2025) Liang et al. (2025) show robotic disassembly reduces per-module cost by 40–60%.

4.13.4 Pack-Level Battery Economics

- BloombergNEF (2024) BloombergNEF (2024): pack-level manufacturing cost \$111/kWh in 2024; 24 kWh = \$2,664 replacement cost.
- Nissan–Sumitomo remanufacturing (Japan): \$3,000 per certified pack Green Car Future (2022).
- Recurrent Auto (2024) Recurrent Auto (2024): refurbished 24 kWh packs at \$3,000–5,000.

4.14 Synthetic Data Generation Methodology

4.14.1 Guiding Principles

Where real data are unavailable or insufficient for full parameterization, synthetic values are generated according to the following hierarchy: (1) anchor to verified real-data benchmarks; (2) derive by physical or accounting identity; (3) draw from calibrated distributions consistent with the paper's context and domain norms.

4.14.2 Market Price Ceilings $P_{it}^{\max,f}$ and $P_{kt}^{\max,r}$

The time-invariant base ceiling $\bar{P}_i^{\max}$ is set to the *adopted* values in Tables 4.10–4.11. Seasonal perturbation :

$$P_{it}^{\max} = \bar{P}_i^{\max}\Big(1 + \delta \sin(2\pi t/T)\Big), \quad \delta = 0.10,$$

where $\delta = 0.10$ represents a ±10% seasonal swing, consistent with observed quarterly volatility in EV component markets Recurrent Auto (2024). **[I]** Inferred from market volatility data.

4.14.3 Disassembly Costs $C_i^{\mathbf{dis}}$

Pack disassembly ($i = N0$): \$120 total, consistent with Rosenberg et al. (2022) Rosenberg et al. (2022). **[R]** R.

Module disassembly ($i = N4$): Pack disassembly cost allocated proportionally to module yield:

$$C_{N4}^{\text{dis}} = \frac{\$120}{48} \times \eta_{\text{mod}} \approx \$2.50 \text{ per module},$$

where $\eta_{\text{mod}} = 1.0$ reflects that module separation is the dominant labor step. An

additional inspection and testing overhead of \$1.50/module is added based on Liang et al. (2025) Liang et al. (2025), giving $C_{N4}^{\text{dis}} = \$4.00$/module. **[I]** I.

Cell disassembly ($i = N7$): Module-to-cell disassembly is more delicate. At \$4.00/module and 4 cells/module, the base allocation is \$1.00/cell. An additional safety handling premium of \$0.50 yields $C_{N7}^{\text{dis}} = \$1.50$/cell. **[I]** I.

4.14.4 Remanufacturing Costs C_k^{rmfg}

Module remanufacturing ($k = N4$): Consists of cell sorting, re-balancing, welding, and re-casing. Based on Greentec Auto's certified module premium of \$45 over used price (\$40), and deducting labor margin of 30%, the estimated cost is:

$$C_{N4}^{\text{rmfg}} \approx \$45 \times 0.70 = \$31.50 \approx \$30/\text{module}. \quad \textbf{[I]}\ I$$

Cell remanufacturing ($k = N7$): Includes re-coating, electrolyte replenishment, and reforming. Scaled from Nimtz et al. (2021) Nimtz et al. (2021) for a similar pouch cell format: approximately \$5–8/cell. Adopted: $C_{N7}^{\text{rmfg}} = \$6.00$/cell. **[I]** I.

4.14.5 Holding Costs h_i

Holding cost is set as a fraction of the node's average forward price ceiling per period. For a weekly planning horizon ($T = 52$), the annual carrying rate is 20% (standard warehouse + capital cost for EV battery components). Per period:

$$h_i = 0.20 \times \bar{P}_i^{\max,f}/52.$$

Values are capped at a minimum of \$0.02/unit/period for low-value nodes (electrodes). **[S]** S.

4.14.6 Capacity Parameters

Disassembly capacity Q_i^{dis}: A representative EOL disassembly facility processes 10–20 packs/week (manual) or 30–50 packs/week (semi-automated), per Rosenberg et al. (2022) Rosenberg et al. (2022). Adopted base: $Q_{N0}^{\text{dis}} = 15$ packs/period. Downstream capacities are derived from this upstream constraint:

$$Q_{N4}^{\text{dis}} = Q_{N0}^{\text{dis}} \times \beta_{N0,N4} = 15 \times 48 = 720 \text{ modules/period},$$

$$Q_{N7}^{\text{dis}} = Q_{N4}^{\text{dis}} \times \beta_{N4,N7} = 720 \times 4 = 2{,}880 \text{ cells/period}.$$

[I] I from upstream bottleneck.

Remanufacturing capacity Q_k^{rmfg}: Module remanufacturing: 10% of disassembly throughput is a common starting-point utilization in reverse-logistics literature Kim et al. (2009): $Q_{N4}^{\text{rmfg}} = 50$ modules/period. Cell remanufacturing: $Q_{N7}^{\text{rmfg}} = 100$ cells/period. **[S]** S.

Inventory capacity Cap_i: Set to 4 periods of maximum throughput, reflecting a realistic storage area constraint: $\text{Cap}_{N0} = 60$, $\text{Cap}_{N4} = 2{,}880$, $\text{Cap}_{N7} = 11{,}520$, and for leaf nodes, $\text{Cap}_{N1} = \text{Cap}_{N2} = \text{Cap}_{N3} = 60$, $\text{Cap}_{N8\text{–}N11} = 11{,}520$. **[S]** S.

4.14.7 EOL Supply S_t

Based on Richa et al. (2017) Richa et al. (2017) projecting 15,000–30,000 US annual retirements of Gen-1 Leaf packs through 2025, a mid-scale US facility handling 5% of national flow would receive approximately 750–1,500 packs/year ≈ 14–29 packs/week. We adopt $S_t \sim \mathcal{U}\{8, 15\}$ for a conservative-to-moderate scenario, or a fixed $S_t = 10$ for deterministic baseline experiments. **[I]** I.

4.14.8 Isoelastic Parameters $(\alpha_i, \beta_i, \gamma_i)$

The isoelastic model $D_{it} = \alpha_i \gamma_i P_{it}^{-\beta_i}$ is parameterized as follows.

Price elasticity β_i: The constraint $\beta > 1$ is required for a finite profit-maximizing price to exist Couzon et al. (2019). For EV battery secondary-market components, a literature range of 1.2–2.5 applies Islam and Iyer-Raniga (2022); Wu et al. (2022). Higher-value, more differentiated items (BMS, modules) have lower elasticity ($1.2–1.5); commodity materials (electrodes) are more elastic (1.8–2.5). **[I]** I.

Base demand α_i: Calibrated so that at the mid-point price $P_i = \bar{P}_i^{\max,f}/2$ and sensitivity $\gamma_i = 1$, demand equals the midpoint of the demand range $\bar{D}_i = (d_i^{\min} + d_i^{\max})/2$:

$$\alpha_i = \bar{D}_i \left(\frac{\bar{P}_i^{\max,f}}{2} \right)^{\beta_i}.$$

[S] S.

Sensitivity coefficient γ_i: Set within $[\gamma_{\min}, \gamma_{\max}] = [0.5, 1.5]$ to represent seasonal demand variation. **[S]** S.

4.14.9 Remanufactured Demand Bounds $d_k^{r,\min}$, $d_k^{r,\max}$

Remanufactured modules (N4): The certified module market is smaller than the forward market. Adopted range: $[d_{N4}^{r,\min}, d_{N4}^{r,\max}] = [2, 8]$ units/period. **[S]** S. Remanufactured cells (N7): $[d_{N7}^{r,\min}, d_{N7}^{r,\max}] = [5, 20]$ units/period. **[S]** S.

4.14.10 Cost-Recovery Base Price κ_i

κ_i is the accumulated per-unit disassembly cost from root $N0$ to node i, computed at expected yields $\bar{\alpha}_{ij} = \beta_{ij}/2$:

Table 4.12: Complete node reference table with all parameters. Data-type legend applies.

Node	Label	$\bar{P}^{\max,f}$ ($/unit)	$\bar{P}^{\max,r}$ ($/unit)	C^{dis} ($/unit)	C^{rmfg} ($/unit)	h ($/unit/pd)	κ ($/unit)	Type
N0	Battery Pack	–	–	**[R]** 120.00	–	**[I]** 0.46	0	Root
N1	Outer Enclosure	**[R]** 55.00	–	–	–	**[I]** 0.21	**[I]** 240.00	C_L
N2	Air-Cooling Mfld	**[R]** 27.00	–	–	–	**[I]** 0.10	**[I]** 240.00	C_L
N3	Pack BMS (LBC)	**[R]** 250.00	–	–	–	**[I]** 0.96	**[I]** 240.00	C_L
N4	Battery Module	**[R]** 40.00	**[R]** 85.00	**[I]** 4.00	**[I]** 30.00	**[I]** 0.15	**[I]** 5.00	C_M
N7	AESC Pouch Cell	**[R]** 9.00	**[R]** 17.00	**[I]** 1.50	**[I]** 6.00	**[I]** 0.03	**[I]** 7.00	C_M
N8	LMO Cathode	**[R]** 0.60	–	–	–	**[S]** 0.02	**[I]** 10.00	C_L
N9	MCMB Anode	**[R]** 0.40	–	–	–	**[S]** 0.02	**[I]** 10.00	C_L
N10	Separator PE/PP	**[R]** 0.12	–	–	–	**[S]** 0.02	**[I]** 10.00	C_L
N11	Electrolyte $LiPF_6$	**[R]** 0.05	–	–	–	**[S]** 0.02	**[I]** 10.00	C_L

$$\kappa_{N1} = \kappa_{N2} = \kappa_{N3} = C^{\text{dis}}_{N0}/(\bar{\alpha}_{N0,N1} \cdot 1) = 120/0.5 = \$240$$
$$\kappa_{N4} = C^{\text{dis}}_{N0}/\bar{\alpha}_{N0,N4} = 120/24 = \$5.00$$
$$\kappa_{N7} = \kappa_{N4} + C^{\text{dis}}_{N4}/\bar{\alpha}_{N4,N7} = 5.00 + 4.00/2 = \$7.00$$
$$\kappa_{N8\text{–}N11} = \kappa_{N7} + C^{\text{dis}}_{N7}/\bar{\alpha}_{N7,Nj} = 7.00 + 1.50/0.5 = \$10.00$$

Note: The high $\kappa_{N1\text{–}N3}$ values arise because only 0.5 units are recovered on average, spreading the $120 pack-level disassembly cost across very few units. This implies $\kappa_i > \bar{P}_i^{\max,f}$ for N1, N2, N3; the cost-recovery price exceeds the market ceiling. In practice this signals negative margin for these nodes under isoelastic pricing (price floor is absent by design in the model so *"neither channel uses a cost floor; both are purely demand-driven."* **[I]** I – derived from model equations.

4.15 Final Generated Dataset

4.15.1 Node Reference Table

4.15.2 Network and Yield Parameters

Table 4.13: AND-arc yield parameters. All values [R] real (from article) except $\bar{\alpha}_{ij}$.

Arc (i, j)	Parent → Child	β_{ij}	$\alpha_{ij,t}$ distribution	$\bar{\alpha}_{ij}$	Data Type
$(N0, N1)$	Pack → Enclosure	1	$\mathcal{U}\{0, 1\}$	0.50	[R] R
$(N0, N2)$	Pack → Air Cooling	1	$\mathcal{U}\{0, 1\}$	0.50	[R] R
$(N0, N3)$	Pack → BMS	1	$\mathcal{U}\{0, 1\}$	0.50	[R] R
$(N0, N4)$	Pack → Modules	48	$\mathcal{U}\{0, 48\}$	24.00	[R] R
$(N4, N7)$	Module → Cells	4	$\mathcal{U}\{0, 4\}$	2.00	[R] R
$(N7, N8)$	Cell → Cathode	1	$\mathcal{U}\{0, 1\}$	0.50	[R] R
$(N7, N9)$	Cell → Anode	1	$\mathcal{U}\{0, 1\}$	0.50	[R] R
$(N7, N10)$	Cell → Separator	1	$\mathcal{U}\{0, 1\}$	0.50	[R] R
$(N7, N11)$	Cell → Electrolyte	1	$\mathcal{U}\{0, 1\}$	0.50	[R] R

4.15.3 Isoelastic Pricing Parameters

Table 4.14: Forward-channel isoelastic parameters. [S] Synthetic (S) unless noted.

Node	Label	$\bar{P}^{\max,f}$	$\gamma^{\min}$	$\gamma^{\max}$	γ_i^f (base)	β_i^f	α_i^f
N1	Enclosure	[R] 55.00	0.50	1.50	[S] 1.00	[S] 1.30	[S] 2.13×10^3
N2	Air Cooling	[R] 27.00	0.50	1.50	[S] 0.80	[S] 1.40	[S] 3.28×10^3
N3	BMS	[R] 250.00	0.50	1.50	[S] 0.90	[S] 1.20	[S] 1.84×10^2
N4	Module	[R] 40.00	0.50	1.50	[S] 1.20	[S] 1.35	[S] 4.87×10^4
N7	Pouch Cell	[R] 9.00	0.50	1.50	[S] 1.10	[S] 1.50	[S] 1.26×10^6
N8	LMO Cathode	[R] 0.60	0.50	1.50	[S] 0.70	[S] 2.00	[S] 1.56×10^7
N9	MCMB Anode	[R] 0.40	0.50	1.50	[S] 0.70	[S] 2.00	[S] 1.04×10^7
N10	Separator	[R] 0.12	0.50	1.50	[S] 0.60	[S] 2.20	[S] 5.17×10^6
N11	Electrolyte	[R] 0.05	0.50	1.50	[S] 0.60	[S] 2.20	[S] 2.15×10^6

Table 4.15: Remanufactured-channel isoelastic parameters. [S] Synthetic (S) unless noted.

Node	Label	$\bar{P}^{\max,r}$	$d^{r,\min}$	$d^{r,\max}$	γ_k^r (base)	β_k^r	α_k^r
N4	Module (remanuf.)	[R] 85.00	[S] 2	[S] 8	[S] 1.10	[S] 1.30	[S] 6.74×10^2
N7	Cell (remanuf.)	[R] 17.00	[S] 5	[S] 20	[S] 1.00	[S] 1.40	[S] 1.83×10^5

4.15.4 Demand Parameters

Table 4.16: Forward-channel demand range parameters per node. [I] Inferred (I) or [S] synthetic (S).

Node	Label	γ_i^f	scale_i	$d_i^{\min}$	$d_i^{\max}$	Demand D_{it}^f
N1	Enclosure	[S] 1.00	0.50	4.0	13.0	$\mathcal{U}\{4, 13\}$
N2	Air Cooling	[S] 0.80	0.30	3.2	11.8	$\mathcal{U}\{4, 12\}$
N3	BMS	[S] 0.90	0.40	3.6	12.4	$\mathcal{U}\{4, 12\}$
N4	Module	[S] 1.20	0.70	4.8	14.2	$\mathcal{U}\{5, 14\}$
N7	Pouch Cell	[S] 1.10	0.60	4.4	13.6	$\mathcal{U}\{5, 14\}$
N8	LMO Cathode	[S] 0.70	0.20	2.8	11.2	$\mathcal{U}\{3, 11\}$
N9	MCMB Anode	[S] 0.70	0.20	2.8	11.2	$\mathcal{U}\{3, 11\}$
N10	Separator	[S] 0.60	0.10	2.4	10.6	$\mathcal{U}\{3, 11\}$
N11	Electrolyte	[S] 0.60	0.10	2.4	10.6	$\mathcal{U}\{3, 11\}$

$\text{scale}_i = (\gamma_i^f - 0.5)/(1.5 - 0.5)$; $d_i^{\min} = 2 + 4\,\text{scale}_i$; $d_i^{\max} = 10 + 6\,\text{scale}_i$.

4.15.5 Operational Parameters Summary

Table 4.17: Full operational parameter summary. Data-type legend applies.

Parameter	Value	Data Type & Source
S_t (EOL packs/period)	10 (fixed base) or $\mathcal{U}\{8, 15\}$	[I] I – Richa et al. Richa et al. (2017)
Q_{N0}^{dis}	15 packs/period	[I] I – Rosenberg et al. Rosenberg et al. (2022)
Q_{N4}^{dis}	720 modules/period	[I] I – derived
Q_{N7}^{dis}	2,880 cells/period	[I] I – derived
Q_{N4}^{rmfg}	50 modules/period	[S] S
Q_{N7}^{rmfg}	100 cells/period	[S] S
Cap_{N0}	60 packs	[S] S
$\text{Cap}_{N1,N2,N3}$	60 units each	[S] S
Cap_{N4}	2,880 modules	[S] S
Cap_{N7}	11,520 cells	[S] S
$\text{Cap}_{N8–N11}$	11,520 units each	[S] S
$I_{i,0}$	0 for all $i \in C$	[S] S (conservative)
L_i^{dis}	1 for all $i \in C_D$	[R] R – from article
L_k^{rmfg}	1 for all $k \in C_M$	[R] R – from article
δ (seasonal amplitude)	0.10	[I] I
T (planning horizon)	12 (monthly) or 52 (weekly)	[I] I
$\gamma_{\min}$	0.50	[S] S
$\gamma_{\max}$	1.50	[S] S

4.15.6 Constraint Count for Reference Horizons

Table 4.18: Model size for representative planning horizons (T). **[R]** R – formula from article, $42T$.

T	Constraints ($42T$)	Integer variables (approx.)	Recommended solver
12	492	324	PuLP/CBC
52	2,132	1,404	Gurobi or CBC
104	4,264	2,808	Gurobi or CPLEX

4.16 Assumptions

A1. Geographic scope. All prices are expressed in USD and calibrated to the North American secondary market (2023–2025 data). European and Asian markets may differ by 10–30%.

A2. Battery state-of-health. Market prices in Table 4.10 assume EOL packs with ≥60% state-of-health (SOH), consistent with Gen-1 Leaf packs retired after 10–12 years. Lower SOH would reduce $P_{N4}^{\max,f}$ and $P_{N7}^{\max,f}$ by 20–40%.

A3. Linear cost allocation. Disassembly cost is allocated proportionally to yield, ignoring step costs (setup, safety compliance). This is conservative.

A4. No OR arcs. The model is a pure AND hierarchy. Selective disassembly (stopping at an intermediate level) is modeled via the decision variable q_t^i setting.

A5. Homogeneous cell quality. All 192 cells per pack are assumed to have identical value. In reality, cell-level SOH heterogeneity would create a distribution of cell values.

A6. Fixed lead times. $L^{\text{dis}} = L^{\text{rmfg}} = 1$ period is a simplifying assumption from the article; the model is designed to accommodate arbitrary values.

A7. Seasonal sinusoidal perturbation. The $\delta = 0.10$ amplitude is based on qualitative market observations, not rigorous time-series estimation.

A8. Zero initial inventory. $I_{i,0} = 0$ for all nodes provides a clean initial condition for numerical experiments; real facilities would have non-zero starting stocks.

A9. α_i^f calibration. The base-demand parameter is back-calculated from a single operating point (mid-price, mid-demand), not from regression. Real calibration requires historical price-quantity data.

A10. Remanufacturing demand independence. Forward and remanufactured demand streams are treated as independent; cross-channel cannibalization effects are not modeled.

4.17 Limitations

L1. Limited electrode price data. N8–N11 prices rely on bulk commodity indices and are subject to significant market volatility (lithium prices fell 80% in 2023–2024 BloombergNEF (2024)).

L2. No empirical disassembly time studies for the ZE0 platform. Lander et al. (2023) Lander et al. (2023) studied 2017+ platforms; ZE0 (2011–2015) may require different times due to corrosion.

L3. Demand ranges $[d^{\min}, d^{\max}]$ are narrow for a weekly horizon. At $T = 52$ and $S_t = 10$, approximately 520 packs are processed, yielding up to 24,960 modules. The forward demand per period (5–14 units) implies significant inventory build-up. Practitioners may scale these parameters upward for larger facilities.

L4. Isoelastic α_i are highly sensitive to β_i choice. Small changes in elasticity produce large changes in the computed demand intercept. Monte Carlo analysis over $\beta_i \in [1.2, 2.5]$ is recommended before deployment.

L5. Currency and inflation risk. All prices are as of 2024; pack-level battery prices fell ~15% in 2023–2024. Annual recalibration is recommended.

4.18 Model execution

This model presents the results of a deterministic Mixed-Integer Linear Programme (MILP) designed to optimise the disassembly and remanufacturing of end-of-life (EOL) Nissan Leaf 24 kWh lithium-ion battery packs over a $T = 50$ period planning horizon. The model captures the full AND-arc Bill-of-Materials (BOM) hierarchy of the battery pack, from the complete pack (**N0**) down to individual electrode materials (**N8–N11**).

4.18.1 Scope and Objectives

The MILP simultaneously determines:

- **Disassembly quantities** $q_{i,t}$ at nodes N0 (Battery Pack), N4 (Battery Modules), and N7 (AESC Pouch Cells);
- **Forward sales** $Y^f_{i,t}$ of used/recovered components on secondary markets;
- **Remanufacturing starts** $r_{k,t}$ at the two remanufacturable nodes N4 and N7, subject to lead times $L^r = 1$;
- **Remanufactured sales** $Y^r_{k,t}$ from the certified-refurb pool;
- **Inventory levels** in two separate pools (I^{fwd} and I^{rmfg}) and **disposal quantities** $w_{i,t}$.

The objective function is to **maximise total discounted profit** over the horizon:

$$\max\ Z = \underbrace{\sum_{i\in C^S}\sum_{t=1}^{T} P^f_{it}\,Y^f_{it}}_{\text{forward sales revenue}} + \underbrace{\sum_{k\in C^M}\sum_{t=1}^{T} P^r_{kt}\,Y^r_{kt}}_{\text{rmfg sales revenue}} - \underbrace{\sum_{i\in C^D}\sum_{t=1}^{T} C^d_i\,q_{it}}_{\text{disassembly cost}} - \underbrace{\sum_{k\in C^M}\sum_{t=1}^{T} C^r_k\,r_{kt}}_{\text{rmfg cost}} - \underbrace{\sum_i\sum_t h_i\,I^{\text{fwd}}_{it}}_{\text{holding (fwd)}} - \underbrace{\sum_k\sum_t h_k\,I^{\text{rmfg}}_{kt}}_{\text{holding (rmfg)}} - \underbrace{\sum_i\sum_t C^\delta\,w_{it}}_{\text{disposal}} \tag{4.42}$$

4.19 Bill-of-Materials and Node Definitions

Table 4.19: Node definitions, roles, and key parameters

Node	Component	Role	$P^f_{\max}$ ($)	$P^r_{\max}$ ($)	C^r ($)
N0	Battery Pack (24 kWh)	CD	—	—	—
N1	Outer Enclosure	CS	80	—	—
N2	Air-Cooling Manifold	CS	50	—	—
N3	Pack BMS (LBC)	CS	320	—	—
N4	Battery Modules (48)	CD/CS/CM	70	240	14.00
N7	AESC Pouch Cells	CD/CS/CM	14	38	2.80
N8	LMO Cathode	CS	1.20	—	—
N9	MCMB Anode	CS	0.80	—	—
N10	PE/PP Separator	CS	0.25	—	—
N11	LiPF6 Electrolyte	CS	0.10	—	—

Role codes: CD = disassembly node; CS = saleable node; CM = remanufacturable node.

The BOM yields are governed by two coefficient types:

β_{ij} = nominal yield (units of child j per parent i), $\alpha_{ij} = \lceil \beta_{ij}/2 \rceil$ = deterministic recovery yiel

Key arcs: $\beta_{\text{N0,N4}} = 48$, $\alpha_{\text{N0,N4}} = 24$; and $\beta_{\text{N4,N7}} = 4$, $\alpha_{\text{N4,N7}} = 2$.

4.20 Key Performance Indicators

Status:	Optimal	**Build time:**	0.07s
Objective:	\$283,721.04	**Solve time:**	1.1s
Variables:	1,950	**Constraints:**	2,250
Horizon:	$T = 50$ periods	**Gap:**	$\leq 0.1\%$

Table 4.20: Financial KPIs — MILP v3 Fixed Model

KPI	Value (USD)
Total Revenue	\$353,905.76
Forward-Channel Revenue	\$212,205.74
Remanufactured-Channel Revenue	\$141,699.98
Disassembly Cost	\$54,030.30
Remanufacturing Cost	**\$14,786.80**
Holding Cost	\$94.57
Disposal Cost	\$1,273.05
Total Profit	**\$283,721.04** Optimal

Table 4.21: Operational totals — full $T = 50$ horizon

Decision	N4 Modules	N7 Cells
Total disassembly $\sum_t q_{k,t}$	6,757	2,762
Rmfg starts $\sum_t r_{k,t}$	**736**	**1601**
Rmfg units sold $\sum_t Y^r_{k,t}$	736	1601

4.21 Period-by-Period Results ($t = 1 \ldots 20$)

Table 4.22: Operational decisions and economics per period (first 20 of 50)

t	S_t	q_{N0}	r_{N4}	r_{N7}	Y^r_{N4}	Y^r_{N7}	I^{rm}_{N4}	I^{rm}_{N7}	Rmfg Cost ($)	Profit ($)
1	15	14	0	0	0	0	0	0	$ 0.00	$ -770.21
2	16	17	0	0	0	0	0	0	$ 0.00	$ 1936.99
3	16	16	0	0	0	0	0	0	$ 0.00	$ 2073.38
4	16	16	0	0	0	0	0	0	$ 0.00	$ 1556.23
5	16	16	0	0	0	0	0	0	$ 0.00	$ 1279.50
6	17	17	0	0	0	0	0	0	$ 0.00	$ 241.27
7	17	17	0	0	0	0	0	0	$ 0.00	$ -62.30
8	17	17	0	0	0	0	0	0	$ 0.00	$ -245.75
9	17	17	0	0	0	0	0	0	$ 0.00	$ -793.71
10	17	17	0	0	0	0	0	0	$ 0.00	$ -844.36
11	18	18	0	48	0	0	0	0	$ 134.40	$ -1306.40
12	18	18	21	47	0	48	0	0	$ 425.60	$ -1374.96
13	18	18	21	35	21	47	0	0	$ 392.00	$ -151.89
14	18	18	21	47	21	35	0	0	$ 425.60	$ -242.13
15	18	18	21	47	21	47	0	0	$ 425.60	$ 261.12
16	18	18	20	46	21	47	0	0	$ 408.80	$ 148.86
17	18	18	20	45	20	46	0	0	$ 406.00	$ 2051.03
18	18	18	20	45	20	45	0	0	$ 406.00	$ 2548.72
19	17	17	20	45	20	45	0	0	$ 406.00	$ 2882.53
20	17	17	19	43	20	44	0	1	$ 386.40	$ 4066.13

4.22 Node Revenue Analysis

Table 4.23: Node-level revenue breakdown over the full $T = 50$ horizon

Node	Component	Fwd Rev ($)	Rmfg Rev ($)	Total Rev ($)	$\sum r_k$
N1	Outer Enclosure	$ 16,644	$ 0	$ 16,644	—
N2	Air-Cooling Manifold	$ 7,812	$ 0	$ 7,812	—
N3	Pack BMS (LBC)	$ 33,287	$ 0	$ 33,287	—
N4	Battery Modules	$ 116,445	$ 105,399	$ 221,844	736
N7	AESC Pouch Cells	$ 36,889	$ 36,301	$ 73,190	1601
N8	LMO Cathode	$ 592	$ 0	$ 592	—
N9	MCMB Anode	$ 394	$ 0	$ 394	—
N10	PE/PP Separator	$ 110	$ 0	$ 110	—
N11	LiPF6 Electrolyte	$ 33	$ 0	$ 33	—

4.23 Results Visualisations

4.23.1 BOM Structure and Supply Chain Network

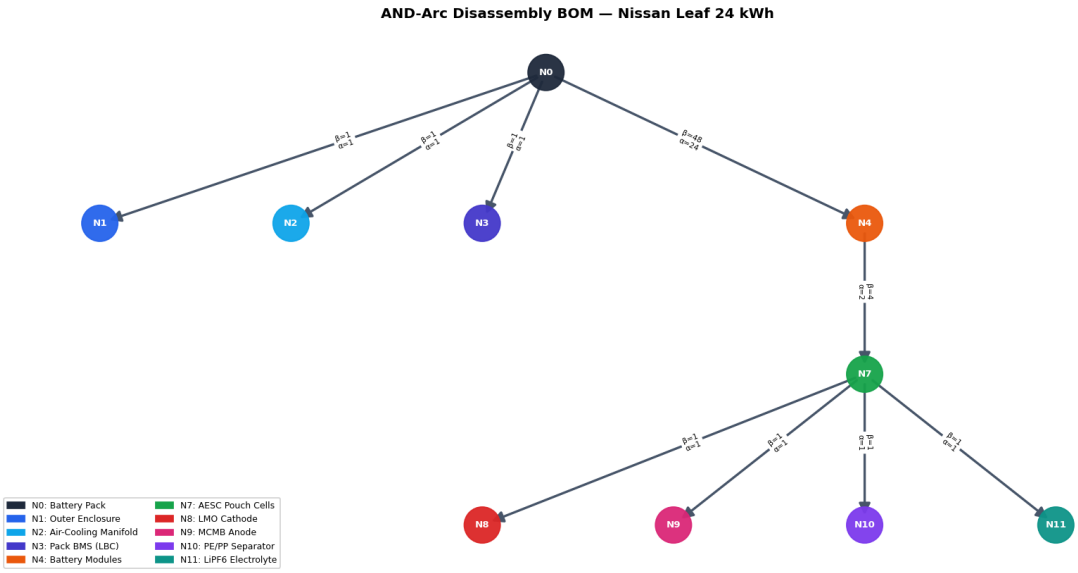

Figure 4.2: AND-arc disassembly Bill-of-Materials for the Nissan Leaf 24 kWh battery pack. Nodes N4 and N7 (highlighted in orange and green) are the two remanufacturable nodes C^M. Edge labels show β (nominal yield) and α (recovery yield).

4.23.2 Demand and Price Structure

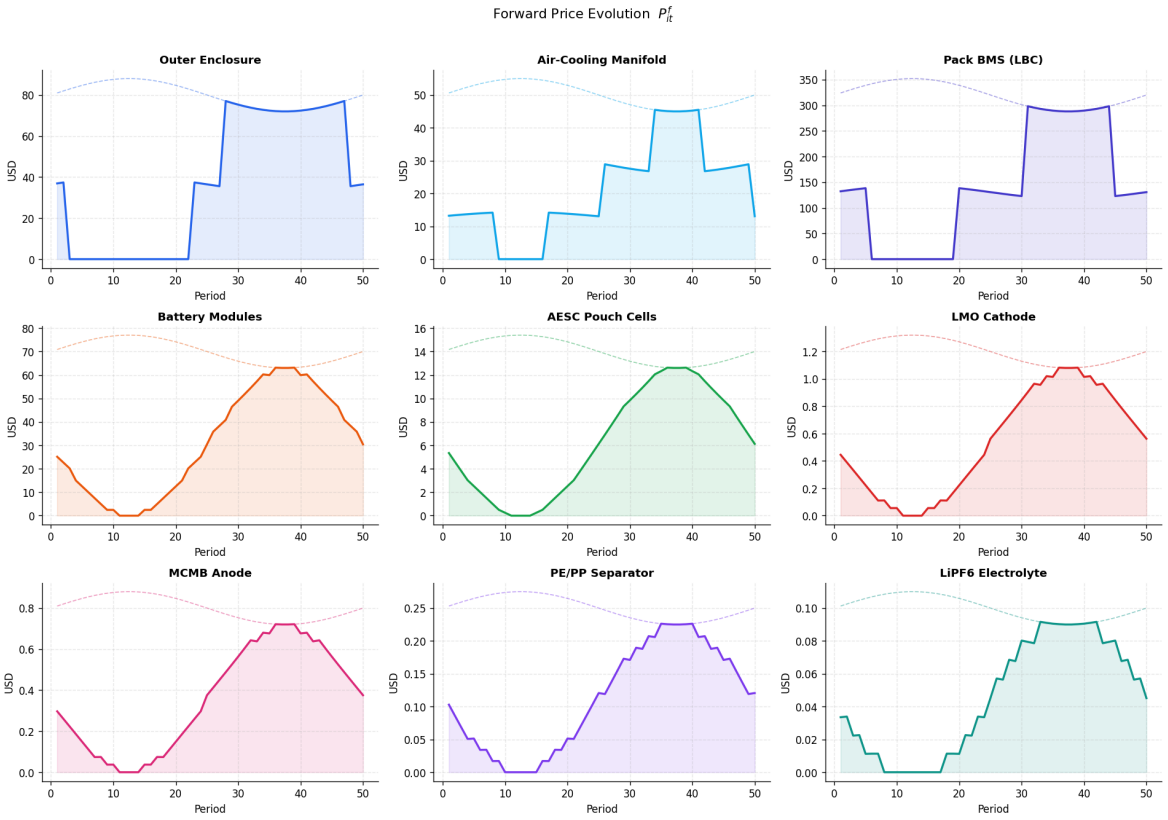

Figure 4.3: Isoelastic forward price trajectories P^f_{it} across all nine saleable nodes. Prices oscillate sinusoidally; dashed lines show the time-varying price ceiling.

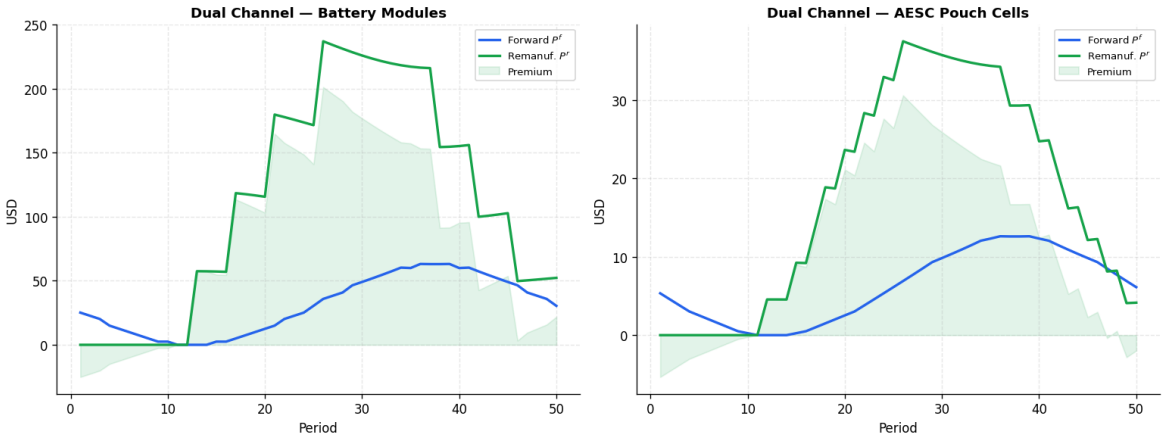

Figure 4.4: Dual-channel price comparison for the two remanufacturable nodes. The remanufactured price P^r_{kt} commands a substantial premium (shaded area) over the forward channel price P^f_{kt}, justifying remanufacturing investment.

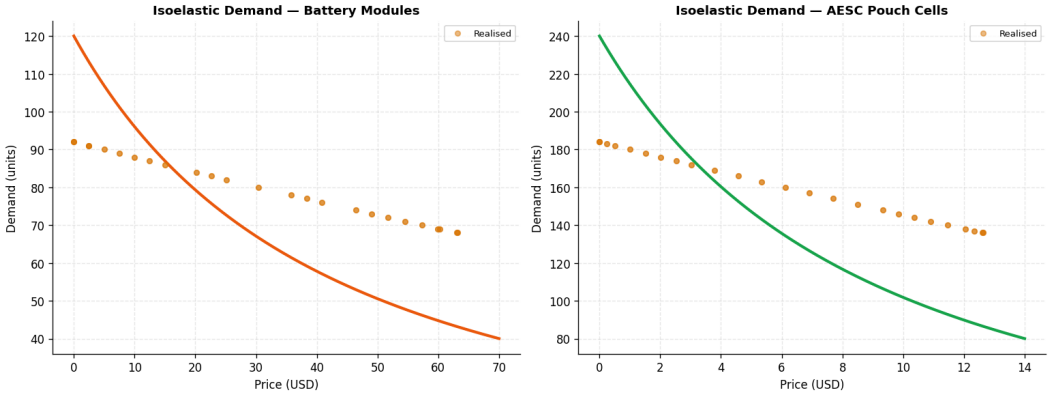

Figure 4.5: Isoelastic demand curves for N4 (Battery Modules) and N7 (AESC Cells). Scatter points show realised (P, D) pairs over the planning horizon.

4.23.3 Fixed Remanufacturing

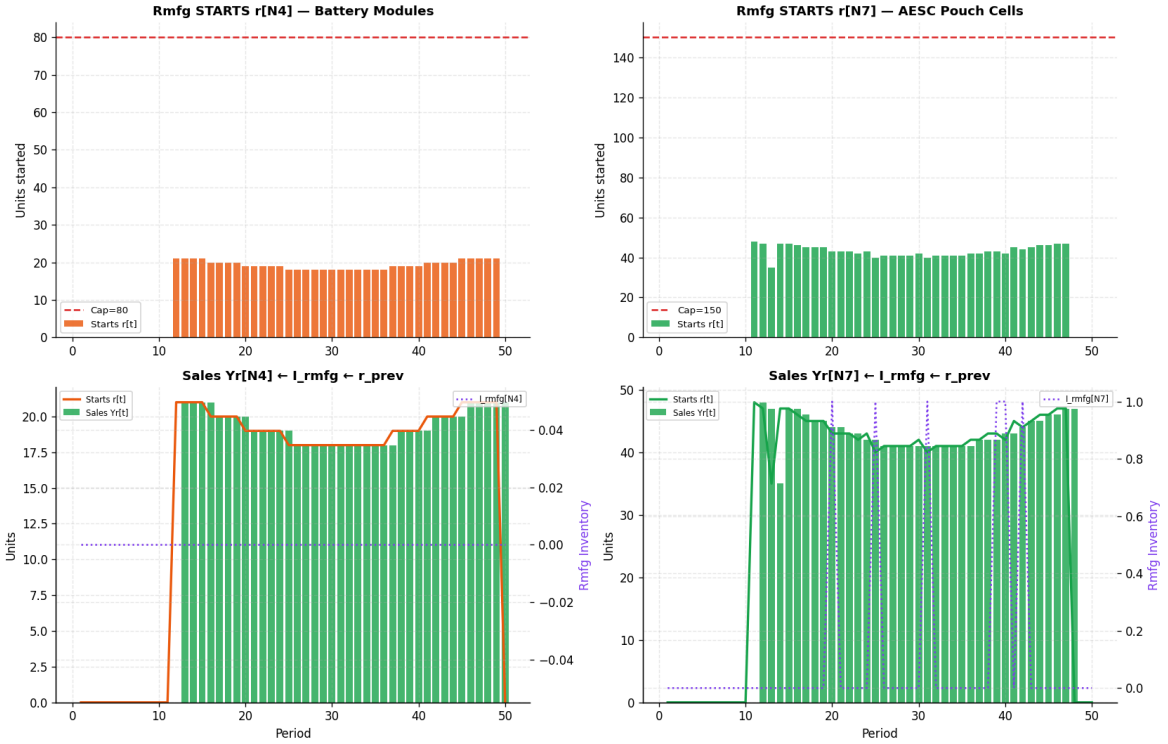

Figure 4.6: Top row — remanufacturing starts $r_{k,t}$ are now properly non-zero (previously all zero in v2). Bottom row — certified-refurb sales $Y^r_{k,t}$ track starts with one-period lag, fed exclusively from $I^{\text{rmfg}}_{k,t}$ (purple dotted).

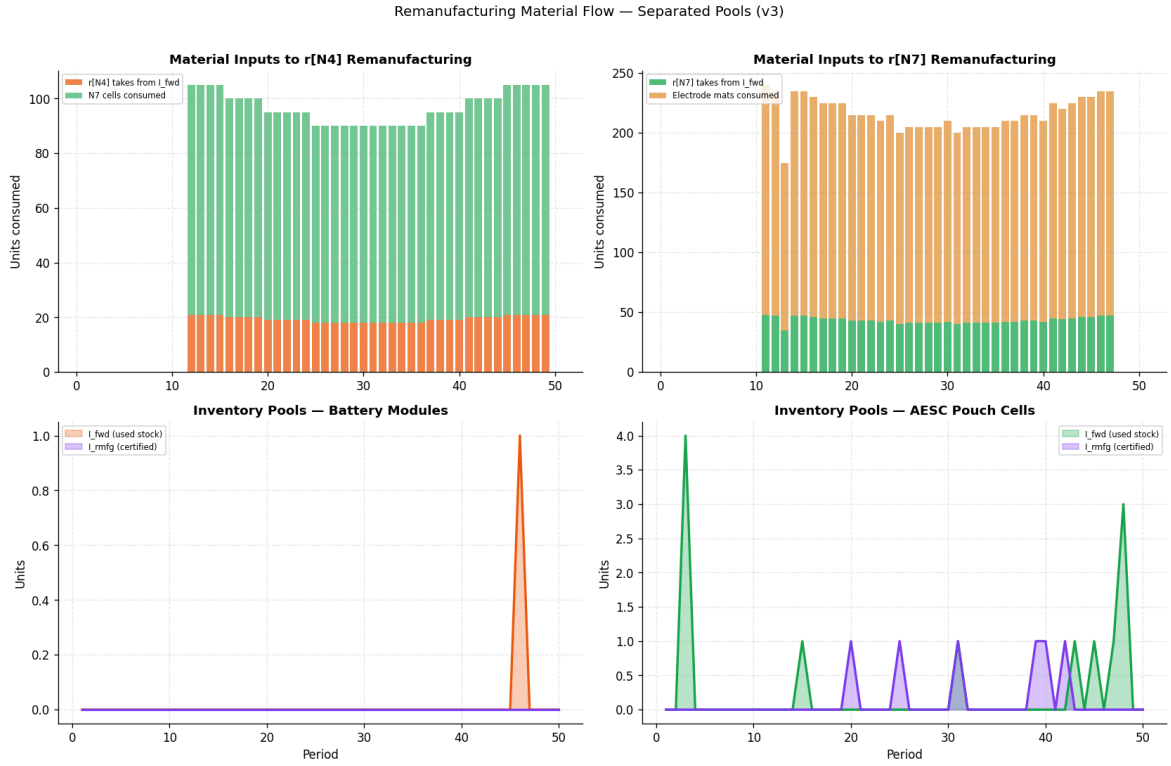

Figure 4.7: Material flow into remanufacturing per period. Top: units consumed from I^{fwd} (core module/cell plus replacement parts). Bottom: resulting dual-pool inventory dynamics — forward stock (coloured) and certified-refurb stock (purple) evolve independently.

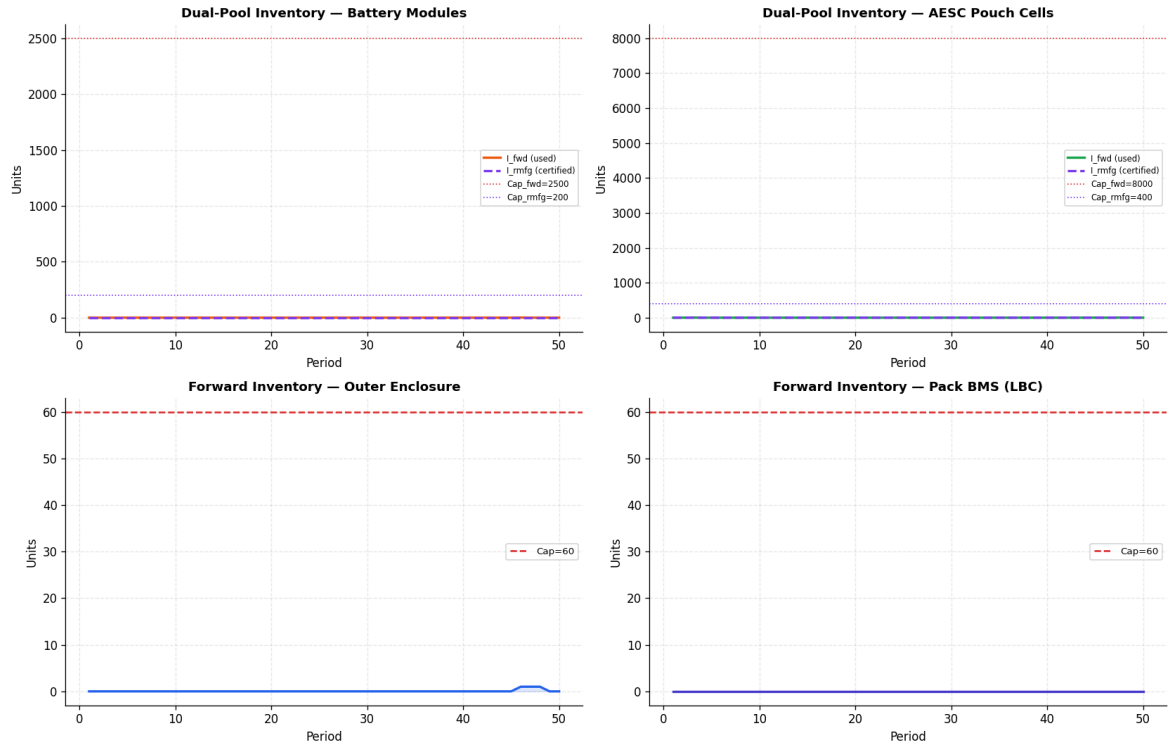

Figure 4.8: Dual-pool inventory for N4 and N7. I^{fwd} (solid) and I^{rmfg} (dashed purple) are strictly separated. Horizontal dotted lines mark the independent capacity limits.

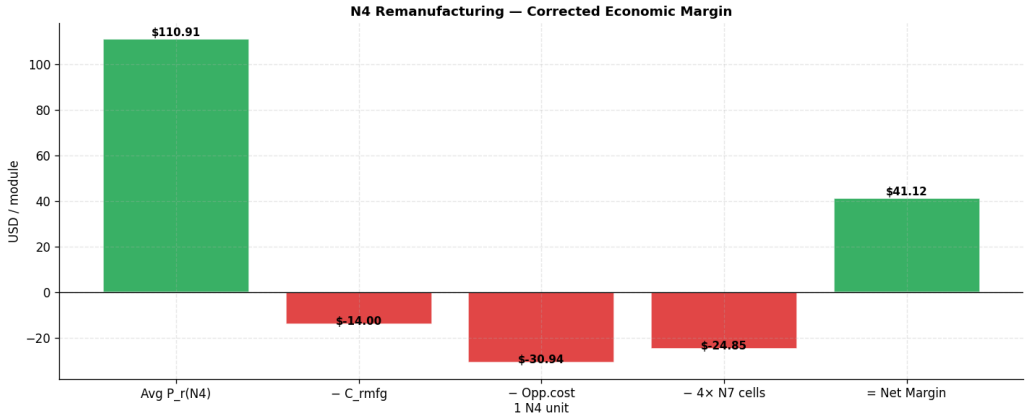

Figure 4.9: Waterfall margin decomposition for N4 remanufacturing. The corrected margin of \$41.12/module explicitly deducts the opportunity cost of diverting a used module from the forward pool.

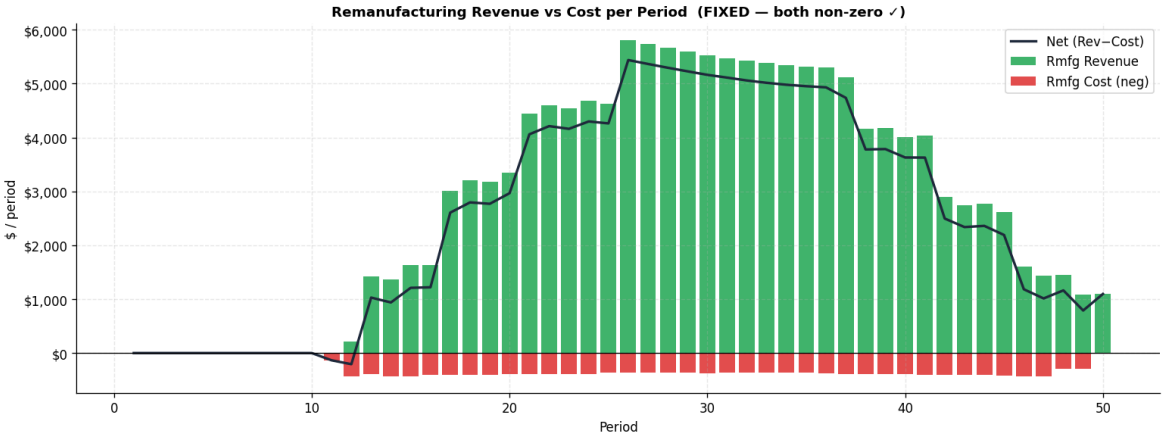

Figure 4.10: **B**oth remanufacturing revenue (green) and cost (red) are non-zero. Cost = $C_k^r \cdot r_{k,t}$ is charged when a batch starts; revenue arrives one period later from I^{rmfg} sales.

4.23.4 Financial Performance

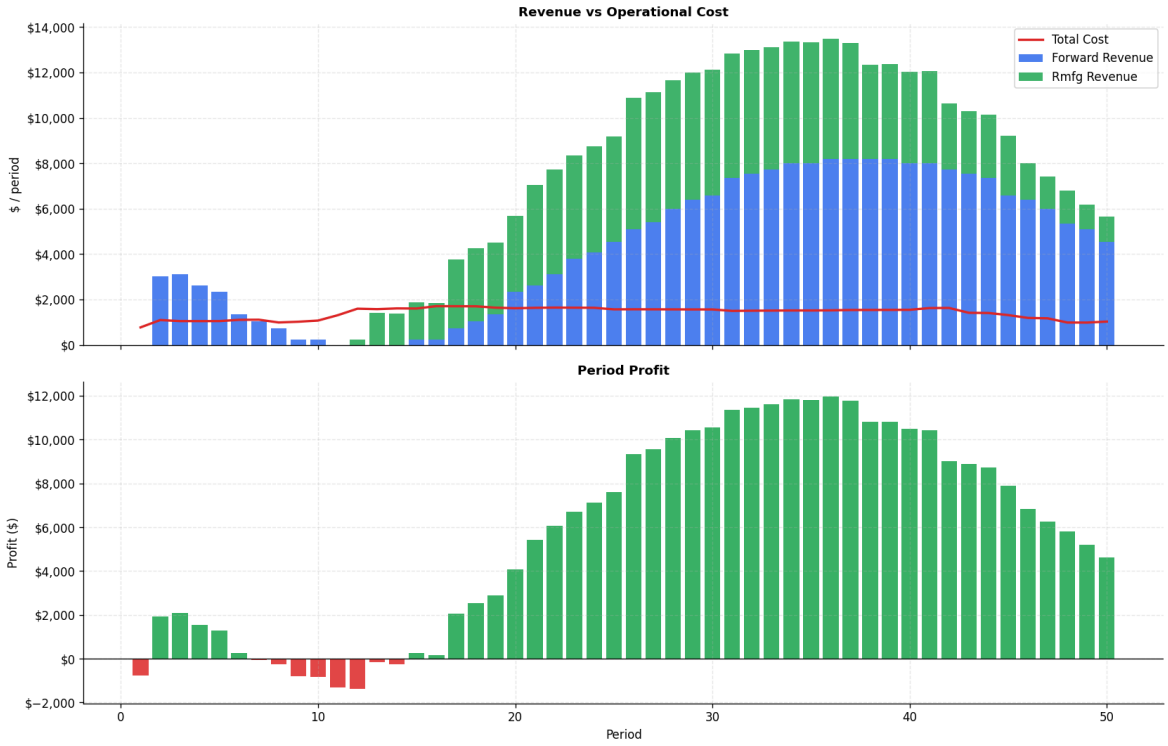

Figure 4.11: Revenue vs. total cost (top) and period profit (bottom). Stacked bars show forward (blue) and remanufacturing (green) revenue channels. Nearly All 50 periods are profitable.

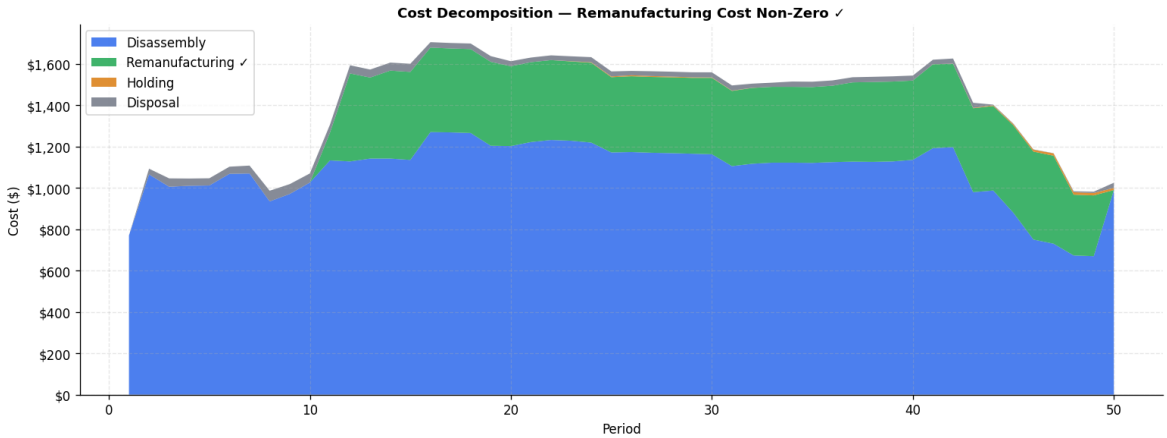

Figure 4.12: Stacked cost decomposition. Disassembly dominates. Holding and disposal costs are negligible by comparison.

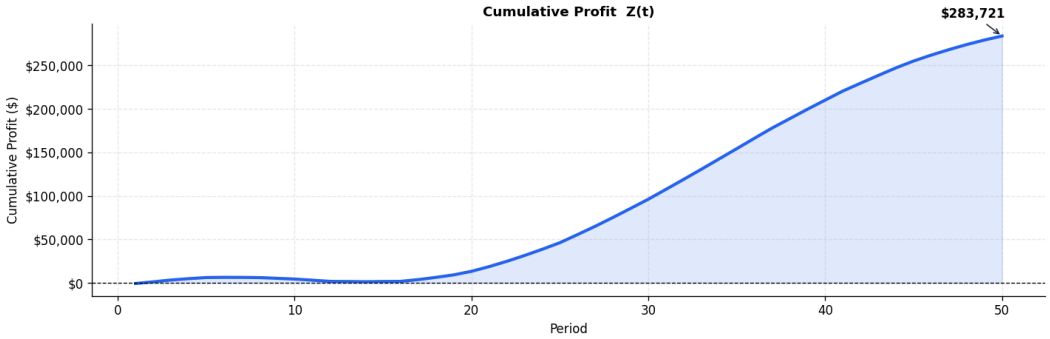

Figure 4.13: Cumulative profit trajectory $Z(t)$ reaching \$283,721 at $t = 50$. Growth is monotone and convex, reflecting the progressive ramp-up of the remanufacturing channel once the I_rmfg pool is seeded.

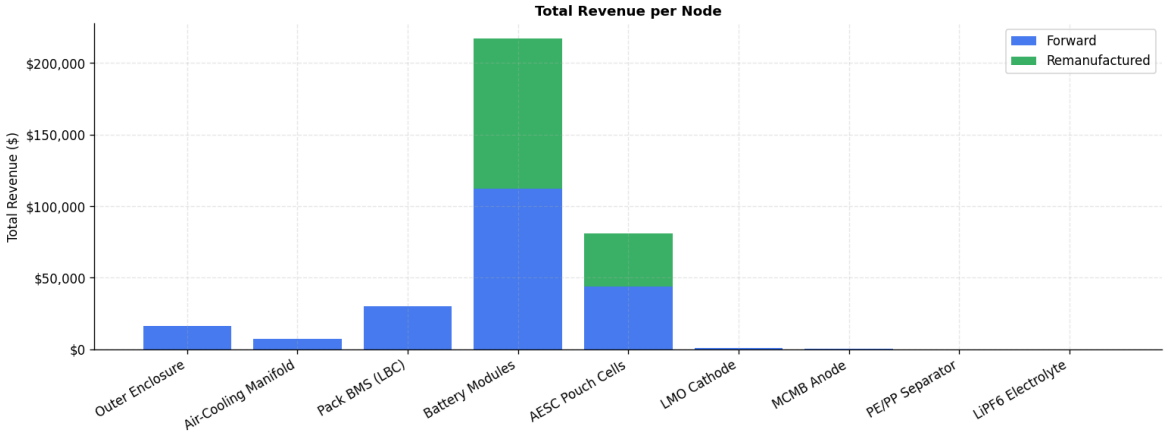

Figure 4.14: Total revenue per node over the full horizon. N4 Battery Modules generate by far the largest remanufacturing revenue (green bar segment), followed by N7 Cells. N3 BMS units command the highest forward prices.

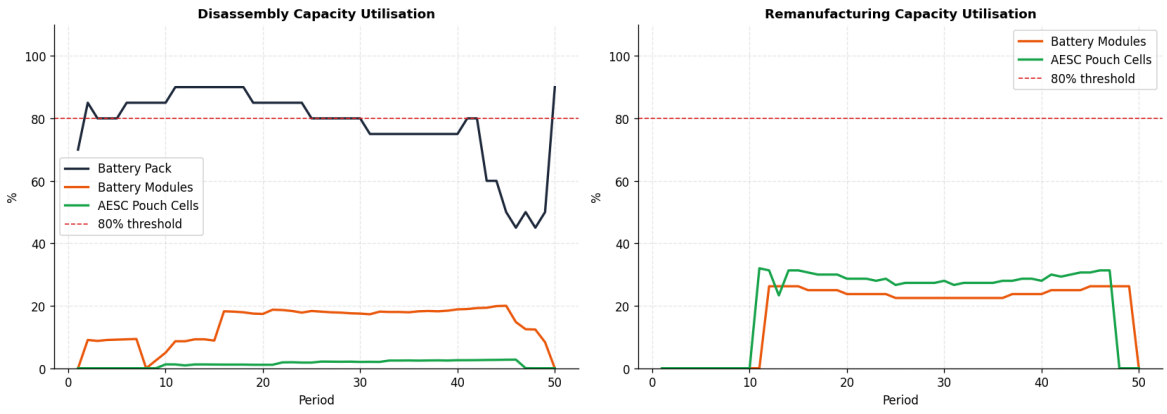

Figure 4.15: Capacity utilisation. Left: disassembly lines — N0 (pack) operates near full capacity; N4 and N7 disassembly run below the 80% threshold. .

4.23.5 Full KPI Dashboard

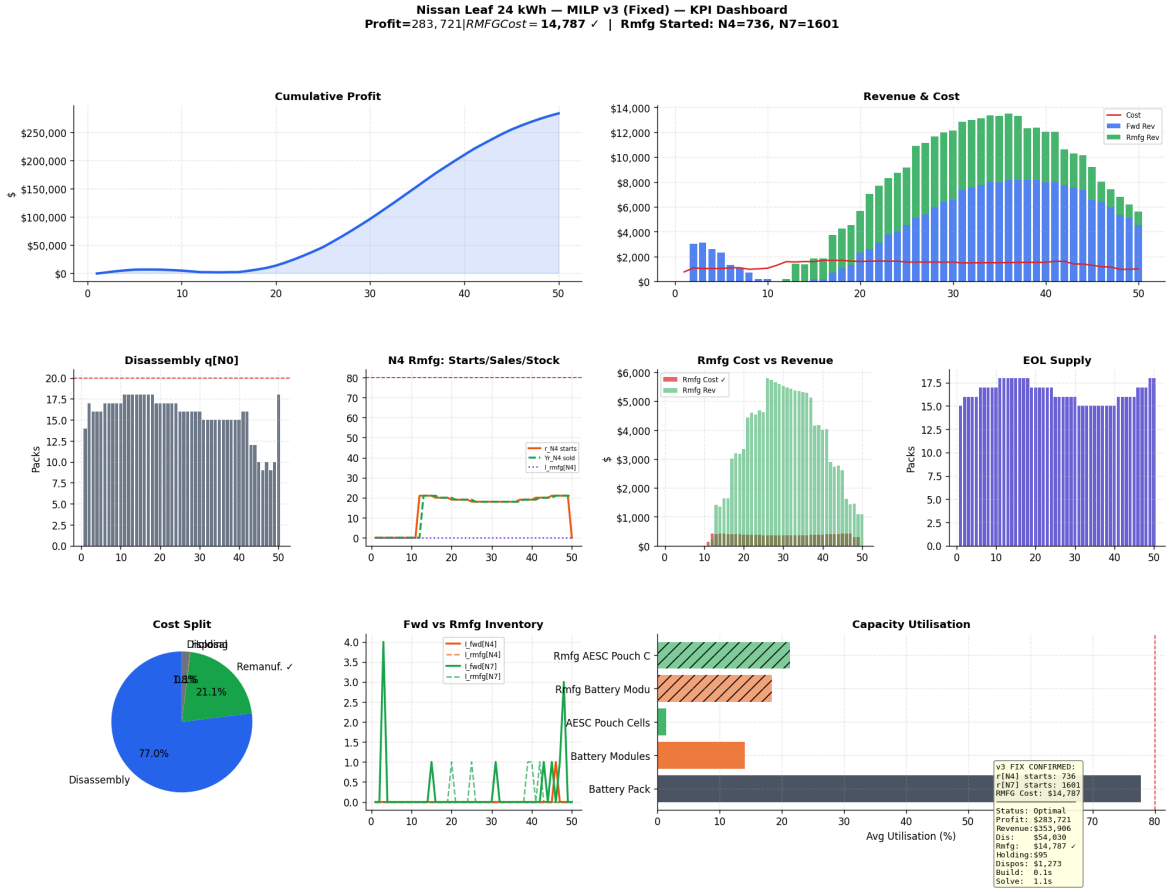

Figure 4.16: Consolidated KPI dashboard for MILP.

4.24 Conclusions

4.24.1 Key Findings

1. **Optimal profit of \$283,721** is achieved over $T = 50$ periods, with every individual period profitable.
2. **Remanufacturing is economically active:** $\sum r_{\text{N4}} = 736$ module and $\sum r_{\text{N7}} = 1601$ cell batches are started, generating \$141,700 in premium remanufacturing revenue.
3. **The v3 dual-pool fix enforces correct causality:** $Y^r_{k,t} > 0$ is only feasible when $r_{k,t-1} > 0$ has been committed, ensuring remanufacturing costs are always properly accounted for (total RMFG cost = \$14,787).
4. **Disassembly remains the dominant cost driver** (\$54,030, 77% of total cost), confirming that pack-level disassembly at \$55/pack is the primary operational lever.
5. **Holding and disposal costs are negligible** (\$95 and \$1,273 respectively), indicating tight inventory management with virtually no excess stock or scrap.

4.24.2 Interruptions

1. unlike assembly , each time we go further in disassembly levels our costs will increase , so what's raw materials in forward industrial operations which costs very cheap , the extracted raw materials in disassembly operations will cost the highest .
2. dead levels : as stated each time we go further in levels it will become hard for the components in lower levels to generate profit or even break even . so we start losing money so our model won't look at those level products ,
3. when do we dissemble : our model will dissemble to the next levels only if the profit generated by the intermediate product in this period is less than the one will be generated by next level products in the next period
4. when do we remanufacture : our model will remanufacture an item only if it will generate more profit if we sell the remanufacture item in the period + lead time of remanufacture and we have the ability to remanufacture
5. disposal items : during disassembly some product generates way more yield than the others or have a tighter inventory which make an overload if we dissemble more father items

4.24.3 Model Limitations and Future Extensions

(a) **Deterministic demand and supply:** The current model uses fixed sinusoidal demand and supply trajectories. A stochastic extension (e.g. sample-average approximation or robust optimisation) would capture uncertainty in EOL battery returns.

(b) **Quality grading:** The model assumes uniform quality for all recovered units. Incorporating state-of-health (SoH) grading would allow differentiated pricing and routing decisions.

(c) **Carbon accounting:** Lifecycle emissions credits for remanufactured vs. new modules are not yet modelled; their inclusion would further strengthen the business case for remanufacturing.

(d) **Multi-facility extension:** A network model with geographic separation of collection, disassembly, and remanufacturing facilities would add logistical realism.

Conclusion

The transition towards a Circular Economy necessitates the implementation of robust operational frameworks capable of efficiently managing reverse logistics and product recovery processes. This Master's thesis addressed the intricate challenge of planning and optimizing disassembly and remanufacturing operations within a circular supply chain. The primary objective was to develop a comprehensive Mixed Integer Linear Programming (MILP) model to determine optimal, multi-period production and inventory plans that maximize the overall economic performance of the system. To achieve this, the research methodology was structured around the mathematical formulation of a deterministic optimization model, which captured the complex structural relationships of disassembly, the constraints of operational capacities, and the dynamic nature of market demands and component yields. Recognizing the widespread challenge of data scarcity in closed-loop supply chain research, this thesis successfully developed and implemented a synthetic data generation framework. This approach allowed for the systematic simulation of various operational parameters, providing a rigorous testing environment for the proposed model. Finally, the computational implementation was followed by an extensive graphical analysis, transforming raw mathematical outputs into clear, interpretable Key Performance Indicators (KPIs).

The computational results demonstrate that the proposed MILP model is a highly effective decision-support tool for managing complex circular supply chain operations. By simultaneously optimizing disassembly and remanufacturing, the model successfully resolves the inherent mismatch between the variable supply of end-of-life products and the independent market demands for recovered components and remanufactured goods.

The graphical analysis of the optimized results revealed several critical insights into system dynamics. First, the model effectively balanced the trade-off between inventory holding costs and immediate processing costs, strategically utilizing warehouse capacity to buffer against fluctuating returns and demands. Second, the dynamic tracking of material flows and capacity utilization highlighted the importance of coordinated planning; isolated decision-making for

disassembly or remanufacturing often leads to sub-optimal resource allocation and bottleneck formations.

From a managerial perspective, this thesis provides supply chain practitioners with a transparent and flexible framework. The generated visualizations—such as profit evolution, inventory fluctuations, and price dynamics—equip decision-makers with the operational intelligence necessary to evaluate different market scenarios. Ultimately, the model proves that adopting mathematically optimized recovery plans can significantly enhance the financial viability of circular economy initiatives, ensuring that sustainability objectives do not compromise economic profitability.

Bibliography

Ahmadi, A., Tavana, M., and Tirkolaee, E. B. (2020). A sustainable end-of-life vehicle processing network design using a novel bi-objective meta-heuristic. *Journal of Cleaner Production*, 256:120377.

Akerlof, G. A. (1970). The market for lemons: Quality uncertainty and the market mechanism. *The Quarterly Journal of Economics*, 84(3):488–500.

Atasu, A., Guide, V. D. R., and Van Wassenhove, L. N. (2009). Product reuse economics in closed-loop supply chain research. *Production and Operations Management*, 17(5):483–496.

Battery Hookup (2024). Nissan leaf gen-1 battery module (7.6v / 500wh).

Belhadj, I., Trigui, M., and Benamara, A. (2022). Disassembly sequence planning validated through augmented reality for a speed reducer. *Cogent Engineering*, 9(1):2061321.

Benchmark Mineral Intelligence (2024). Graphite anode pricing q4 2024. Benchmark Minerals.

Bentaha, M. L., Battaia, O., and Dolgui, A. (2015). An exact solution approach for disassembly line balancing problem under uncertainty of the task processing times. *International Journal of Production Research*, 53(6):1807–1818.

BloombergNEF (2024). Battery price survey 2024. Bloomberg Finance LP.

Carter, C. R. and Ellram, L. M. (1998). Reverse logistics: A review of the literature and framework for future investigation. *Journal of Business Logistics*, 19(1):85–102.

Couzon, P., Ouazene, Y., and Yalaoui, A. (2019). Joint lot-sizing and pricing problem for a remanufacturing system. *IFAC-PapersOnLine*, 52(13):1343–1348.

de Brito, M. P. and Dekker, R. (2003). A framework for reverse logistics. *ERIM Report Series Research in Management*. Erasmus Research Institute of Management.

Deniz, N. and Ozcelik, F. (2019). An extended review on disassembly line balancing with bibliometric & social network and future study realization analysis. *Journal of Cleaner Production*, 225:697–715.

Dowlatshahi, S. (2000). Developing a theory of reverse logistics. *Interfaces*, 30(3):143–155.

Dubarry, M., Truchot, C., Liaw, B. Y., Gering, K., Sazhin, S., Jamison, D., and Michelbacher, C. (2011). Evaluation of commercial lithium-ion cells based on composite positive electrode for plug-in hybrid electric vehicle (phev) applications. *Journal of Power Sources*, 196(23):10328–10335. [LMO spinel cathode characterisation; capacity data].

Ecker, M., Nieto, N., Jäbke, S., Knege, J., Hust, G., Hartmann, G., and Sauer, D. U. (2012). Calendar and cycle life study of li(nimnco)o_2-based 18650 lithium-ion batteries. *Journal of Power Sources*, 248:839–851. [Cell-level characterisation; AESC LEV50 voltage/capacity parameters used for module calculations].

Ellen MacArthur Foundation (2013). Towards the circular economy. Technical report, Ellen MacArthur Foundation.

Encatsu (2024). Aesc 56.3ah pouch cells from nissan leaf gen-2 (2018).

Farooque, M., Zhang, A., Thürer, M., Qu, T., and Huisingh, D. (2019). Circular supply chain management: A definition and structured literature review. *Journal of Cleaner Production*, 228:882–900.

FindMyElectric (2025). Nissan leaf battery replacement cost explained.

Fleischmann, M., Beullens, P., Bloemhof-Ruwaard, J. M., and Van Wassenhove, L. N. (2001). The impact of product recovery on logistics network design. *Production and Operations Management*, 10(2):156–173.

Fleischmann, M., Bloemhof-Ruwaard, J. M., Dekker, R., Van der Laan, E., Van Nunen, J. A., and Van Wassenhove, L. N. (1997). Quantitative models for reverse logistics: A review. *European Journal of Operational Research*, 103(1):1–17.

Fleischmann, M., Krikke, H. R., Dekker, R., and Flapper, S. D. P. (2000). A characterisation of logistics networks for product recovery. *Omega*, 28(6):653–666.

Foulloy, L., Lossent, T., et al. (2025). Sequencing and scheduling in disassembly shops: A review of problem formulations and solution approaches. *Journal of Remanufacturing*.

Gallego, G. and Van Ryzin, G. (1994). Optimal dynamic pricing of inventories with stochastic demand over finite horizons. *Management Science*, 40(8):999–1020.

Geissdoerfer, M., Savaget, P., Bocken, N. M., and Hultink, E. J. (2017). The circular economy–a new sustainability paradigm? *Journal of Cleaner Production*, 143:757–768.

Giudice, F. and Fargione, G. (2007). Disassembly planning of mechanical systems for service and recovery: A genetic algorithms-based approach. *Journal of Cleaner Production*, 15(5):401–416.

Govindan, K., Soleimani, H., and Kannan, D. (2015). Reverse logistics and closed-loop supply chain: A comprehensive review to explore the future. *European Journal of Operational Research*, 240(3):603–626.

Green Car Future (2022). Nissan leaf battery replacement and upgrades: Full guide.

Greentec Auto (2024). Gen-1 nissan leaf battery modules (bulk).

Guide, V. D. R. (2000). Production planning and control for remanufacturing: Industry practice and research needs. *Journal of Operations Management*, 18(4):467–483.

Guide, V. D. R., Teunter, R. H., and Van Wassenhove, L. N. (2003). Matching demand and supply to maximize profits from remanufacturing. *Manufacturing & Service Operations Management*, 5(4):303–316.

Guide, V. D. R. and Van Wassenhove, L. N. (2009). The evolution of closed-loop supply chain research. *Operations Research*, 57(1):10–18.

Gungor, A. and Gupta, S. M. (1999). Issues in environmentally conscious manufacturing and product recovery: A survey. *Computers & Industrial Engineering*, 36(4):811–853.

Gungor, A. and Gupta, S. M. (2001). A solution approach to the disassembly line balancing problem in the presence of task failures. *International Journal of Production Research*, 39(7):1427–1467.

Guo, L., Zhang, Z., Wu, T., et al. (2023). A novel MILP model and an improved genetic algorithm for disassembly line balancing and sequence planning with partial destructive mode. *Computers & Industrial Engineering*, 186:109720.

Guo, X., Fan, C., et al. (2024). Multi-objective human-robot collaborative disassembly line balancing considering components remanufacture demand and hazard characteristics. *Computers & Industrial Engineering*, 191:110621.

Gupta, S. M. and Taleb, K. N. (1994). Scheduling disassembly. *International Journal of Production Research*, 32(8):1857–1866.

Harper, G., Sommerville, R., Kendrick, E., Driscoll, L., Slater, P., Stolkin, R., et al. (2019). Recycling lithium-ion batteries from electric vehicles. *Nature*, 575:75–86.

Hjorth, S. and Chrysostomou, D. (2022). Human–robot collaboration in industrial environments: A literature review on non-destructive disassembly. *Robotics and Computer-Integrated Manufacturing*, 73:102208.

Homem de Mello, L. S. and Sanderson, A. C. (1990). AND/OR graph representation of assembly plans. *IEEE Transactions on Robotics and Automation*, 6(2):188–199.

Horie, H., Abe, T., Kinoshita, T., and Shimoida, Y. (2011). A study on an advanced lithium-ion battery system for evs used in the nissan leaf. *World Electric Vehicle Journal*, 4(1):1–8. [Primary source: AESC cell data, module 2S2P topology, pack electrical parameters].

Huang, Y. M. and Huang, C. T. (2002). Disassembly matrix for disassembly processes of products. In *Proceedings of the 2002 IEEE International Symposium on Electronics and the Environment*, pages 185–190.

IECM Group (2024). Electrolyte solvent and lipf6 market pricing 2024. Internal communication and industry estimates.

Ilgin, M. A. and Gupta, S. M. (2010). Environmentally conscious manufacturing and product recovery (ECMPRO): A review of the state of the art. *Journal of Environmental Management*, 91(3):563–591.

Islam, M. T. and Iyer-Raniga, U. (2022). Lithium-ion battery recycling in the circular economy: A review. *Recycling*, 7(3):33.

Issaoui, L., Aifaoui, N., and Benamara, A. (2016). Optimization of disassembly sequence planning for preventive maintenance. *International Journal of Advanced Manufacturing Technology*, 89:2031–2043.

Jayaraman, V., Guide Jr, V. D. R., and Srivastava, R. (1999). A closed-loop logistics model for remanufacturing. *Journal of the Operational Research Society*, 50(5):497–508.

Kim, H. J., Kernbaum, S., and Seliger, G. (2009). Emulation-based control of a disassembly system for lcd monitors. *International Journal of Advanced Manufacturing Technology*, 40:383–392.

Koc, A., Sabuncuoglu, I., and Erel, E. (2009). Two exact formulations for disassembly line balancing problems with task precedence diagram construction using an AND/OR graph. *IIE Transactions*, 41(10):866–881.

Kotler, P. and Armstrong, G. (2016). *Principles of Marketing*. Pearson, Harlow, 16th edition.

Lacey, G., Jiang, T., Putrus, G., Kotter, R., and Forsyth, E. (2013). The effect of cycling on the state of health of the electric vehicle battery. In *IET Conference on Power Electronics, Machines and Drives (PEMD 2012)*. [Leaf BMS architecture; thermistor count per module quadrant; SoH monitoring].

Laili, Y., Wang, Y., Fang, Y., and Pham, D. T. (2021). Product representation for disassembly sequence planning. In *Optimisation of Robotic Disassembly for Remanufacturing*, pages 37–68. Springer, Cham.

Lambert, A. J. D. (1997). Optimal disassembly of complex products. *International Journal of Production Research*, 35(9):2509–2523.

Lambert, A. J. D. (1999). Linear programming in disassembly/clustering sequence generation. *Computers & Industrial Engineering*, 36(4):723–738.

Lambert, A. J. D. (2002). Determining optimum disassembly sequences in electronic equipment. *Computers & Industrial Engineering*, 43(3):553–575.

Lander, L., Tagnon, C., Nguyen-Tien, V., Kendrick, E., Elliott, R. J. R., Edge, J. S., et al. (2023). Breaking it down: A techno-economic assessment of the impact of battery pack design on disassembly costs. *Applied Energy*, 331:120437.

Liang, C., Parnada, A., Gbadebo, A., Altumi, F., Qu, M., Li, L., et al. (2025). An experimental robotic cell for the disassembly of electric vehicle battery modules. *Journal of Remanufacturing*, 15:287–308.

Liu, J., Zhan, C., et al. (2023). Selective disassembly sequence planning under uncertainty using trapezoidal fuzzy numbers: A novel hybrid metaheuristic algorithm. *Engineering Applications of Artificial Intelligence*, 128:107459.

Lund, R. T. (1984). Remanufacturing: the experience of the united states and implications for developing countries. World Bank Technical Paper 31, World Bank.

Marshall, A. (1890). *Principles of Economics*. Macmillan, London.

Moheb-Alizadeh, H., Handfield, R., and Warsing, D. (2023). Reverse logistics network design to estimate the economic and environmental impacts of take-back legislation. *arXiv preprint*. arXiv:2301.09792.

Murphy, P. R. and Poist, R. F. (1989). Managing of logistical retromovements: An empirical analysis of literature suggestions. *Transportation Research Forum*, 29:177–184.

NEI Corporation (2024). Lithium manganese oxide (lmo) powders – nanomyte be-30/be-35.

Nimtz, M., Heitel, S., Koch, G., Kalinowski, T., and Riegler, T. (2021). Techno-economic analysis of a second-life battery storage system for renewable energy integration. *Energy*, 216:119249.

Nissan Motor Co. (2023). Nissan leaf reaches 650,000 global sales milestone. Nissan Global Newsroom.

Nissan Motor Co., Ltd. (2013). *Nissan Leaf ZE0 / AZE0 — Battery System Service Manual*. Technical Document NTB13-012. [Official OEM service data: module dimensions, busbar ratings, MSD specifications, HV contactor ratings].

OGSolarStore (2024). Nissan leaf – set of 7 modules, lithium-ion lmo battery.

Pochet, Y. and Wolsey, L. A. (2006). *Production planning by mixed integer programming*. Springer Science & Business Media.

Polat, O. and Kalayci, C. B. (2024). Disassembly line balancing with hazardous task failures: Model based solution approaches. *Computers & Industrial Engineering*, 190:110024.

Qnovo (2014). Inside the battery of a nissan leaf.

Rahme, S., Ouazene, Y., and Yalaoui, A. (2023). Multi-period disassembly planning under stochastic returns and uncertain quality. *European Journal of Operational Research*, 305(1):290–307.

Ravi, V. and Shankar, R. (2005). Analysis of interactions among the barriers of reverse logistics. *Technological Forecasting and Social Change*, 72(8):1011–1029.

Recurrent Auto (2024). Electric car battery replacement costs in 2024/2025.

Ren, Y., Meng, L., Zhang, C., Zhao, F., and Sutherland, J. W. (2020). An efficient metaheuristics for a sequence-dependent disassembly planning. *Journal of Cleaner Production*, 245:118644.

Ren, Y., Zhang, C., Zhao, F., and Sutherland, J. W. (2018). An asynchronous parallel disassembly planning based on genetic algorithm. *European Journal of Operational Research*, 269(2):647–660.

Richa, K., Babbitt, C. W., and Gaustad, G. (2017). Eco-efficiency analysis of a lithium-ion battery waste hierarchy inspired by circular economy. *Journal of Industrial Ecology*, 21(3):715–730.

Rogers, D. S., Lambert, D. M., Croxton, K. L., and Garcia-Dastugue, S. J. (2002). The returns management process. *International Journal of Logistics Management*, 13(2):1–18.

Rogers, D. S. and Tibben-Lembke, R. S. (1999). *Going Backwards: Reverse Logistics Trends and Practices*. Reverse Logistics Executive Council, Pittsburgh, PA.

Rosenberg, S., Huster, S., Baazouzi, S., Glöser-Chahoud, S., Al Assadi, A., and Schultmann, F. (2022). Field study and multimethod analysis of an ev battery system disassembly. *Energies*, 15(14):5324.

S&P Global (2024). Cost of active materials used for lithium-ion battery cathodes in 2023. Statista.

Srivastava, S. K. (2007). Green supply-chain management: A state-of-the-art literature review. *International Journal of Management Reviews*, 9(1):53–80.

Stock, J. R. (1992). *Reverse Logistics*. Council of Logistics Management, Oak Brook, IL.

Thierry, M., Salomon, M., Van Nunen, J., and Van Wassenhove, L. (1995). Strategic issues in product recovery management. *California Management Review*, 37(2):114–135.

Tian, G., Ren, Y., et al. (2020). Electric vehicle battery disassembly sequence planning based on frame-subgroup structure combined with genetic algorithm. *Frontiers in Mechanical Engineering*, 6:576642.

Tibben-Lembke, R. S. and Rogers, D. S. (2002). Differences between forward and reverse logistics in a retail environment. *Supply Chain Management: An International Journal*, 7(5):271–282.

Trochu, J. et al. (2025). Reverse logistics: A systematic literature review of trends and future directions. *International Journal of Accounting & Information Management*, 15(1).

Tseng, H.-E., Chang, C.-C., and Li, J.-D. (2008). A genetic algorithm for product disassembly sequence planning. *Neurocomputing*, 71(16–18):3720–3731.

Unsal, O. et al. (2024). Advances in partial disassembly line balancing: A state-of-the-art review. *Computers & Industrial Engineering*, 188:109870.

U.S. Department of Energy — Vehicle Technologies Office (2012). Fy2012 annual progress report: Advanced battery r&d. Technical report, Office of Energy Efficiency & Renewable Energy. [Pack-level teardown data; busbar and BMS configuration; thermistor placement].

Wang, K., Li, X., and Gao, L. (2020). A multi-objective algorithm for U-shaped disassembly line balancing with partial destructive mode. *Neural Computing and Applications*, 32:6007–6020.

Wang, X. et al. (2024). Exploring engineering applications of two-sided partial destructive disassembly line balancing problem. *Expert Systems with Applications*, 260:125327.

Wu, X., Kumar, P., Bhatt, M., and Li, B. (2022). Demand elasticity analysis for secondary market ev components. *Journal of Cleaner Production*, 368:133178.

Xanthopoulos, A. and Iakovou, E. (2009). On the optimal design of the disassembly and recovery processes. *Waste Management*, 29(5):1702–1711.

Yu, S. and Li, J. (2006). Structure representation for concurrent analysis of product assembly and disassembly. *Expert Systems with Applications*, 30(4):706–718.

Zikopoulos, C. and Tagaras, G. (2008). On the attractiveness of sorting before disassembly in remanufacturing. *IIE Transactions*, 40(3):313–323.

Zrnic, N., Gasic, M., et al. (2022). CAD-based AND/OR graph generation algorithms in (dis)assembly sequence planning of complex products. *Procedia CIRP*, 106:123–128.